1986

A nuclear magnetic resonance study of deuterated poly(vinylidene fluoride) and a copolymer of deuterated vinylidene fluoride and tetrafluoroethylene

Montee A. Doverspike
College of William & Mary - Arts & Sciences

INFORMATION TO USERS

While the most advanced technology has been used to photograph and reproduce this manuscript, the quality of the reproduction is heavily dependent upon the quality of the material submitted. For example:

- Manuscript pages may have indistinct print. In such cases, the best available copy has been filmed.
- Manuscripts may not always be complete. In such cases, a note will indicate that it is not possible to obtain missing pages.
- Copyrighted material may have been removed from the manuscript. In such cases, a note will indicate the deletion.

Oversize materials (e.g., maps, drawings, and charts) are photographed by sectioning the original, beginning at the upper left-hand corner and continuing from left to right in equal sections with small overlaps. Each oversize page is also filmed as one exposure and is available, for an additional charge, as a standard 35mm slide or as a 17"x 23" black and white photographic print.

Most photographs reproduce acceptably on positive microfilm or microfiche but lack the clarity on xerographic copies made from the microfilm. For an additional charge, 35mm slides of 6"x 9" black and white photographic prints are available for any photographs or illustrations that cannot be reproduced satisfactorily by xerography.

Doverspike, Montee A.

A NUCLEAR MAGNETIC RESONANCE STUDY OF DEUTERATED POLY(VINYLIDENE FLUORIDE) AND A COPOLYMER OF DEUTERATED VINYLIDENE FLUORIDE AND TETRAFLUOROETHYLENE

The College of William and Mary in Virginia PH.D. 1986

PLEASE NOTE:

In all cases this material has been filmed in the best possible way from the available copy. Problems encountered with this document have been identified here with a check mark __✓__.

1. Glossy photographs or pages _____
2. Colored illustrations, paper or print _____
3. Photographs with dark background _____
4. Illustrations are poor copy _____
5. Pages with black marks, not original copy __✓__
6. Print shows through as there is text on both sides of page _____
7. Indistinct, broken or small print on several pages __✓__
8. Print exceeds margin requirements _____
9. Tightly bound copy with print lost in spine _____
10. Computer printout pages with indistinct print _____
11. Page(s) _____ lacking when material received, and not available from school or author.
12. Page(s) _____ seem to be missing in numbering only as text follows.
13. Two pages numbered _____. Text follows.
14. Curling and wrinkled pages _____
15. Dissertation contains pages with print at a slant, filmed as received _____
16. Other _____

_____

_____

University
Microfilms
International

A NUCLEAR MAGNETIC RESONANCE STUDY OF DEUTERATED POLY(VINYLIDENE FLUORIDE) AND A COPOLYMER OF DEUTERATED VINYLIDENE FLUORIDE AND TETRAFLUOROETHYLENE

A Dissertation

Presented to

The Faculty of the Department of Physics

The College of William and Mary in Virginia

In Partial Fulfillment

of the Requirements for the Degree of

Doctor of Philosophy

by

Montee A. Doverspike

November 1986

APPROVAL SHEET

This dissertation is submitted in partial fulfillment of the requirements for the degree of

Doctor of Philosophy

Author

Approved, November 1986

Mark S. Conradi

Roy L. Champion

Henry Krakaur

Harlan Schone

Morty Eckhause

Gary C. Defotis

Chemistry Department

Table of Contents

LIST of FIGURES

ABSTRACT

Pulsed deuterium NMR experiments have been performed on deuterated samples of poly(vinylidene fluoride), PVF_2, repeat unit CH_2CF_2 and the copolymer poly(vinylidene fluoride)-tetrafluoroethylene (80-20), (PVF_2–F_4E). A deuterium line shape study has been employed to characterize the orientational distribution of the dipole moments in both poled and unpoled samples. In addition, the orientational distributions of chain axis alignment has been measured in stretched samples.

PVF_2 and PVF_2–F_4E exhibit unique piezoelectric and pyroelectric properties which are due to their crystalline components (approximately 50% in typical material). Four crystalline phases exist in the homopolymer (PVF_2), the α, β, γ, and the δ. The relatively electrically inactive, melt solidified α phase can be transformed into the ferroelectric β phase by mechanical deformation (stretching) or by application of large electric fields (poling- 200 Mv/meter). The copolymer melt solidifies directly into the β phase. The β phase is characterized by a net dipole moment per unit cell due to the parallel alignment of the CF_2 dipole moments in the unit cell. The orthorhombic unit cell dimensions of the β phase render a nearly pseudohexagonal packing structure of the molecular chains and is thought to allow for dipole reorientations via 60° steps during the poling process.

The orientationally dependent quadrupole interaction has been used to characterize the orientational distributions of the molecular dipole moments about the poling direction in both poled and unpoled samples of PVF_2 and PVF_2–F_4E. No orientational dependence was found in either the poled or unpoled samples. This is in contrast to recent x-ray results which report substantial orientational anisotropy in rolled, poled protonated films. We have also measured the degree of chain axis alignment in stretched samples of both PVF_2 and PVF_2–F_4E. Alignment in both samples is characterized by a gaussian distribution function about the stretch direction with a half width 1/e maximum of 22° and 18° respectively.

The characterization of the experimental results was done by comparing computer simulated line shapes with the experimental line shapes.

A NUCLEAR MAGNETIC RESONANCE STUDY OF DEUTERATED POLY(VINYLIDENE FLUORIDE) AND A COPOLYMER OF DEUTERATED VINYLIDENE FLUORIDE AND TETRAFLUOROETHYLENE

Chapter I

INTRODUCTION

The polymer poly(vinylidene fluoride), PVF_2, has been known for many decades but has only in the last 10 to 15 years become a topic of intense study. Its unique piezoelectric and pyroelectric properties were first reported on in 1969.[1] These electrical characteristics are a consequence of the macroscopic polarization induced in the polymer by the application of large electric fields.[1-4] The polymer's physical consistency is very similar to Saran wrap. Its special electrical properties combined with its mechanical durability have made it very popular for many uses, i.e., ultrasonic transducers,[1,3,5-6] stress-wave monitors,[1] pressure measuring devices,[1,6] and infrared detectors.[1,7-8]

As a consequence of its commercial applications, it is not surprising to find numerous reports on its structure, crystallization and morphology.[1,9-11] Included in these reports is a very extensive review article by Lovinger (1983) covering the historical development, recent experimental studies and discussions on theoretical models of PVF_2.[1] We note that his review will be referenced frequently in the following report but by no means exclusively. Several techniques have been employed to study the properties of PVF_2 : x-ray diffraction,[1,8,11-16] infrared spectroscopy,[1,7,17-20] electron diffraction,[1] high resolution NMR,[1,21-22] wideline NMR[1,9,23] and dielectric studies.[1,8,24-28]

PVF_2, polymerized from the monomer unit $CH_2=CF_2$,[1,4] contains approximately a 50/50 mixture of amorphous and crystalline components.[1,4] The molecular structure consists of a carbon backbone with two protons and two fluorines attached alternately to the carbon atoms.[1,4] The amorphous region plays very little role in the macroscopic electrical properties.[1,6,9,12,28] The cystalline portion of the polymer can exist in four different phases.[1,10-11] The process used to produce the polymer film and the

film's thermal and mechanical history determine the crystalline phase found in the film.[1,4] Of the four phases, the α, β, γ, and δ phases, the β phase is the most electrically active[1] and is the phase that will be reported on in this work. The β phase contains two molecules per unit cell.[1,4] The molecular unit CF_2 has an electrical dipole moment of 7.0×10^{-30} C cm,[29] bisecting the two C-F bonds (figure 1.1). The molecules are oriented in the unit cell such that there is a net dipole moment per unit cell.[1,4] That is, all the dipole moments of the CF_2 groups in the unit cell are parallel.[4] The electrical properties exhibited by the polymer are thought to be due to the reorientation of the dipole moments in the unit cell.[1-2,4,8,27,30-31] When an external electric field is applied, the dipoles align themselves in a cooperative manner along the applied field. Several models for the reorientational process have been proposed,[1,12,26,29] but the experimental data are still inconclusive as to how this process takes place.[1] Regardless of the mechanism, the end result is that the polymer molecules rotate about their long axes.[1] Another question still unresolved concerns the orientational distribution function of the b-axis (polar axis) before and after poling.[20,29,32] The NMR experiments performed here address both these issues in order to gain a fuller understanding of the microscopic behavior of this material.

Deuterium NMR has been used extensively to study the orientational properties of many systems at the molecular level.[33-43] Its use has proved invaluable in determining the molecular orientations and molecular dynamics in many polymer system.[37,43-45] Quadrupolar broadening of the deuterium NMR spectrum provides information on the orientation of the molecule (carbon-deuterium (C-D) bond orientation in our specific case) containing the deuterium nucleus with respect to an applied magnetic field. The quadrupole moment of the deuterium nucleus (spin 1) interacts with a local electric field gradient to produce an orientationally dependent splitting of the three level, spin 1 system.[33,46] The splitting is a function of the angle between the applied magnetic field and the C-D bond.[33,34] By inspection of the resulting line shapes, it is possible to infer qualitative as well as quantitative information about the molecular dynamics and orientational properties.[35-37,44-45]

We report here a nuclear magnetic resonance line shape study of deuterated PVF_2 and its copolymer poly(vinylidene fluoride) - tetrafluoroethylene, PVF_2–F_4E. The purpose of these experiments is to characterize the orientational distribution functions $f(\theta)$ and $g(\phi)$ of the carbon-deuterium bonds as a function of stretching and electrical polarizing (poling). The angle θ refers to the orientation of the chain axis with respect to the stretch direction. The angle ϕ refers to the orientation of the electric dipole moments with respect to the direction of the applied poling field. We will address the questions raised above by the use of line shape analysis and comparison to simulated line shape calculations. What is the orientational distribution of chain axes in stretched films? To what extent do the dipole moments reorient upon poling and what is the final orientational distribution of dipole moments characterizing these films? Do the reorientations take place via 180° flips as has been originally proposed[1] or is the process performed via 60° steps as has been recently suggested?

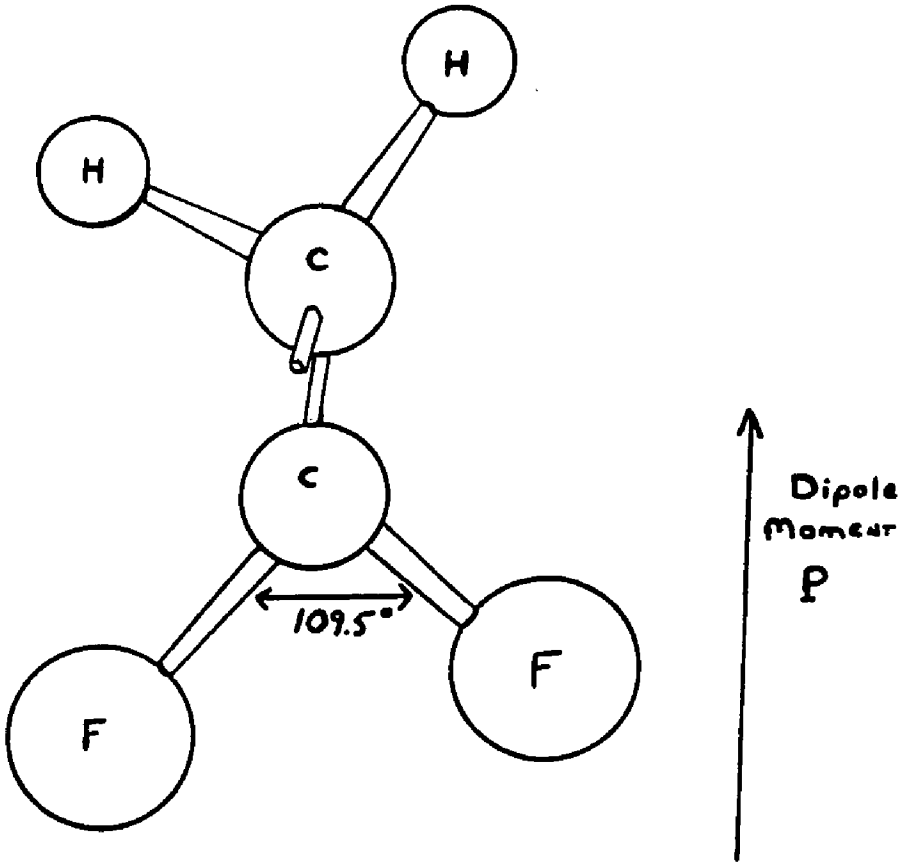

Figure 1.1 : Monomer unit of PVF_2 showing the net dipole moment

Chapter II

EXPERIMENTAL PROCEDURE

2.0 NMR Spectrometer

A NMR spectrometer consists of three major parts, a transmitter, an antenna, and a receiver. Since an in depth explanation of each of these is available in standard publications,[47,48] only a brief description will be presented here. A description of the magnet and data acquisition equipment will also be presented.

An NMR spectrometer is very similar in operation to a radio broadcasting network. The transmitter section produces a radio frequency (rf) signal which is sent to the antenna section (the probe in this case) via coaxial lines. The returning rf signal is picked up by the receiver and heterodyned down to audio frequencies, typically hundreds of hertz.

2.0.1 Transmitter

The transmitter section of our super-heterodyned pulse spectrometer consists of a crystal controlled coherent rf synthesizer (.1 to 160 MHz), a transmitter assembly containing rf phasing and gating components, and pulse generators. The rf phasing and gating are done at an intermediate frequency of 30 MHz obtained from a fixed 30 Mhz output on the synthesizer. The 30 MHz signal is heterodyned with the synthesizer's tuneable output (10 dBm) at 30 MHz $+f_o$ to produce the properly phased and gated rf signal at f_o . This rf signal is preamplified by an ENI class A amplifier to approximately 30 watts. The signal is then amplified to 200 watts by a home-modified TTI class C amplifier and then sent to the tuned probe via 50 ohm triaxial line (double shielded coaxial line).

A 52 MHz bandpasss filter is used just before the ENI to remove noise and spurious heterodyne outputs due to the mixing elements in the transmitter assembly.

A high pass filter follows the ENI to remove any low frequency noise generated by the ENI . In addition to rf filters, several crossed diodes are placed after the TTI amplifier to reduce noise output[49] and hence, increase transmitter to receiver isolation during the transmitter off-time.

Both manually and computer operated home-built pulse generators are used to produce the necessary timing for pulse lengths and delays. The pulse generators control the gating of the transmitter assembly section.

2.0.2. Receiver

The receiver section of the spectrometer consists of a preamplifier, a frequency mixer, an intermediate frequency (IF) amplifier, and a phase sensitive detector. The NMR sample generates a signal at $f_o + \Delta f$ (i.e. near f_o) which is preamplified at $f_o + \Delta f$, and is then heterodyned in a single sideband mixer producing a signal at 30-Δf Mhz. This in turn is amplified in the variable gain IF amplifier and then phase sensitive detected[49] to produce an in phase and quadrature audio signal at Δf. The detected signals are then low-pass filtered in a variable RC network setting the receiver bandwidth, and sent to the transient digitizer.

Due to the sensitivity of the receiver input (typically it amplifies signals at the microvolt level), the receiver input stage should always be isolated from the transmitter section, especially when the transmitter is pulsed on.[49] Typical transmitter pulse voltages are of the order of 100 volts and result in receiver " deadtime ", due to amplifier saturation and ringing of LC circuits of the probe. The deadtime persists after the pulse is applied and obscures the initial part of the NMR signal. The deadtime can be minimized by turning the receiver off during the pulse and by using crossed diodes at the receiver preamplifier input.[49] The receiver deadtime for these experiments is typically 10-20 microseconds. Since the line shapes measured were of the order of 250 KHz wide, it was necessary to look at echoes instead of free induction decays (FID) since FIDS were obscured by the receiver deadtime.

2.0.3. Data Acquisition

A Biomation 2805M transient digitizer was used to digitize the dual audio frequency signals. The maximum conversion rate was 5 MHz with a memory size of 2048 8-bit words per channel. Only the first half of memory of each channel was transferred to the Apple II microcomputer for signal averaging and data storage. In addition to data acquisition, the Apple II could also control the pulse timing sequences via a computer hook up to the pulse generators. The experimental data were stored on diskettes for permanent record. The Apple II was also used for data analysis and theoretical computations.

2.0.4. Magnet

The magnet used in the following experiments was an 8.0 Tesla Oxford superconducting solenoid with a two inch room temperature bore. Superconducting shim coils provided homogeneity improvement. The magnet was replenished with liquid helium every five days to keep the coils superconducting. Liquid nitrogen was also used as a cryogen in the outside jacket which surrounded the inner He dewar and was filled every 1 or 2 days. Liquid helium storage dewars (≈100 liters) were hoisted onto a hydraulic lift dolly and then positioned approximately 1 meter from the magnet filling port which exited vertically from the top of the magnet. Care was taken with the placement of the dolly and storage dewar near the magnet to avoid the risk of the steel dolly being attracted to the magnet. A vacuum jacketed stainless steel transfer tube was used for the liquid helium transfers. During transfers, the transfer tube was precooled by inserting the storage dewar side of the tube in the dewar until it reached the liquid helium level. The exiting gas was dumped into the room until the gas stream became more dense and appeared to be light blue in color. This indicated that liquid helium was then coming through the tube. The magnet side of the transfer line was then inserted into the magnet fill port. The fill time was approximately 30 minutes with a pressure of 45 inches of water on the storage dewar. The pressure was maintained by an external helium gas cylinder and regulator hosed to the storage dewar. When the magnet was full the transfer line was then removed and the magnet fill port was resealed. Twenty liters was the amount typically required for each refill.

The magnet field stability and spatial homogeneity remained constant over the experimental time span of about six months. Periodic measurements of the field strength were performed using a D_2O sample in the experimental probe. Field drift was approximately 800 hertz over the entire time span. Most of the drift occurred during the first few weeks after the initial cool down of the magnet.

2.0.5 Probe and Matching Network

The NMR probe consists of a handwound coil in an LC tank circuit combined with a rf matching network for efficient coupling to the transmitter and receiver.[48,49] The function of the probe is two-fold. First, it delivers rf power to the sample in the form of an oscillating magnetic field H_1, and secondly, it serves as a receiving antenna which picks up the NMR signal (precessing magnetization).[49]

The double duty of the single coil as the transmitter and receiver antenna poses problems for the receiver section.[49] The receiver is designed to amplify signals at the microvolt level. But the transmitter pulses are of the order of hundreds of volts. Hence the receiver must be isolated from the transmitter during rf pulsing.[49] This is accomplished by placing shunt diodes at the input of the receiver preamplifier. The diodes turn on during transmitting pulses (>.6volts) and are off for small signals.[48] Hence, they act like automatic switches for large and small signals. Further isolation was accomplished during the off time of the transmitter by placing diodes in series with the transmitter directly after the main power amplifier. This reduces broadband noise seen by the receiver which is emitted by the power amplifier even during its off state.

The probe circuit consists of a LC parallel resonant tank circuit. [49] The parallel circuit has a high impedance at the resonance condition $\omega^2LC=1$, where L is the inductance of the NMR coil, C is the parallel capacitance, and ω is 2π times the NMR frequency f_o. Typical Q values for the circuit are ≈ 100,[49] where Q, the quality factor of the tank circuit, is defined as $Q=\omega L/R$.[48] R is the ohmic resistance of the coil (measured at f_o, generally larger than its dc resistance).

Values for the rotating field H_1 range between 50 to 100 gauss. The strength of

the rotating field H_1 is given by :[49]

$$H_1 \approx 3(PQ/V\omega_0)^{1/2}.$$

P is the power in watts of the transmitter, Q is the quality factor of the circuit , V is the volume of the NMR coil, and ω_0 is the resonance frequency. For a given transmitter power output, the easiest way to produce large H_1 fields is to reduce the sample coil volume. This was necessary in the following experiments in order to produce reasonable $\pi/2$ pulse times. The NMR sample coils were of the order of .125 inches in diameter and .250 inches long.

To insure that the maximum amount of power possible is transmitted to the probe during a pulse (also maximizes the received signal), the high impedance tank circuit (5000 ohms at resonance) must be impedance matched to the transmitter and receiver, i.e., to 50 ohms.[48,49] This is accomplished using capacitive coupling to the tank circuit. By appropriate choices of both the tuning and coupling capacitors, the probe coil is transformed to 50 ohms resistive at the input for the desired frequency.[48] Typical capacitive values used are 10 to 100 picofarads; the usual inductance for NMR coils is 1 to 3 μhenries. To avoid spurious acoustic signals from the probe components, care must be taken in the choice of capacitors and design of the NMR coil. Before each experiment was performed, care was taken to tune the probe and check for coherent and incoherent rf noise.

The homebuilt rf probe had two Johanson quartz trimmer capacitors which served as the variable tuning and coupling capacitors for the rf tank circuit. Additional fixed capacitors were used when needed. All NMR coils were handwound and epoxied to maintain their rigidity. The probe body consisted of a copper pipe 1.5 inches in diameter and approximately 4 inches in length. Both ends of the probe body were capped off with copper plate disks. The rf circuitry including the coil was supported by the top cap. The tuning and coupling capacitors protruded through the top of the cap along with a BNC connector that provided the rf input to the probe. The probe body had a 3/16 inch hole drilled into the side of the tube so the sample could be inserted into the probe and into the NMR coil. The sample could then be oriented with respect to the magnetic field H_0 without taking the probe apart. Scribe marks

every 5° were placed on the side of the probe body and indicated the orientation of the sample with respect to the magnetic field H_o.

2.0.6 Hysteresis Electronics

A homebuilt ferroelectric hysteresis measuring device was used for studying hysteresis loops of samples. A schematic diagram of the hysteresis measuring electronics is shown in figure 2.1.

The positive and negative voltages were supplied by Fluke and Power Design high voltage power supplies. Typical voltages used in running the hysteresis loop poling scans ranged between 1.5 to 3.0 Kv. To stiffen the output voltages of the supply, the homebuilt circuit included a 1.0 μfarad shunt capacitor on the hi voltage input.

During a hysteresis loop run, the voltage applied to the sample is monitored at the x output where it is divided down by 1000 to 1. A measuring capacitor (10 μf) in series with the sample capacitance is used to measure the polarization (or charge) developed on the sample. A manual grounding switch is in shunt with the reference capacitor in order to drain off charge when desired. A neon bulb is included as a safety precaution, limiting the voltage across the measuring capacitor. The charge developed across the sample is measured by monitoring the voltage drop across the 10 μf standard capacitor with a high impedance voltmeter ($\approx 10^{13}\Omega$). A buffered output on the voltmeter provides a y output. An electric field vs. polarization plot is produced by sending the x and y outputs to a plotter.

2.1. Sample Preparation

Deuterated samples of poly(vinylidene fluoride), PVF_2–D_2, (hompolymer) and a copolymer of poly(vinylidene fluoride) and tetrafluoroethylene, PVF_2–F_4E, were obtained in powder form from Dr. Ted Cais of Bell Labs. The homopolymer powder came in two different molecular weights, 147 mg of high molecular weight material and 438 mg of a low molecular weight sample. These molecular weights proved to be much higher and much lower than the molecular weights normally found in the commercially available protonated PVF_2.[50] The deuterated material therefore exhibited different pressing, stretching, and poling characteristics. As a result it was very

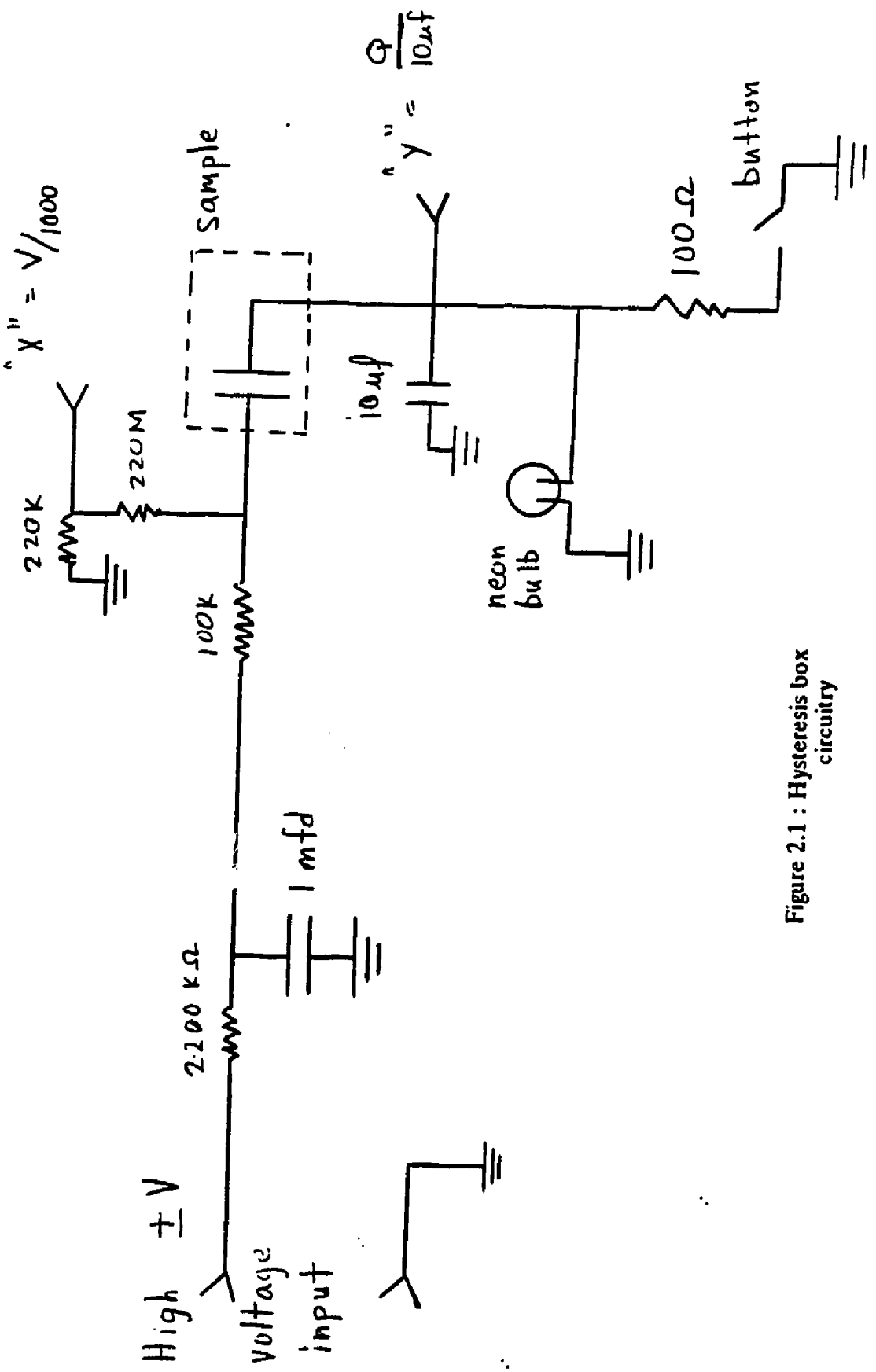

Figure 2.1 : Hysteresis box circuitry

difficult to produce poled samples of the homopolymer.

The copolymer on the other hand had similar processing characteristics to the commercial PVF_2 and consequently it was relatively easy to produce poled films.[50]

The film making process will be described below along with the difficulties due to the low and high molecular weight characteristics.

2.1.1. Pressing films[51]

The basic procedure in making the films involved simultaneously heating and pressing the powder in a hydraulic press. Approximately 6 mg of powder was placed between two 2 mil thick sheets of Kapton (polycarbonate film). A thinner sheet of kapton with the center removed was also placed between the two outside sheets and served as a shim to gauge the final thickness of the film. This assembly was then placed in a temperature regulated hydraulic press where the temperature and pressure could be controlled. The press was heated just below the melting point of the powder ($190^{\circ}C$ – homopolymer, $160^{\circ}C$ – copolymer)[1] and then pressure was slowly applied to the sandwiched sheets. When the pressure was $\approx$ 4000 lbs/in.^{2}, the press was quickly released and the pancaked sheets were removed and allowed to cool down to room temperature. Then the kapton sheets were peeled away leaving a circular film varying from 25 to 75 microns thick and 4 to 6 cm in diameter. Control samples of commercial, protonated material were first attempted to insure that the procedure to be used would give satisfactory results. Several films of commercial PVF_2 were successfully pressed and stretched using the procedure described above.

2.1.2. Low Molecular Weight Film[51]

The low molecular weight (m.w.) homopolymer was used for the first attempt in making a deuterated pressed film. The low m.w. films proved to be impossible to make due to their flow and stretch characteristics. The melt viscosity of the powder was so low that the material flowed almost like water when heated. This produced films so thin that it was impossible to peel them from the Kapton sheets without tearing. In addition, the films cooled to form a very brittle structure and were not malleable like the commercial material. Stretching the films was impossible. Consequently,

no films were made from the low m.w. homopolymer.

2.1.3. High Molecular Weight Film.[51]

The high molecular weight material had the opposite problem of the low molecular weight films. The melt viscosity was so high that a considerable amount of pressure (6000 lbs/in.^{2}) was required to pancake the film. However, the films were malleable enough to peel from the Kapton sheets without tearing or otherwise damaging the films. Due to the poor flow characteristics, the melt would develop small air pockets in the films even after pressing. The density inhomogeneity of the cooled films made it very difficult to produce stretched, poled samples.

2.1.4. Stretching Films[51]

The final stage in the film making process involved stretching the pressed films on a Nystron stretching machine. The films were first cut into strips approximately 4-6 cm by .5-1.5 cm. A temperature regulated chamber kept the films at 85° C during the stretching process. Films were placed in retracting jaws and stretched at a rate of .1 inches per minute. The homopolymer films attained a 3:1 stretch ratio. After stretching, the films were cooled to room temperature while under tension and then removed.

The high molecular weight homopoymer material was very difficult to stretch due to its high shear strength. Many of the films tore in half instead of stretching like the commercial protonated material. Most of the problems encountered with stretching the high m.w. films were due to air pockets and density inhomogeneity in the pressed films. Uneven stretching would occur around the air pockets and thin spots and the films would eventually tear. After numerous attempts, a few high m.w. homopolymer stretched films were finally produced. Their final thicknesses ranged between 12 to 25 microns and length varied between 3 to 8 cm.

2.1.5. Copolymer Film

The copolymer samples were far easier to produce than the homopolymer films. The flow characteristics of the copolymer melt made it easy to press out smooth,

homogeneous circular films. The cut strips were easily stretched, attaining a 4:1 stretch ratio forming homogeneous films approximately 25 microns thick.

2.2 Plating and Poling

2.2.1. Plating

The plating and poling process was done both at the National Bureau of Standards and at Washington University in St. Louis, MO.. All the films were evaporatively plated with aluminum in an evacuated evaporation unit. The stretched films were placed between two aluminum masks and plated with approximately 1000 angstroms of aluminum on both sides. A small area around the perimeter of the film was left unplated to prevent electrical arcing around the edge during the poling process. Care was taken to prevent radiative heating of the films during the plating process.

2.2.2. Poling

The poling process involved running electrical hysteresis experiments on the stretched samples, i.e., measuring polarization vs. electrical field strength. The ferroelectric films are polarized by application of a large electric field.[1] The electrical connection to the films was provided by small copper leads which were silver epoxied to the plated aluminum surface. The samples were submerged in silicone oil to prevent electrical arcing around the sample edge. Preliminary trials of poling with the samples exposed to air were unsuccessful due to an edge arcing effect. At NBS, a digital, high voltage (10 Kv) power supply was used to produce the large electric fields. A homebuilt charge-measuring device was used to measure the polarization as a function of the applied electric field. The voltage source was sinusoidally driven at a repetition rate of one cycle per 100 seconds. Signals proportional to the applied voltage and accumulated charge were sent to a plotter which produced hysteresis diagrams.

The poling process at Washington University was performed using the hysteresis box already described in section 2.0.6.. A 3 Kv power supply provided the necessary

voltage. The voltage was varied by turning the knobs in 100 volt increments. There was no difference between hysteresis loops run on the two different rigs. Both setups gave reproducible and reliable results.

The most reliable indication that samples were successfully poled was the measurement of remnant polarization from the hysteresis plots. The values typically measured on commercial films range from 5 to 10 μcoulombs per cm^2.[1,6,8,24,27] The deuterated films showed lower remnant polarization values ranging between 1 to 3 μcoulombs per cm^2. We note that electric breakdown would sometimes occur in the films due density inhomogeneity before full hysteresis curves could develop. This could be the reason for the lower values of polarization in both the PVF_2 and PVF_2–F_4E films.

Two other methods of measuring polarization were utilized at the National Bureau of Standards: a light pulse technique and a thermal pulse measurement which made use of both the piezo-pyro electrical properties of PVF_2. [52] Both methods confirmed that the films were poled.

Chapter III

MATERIAL BACKGROUND

3.0 General Information

Poly(vinylidene fluoride) and its copolymers have been the focus of extensive research, their conformational and electrical properties having been studied by several techniques: x-ray[10-16,29,31,53] and infrared analysis,[1,7-8,17-20] and electron and Raman spectroscopy.[1] The crystal structure and electrical properties of PVF_2 are well documented and will be reviewed below. Since very extensive reviews exist,[1] the discussion below will be brief and general in nature. The discussion will focus mainly on the particular crystalline phase β, since it is the β phase that exhibits special electrical properties and hence, was the crystalline structure studied in this research. Polarization theories will also be discussed along with experimental evidence for each.

3.1 Amorphous Phase

The monomer unit of poly(vinylidene fluoride) is CH_2CF_2. The homopolymer, PVF_2, and its various copolymer blends form approximately a 50/50 mix of crystalline /amorphous components. The root mean square length of the amorphous chains is approximately 65 nm, i.e., $\langle r^2 \rangle_o^{1/2} \approx 65$ nm , for a typical molecular weight of one million.[54] Below the glass transition (-60° C), the motion of the amorphous chains are substantially reduced and freeze into disordered configurations.[1,6] Due to the relatively unrestricted motion of the amorphous chains at room temperature,[55] the amorphous component is thought to contribute very little to the macroscopic electrical properties of the polymer.[1]

3.2 Crystalline Phases

The piezo-pyro electrical properties of the polymer are a direct consequence of its four crystalline structures. Each crystalline structure shows varying amounts of

electrical activity, ranging from the most active polymorph, the electrically polar β phase, to the three relatively inactive polymorphs, the α, γ, and δ phases.

3.2.1 α Phase

The most common polymorph, the α phase, is obtained by crystallization from the melt.[1] The unit cell has orthorhombic symmetry, dimensions a=4.96, b=9.64, c=4.62 ang., and contains four molecules per unit cell.[1] Though the monomer unit itself has an electrical dipole moment, the unit cell shows no net dipole moment due to the antiparallel packing of the chains (see figure 3.1). The c - axis repeat distance is consistent with a *cis –trans* conformation. [1] Though the α phase is formed from the melt, it can be transformed to the polar β phase by various mechanical deformations of the film.[1,6,15]

3.2.2. β Phase

The β -phase is obtained from melt-crystallized films by mechanical deformation such as stretching or rolling, or by application of large electric fields (200 Mv/meter).[1] The unit cell contains two molecules in orthorhombic symmetry with lattice constants a=8.45, b=4.88, c=2.55 ang..[1] The unit cell is shown in figure 3.2. The repeat distance along the c-axis is uniquely characteristic of an all *trans* conformation.[1] In contrast to the antiparallel arrangement in the α phase, the β phase structure contains two dipoles in the unit cell whose moments are parallel to the b-axis, giving rise to a net polarization per unit cell.[1] The dipole moment of an individual monomer unit of the β-chains is 7.0×10^{-30} coulombs-cm and lies normal to the chain axis.[1]

When a film is formed from the melt, the resulting α phase crystallites grow to form spherulites, with the b-axis emerging in the radial direction.[1] The c-axes of the crystallites lie normal to the spherulite. The spherulites have diameters of approximately 100 microns and thicknesses of the order of 100 angstroms, depending on the growth conditions.[1]

Stretching melt-crystalized films by approximately 400% induces the transformation to the β phase and is accompanied by a preferential alignment of the crystallite c-axis along the stretch direction.[4,9] X-ray diffraction, electron microscopy and

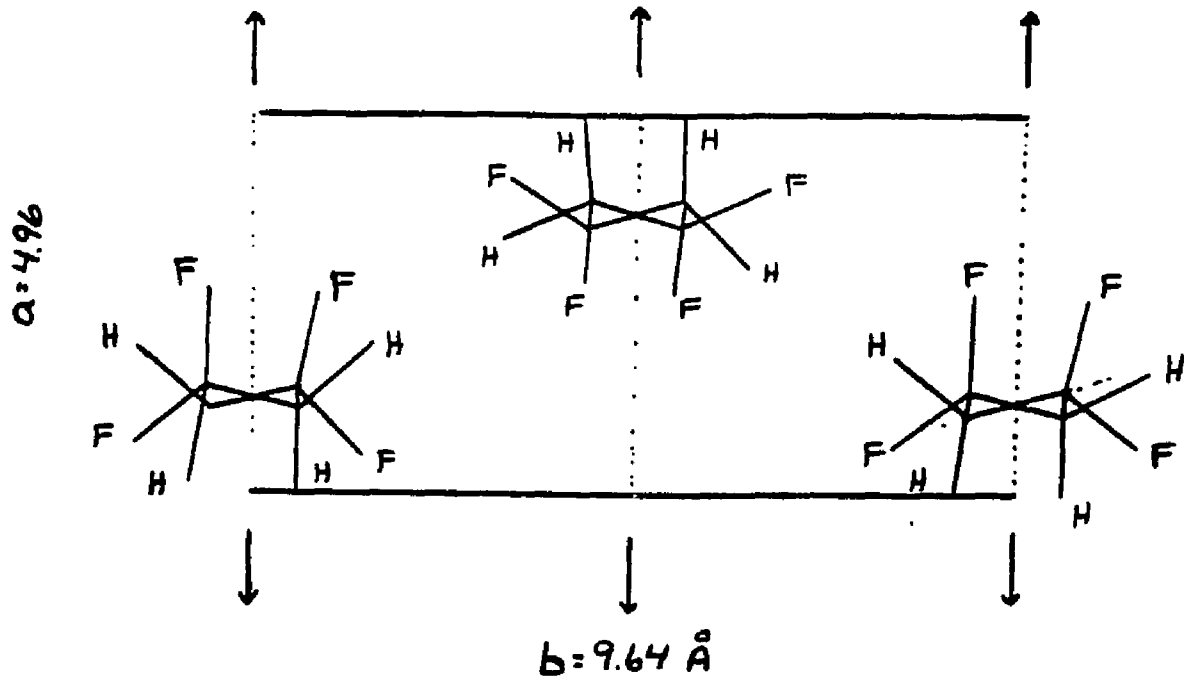

Figure 3.1 : Unit cell of α–PVF_2.
Note the antiparallel packing of dipole moment vectors.

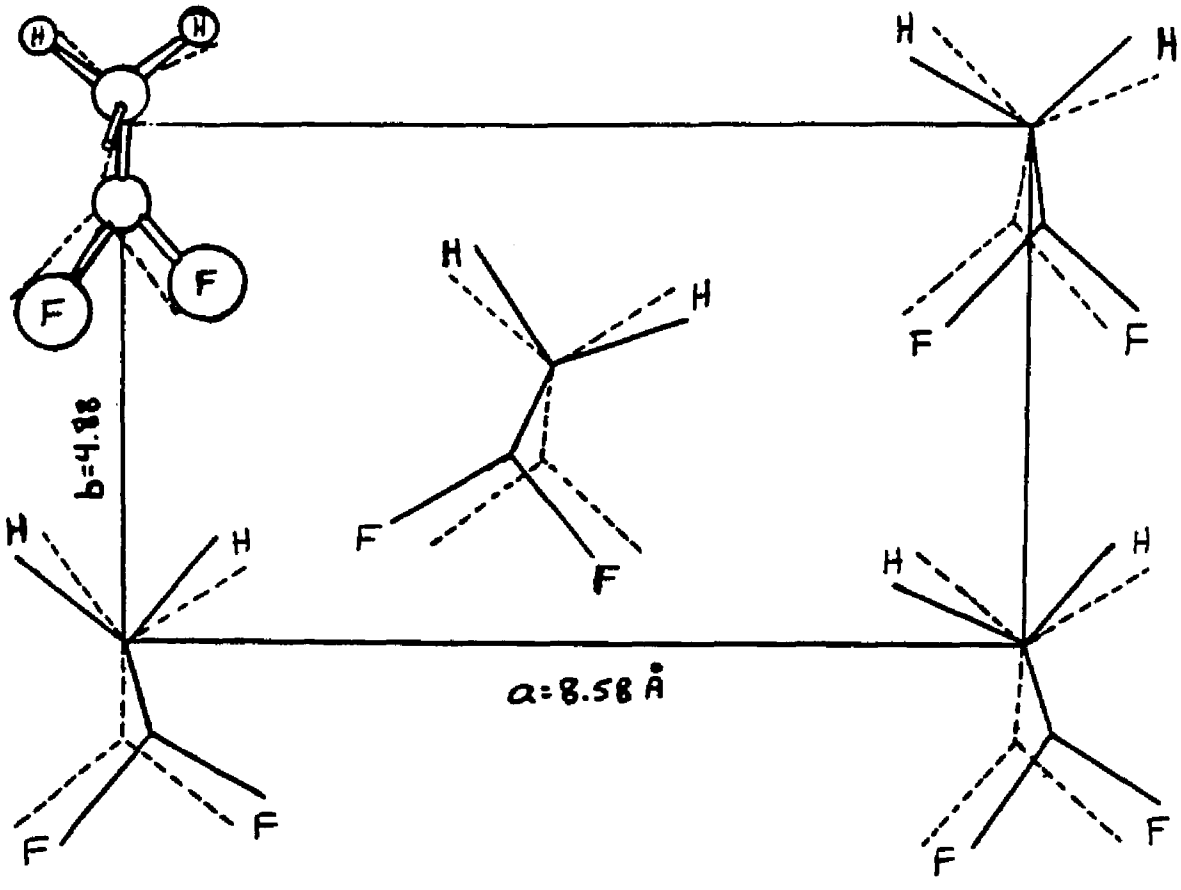

Figure 3.2 : Unit cell of β–PVF_2.
Note the parallel alignment of the dipole moment vectors.

electron diffraction, and infrared spectroscopy, as well as our own NMR results confirm chain axis alignment along the stretch axis.[1] A simple minded model has the crystallites suspended in a matrix of amorphous chains, with the crystallites attached to each other by connecting chains.[6,56] When the film is stretched, the chains exert tension along the c-axes in the crystallites, thereby elongating the crystallites along the c-axis.[1,6,56] The elongation is accompanied by the rotation of carbon-carbon bonds along the molecular backbone. The α to β transition is then simply described as a rotation of *cis* to *trans* configuration about every other bond.[1]

The crystalline component of the copolymer PVF_2–F_4E occurs in the $\mathcal{B}$ phase structure directly from the melt.[1,24,31,57] The monomer units CF_4 occur every 5 or 6 monomer lengths on the PVF_2 chain.[1] The reason that the copolymer blend forms into the β phase directly from the melt is thought to be due to steric effects associated with the van der Waals radii of fluorine (1.35 ang.) and hydrogen (1.2 ang.).[1] We note that if a monomer unit in the PVF_2 β-structure was reversed by 180°, this would actually relieve some of the stress on the fluorine side of the chain due to the nearly overlapping van der Waals radii of the fluorines.[1] But a similar reversal in the α phase would in fact create more strain because it would put the fluorines even closer together (.4 ang.) than the sum of their van der Waals radii.[1] So the lowest energy conformation for the copolymer form is the β phase. We note that the copolymer still has randomly oriented b-axes and consequently shows no electrical activity until it is poled.[1] The electrical properties of the copolymer are the same as the homopolymer,[1] so the discussion to follow pertains to both materials. We add that the PVF_2 monomer units of the copolymer blends were deuterated in the following experiments.

3.2.3 Electrical Properties

The electrical properties of PVF_2, piezoelectricity and pyroelectricity, are direct consequences of its ferroelectric nature.[1] A material is piezoelectric if a mechanical deformation induces a change in the macroscopic polarization.[1] Pyroelectrical activity is characterized by a change in polarization due to a change in temperature.[1] Though some theories have suggested that the trapping of real charges during the poling process might be responsible for the electrical activity,[4] the most widely held view is that PVF_2 is a ferroelectric material: a material that contains electrically polar crystals giving rise to a macroscopic polarization that can be reversed by application of an electric field. The reorientation process however is still not clearly understood.[1,4,8,14,16,20,29,32]

3.3 Polarization Theories

Several reorientation theories have been proposed to explain the polarization behavior at the microscopic level.[1,26,29] One of the first models proposed suggested a 180° rotation of dipoles about the chain axis via a *kink* propagation down the chain.[1] But recent calculations show that such a reorientation process would take substantially longer than is experimentally seen.[1,28]

A more plausible model which is consistent with the pseudohexagonal packing of the molecular chains, suggests that the reorientation of the dipolar monomer unit takes place in 60° increments.[1,26,29] The model is supported by results from x-ray experiments on rolled, uniaxially stretched films.[15,16] In these experiments the total scattering intensity was measured as a function of the angle between the scattering plane and the direction normal to the film. Both poled and nonpoled samples were investigated. The reflected intensity showed an angular dependence in poled films which was not evident in the unpoled material. The reflected intensity varied periodically every 60°. It was concluded that the poling process does reorient the molecular dipoles of the unit cells. A 6-site potential well model was used to calculate an angular distribution function for dipole orientation about the c-axis as a function of applied electric field.[15] A theoretical value for the macroscopic polarization was calculated

using the distribution function and a fit to the x-ray data on poled films. The theoretical value was in good agreement with the experimentally measured value.[15] A similar 6-site potential well cooperative model has yielded theoretical hysteresis curves similar to experimentally observed hysteresis plots.[26,56]

Another experiment supporting dipole reorientation utilizes infrared spectroscopy.[20] In these experiments, infrared transmittance through the film at 512 cm^{-1} and 446 cm^{-1} show hysteresis type behavior as a function of the applied electric field. The transition moment at 512 cm^{-1} is oriented along the dipole moment of the CF_2 dipole. The transition moment at 446 cm^{-1} is perpendicular to the dipole moment. Both transitions are due to CF stretching motion . As the dipoles are reoriented by an applied electric field, the infrared absorption varies in magnitude as the transition moments are reoriented from parallel to perpendicular with respect to the film surface. It should be noted that the variation between maximum and minimum transmission is only about 7 % .

In conclusion, experimental evidence clearly shows that the application of large electric fields induces dipolar reorientation in PVF_2 films. The current view is that the piezo-pyro electrical properties characterizing PVF_2 after it has been poled are direct consequences of induced dipolar alignment due to the reorientation of the molecules and the creation of polarized domains.[1] But it is not conclusive as to how and to what extent these reorientations take place. This work hopes to address these questions in a more conclusive manner.

Chapter IV

NMR THEORY

Preface

A short and concise review of the fundamental NMR interactions pertinent to the following experiments are presented. The discussion will follow the general format presented by Abragam.[33] Other references used include C.P. Slichter[34] and a treatise on quadrupolar interactions by Cohen and Reif.[46]

4.0 Zeeman Interaction

The nucleus possesses a total magnetic moment μ and a total spin angular momentum J. They are proportional to each other and the proportionality constant is a scalar, defined as the *gyromagnetic ratio* , γ :[33]

$$\mu = \gamma \mathbf{J}.$$

We also define a dimensionless angular momentum operator I by

$$\mathbf{J} = \hbar \mathbf{I}.$$

The application of a large magnetic field H produces a Zeeman interaction with the nucleus and the Hamiltonian is given by

$$H = -\boldsymbol{\mu} \cdot \mathbf{H}.$$

If the field H is taken to be along the z axis, the Hamiltonian becomes

$$H = -\gamma \hbar H_o I_z.$$

The allowed energies are given by[34]

$$E = -\gamma \hbar H_o m \qquad m = I, I-1, , , -I.$$

Transitions of $\Delta m = \pm 1$ (the magnetic dipole selection rule) between the different energy levels are induced by a time dependent interaction of angular frequency ω, where

$$\omega = \gamma H_o.$$

4.0.1 Electric Quadrupole Interaction

Nuclei with spin I > 1/2 have an electric quadrupole moment due to a nonspherical charge distribution within the nucleus itself.[34] This nonspherical charge distribution interacts with electric field gradients (EFG) at the nuclear site resulting in an orientationally dependent electrostatic interaction. The Hamiltonian is given by[34,46]

$$H_Q = \frac{eQ}{4I(2I-1)} [V_{zz}(3I_z^2 - I^2) + (V_{xx} - V_{yy})(I_x^2 - I_y^2)]. \quad (4.1)$$

Q is called the *quadrupole moment* of the nucleus, e is the proton charge, and V_{zz}, V_{xx}, and V_{yy} are the second partial derivatives of the potential at the nuclear site due to external charges. Equation 4.1 shows that only two parameters are needed to characterize the derivatives of the potential, V_{zz}, and $V_{xx} - V_{yy}$. **q** and η, referred to as the *field gradient* and the *asymmetry parameter* respectively, are commonly defined by the equations :[34]

$$eq = V_{zz}$$

$$\eta = \frac{V_{xx} - V_{yy}}{V_{zz}} .$$

We can then rewrite the quadrupolar Hamiltonian as

$$H_Q = \frac{e^2qQ}{4I(2I-1)} [(3I_z^2 - I^2) + \eta(I_x^2 - I_y^2)]. \quad (4.2)$$

The potential V at the site of the nucleus is due to external charges, i.e., orbiting electrons or other nuclei. Since V_{zz} has a r^{-3} radial dependence from point charges, the dominant EFGs are due the electrons closest to the nucleus. An exception to this would arise when there is a closed electron shell, then the charge distribution is spherically symmetric and there is no quadrupole coupling due to the atomic electron structure. Different types of atomic bonds give rise to different symmetries of charge distribution and hence affect the magnitude and orientational properties of the quadrupolar interaction. In many cases it is a good approximation to assume axial symmetry for the charge distribution near the nucleus. η is then set to zero in Eq. 4.2.

4.0.2 Quadrupole Perturbation to a Strong Zeeman Interaction

Now we will consider the specific case of a quadrupole interaction in the presence of a large Zeeman interaction. The quadrupole interaction then becomes a perturbation to the Zeeman interaction. Assuming axial symmetry, the Hamiltonian can be written as :[34,46]

$$H = -\gamma\hbar I I_0 I_z + e^2 q \frac{Q}{4I(2I-1)} \frac{(3\cos^2\theta - 1)}{2} [3I_z^2 - I(I+1)]. \qquad (4.3)$$

where θ is the angle between the magnetic field H_0 and the unique principal axis of the EFG. For the specific case of spin 1, the different energy levels become :

$$\begin{aligned} E_{-1} &= \omega_0\hbar + e^2 q \frac{Q}{4} P_2(\cos\theta) \\ E_0 &= -e^2 q \frac{Q}{2} P_2(\cos\theta) \\ E_{+1} &= -\omega_0\hbar + e^2 q \frac{Q}{4} P_2(\cos\theta) \end{aligned} \qquad (4.4)$$

where

$$P_2(\cos\theta) = \frac{3\cos^2\theta - 1}{2}$$

is the second Legendre polynomial. The NMR transition frequency with respect to the center resonance ω_0 becomes

$$\omega = \omega_0 \pm \omega_Q P_2(\cos\theta) \qquad (4.5)$$

where

$$\omega_Q \equiv \frac{3e^2 qQ}{4\hbar}.$$

The plus and minus refer to the $E_0 \rightarrow E_{-1}$ and $E_{+1} \rightarrow E_0$ transitions respectively.

The effect of the quadrupole interaction on the Zeeman splittings is shown in figure 4.1.. Two characteristics of the perturbation should be noted. First, the shift of the +m and -m levels are the same. Second and most importantly, the magnitude of the splittings are orientationally dependent. Spectral absorption in the NMR line will occur at different frequencies for different values of $P_2(\cos\theta)$, i.e., different orientations of the EFG unique principal axis with respect to the magnetic field H_0. In the specific case (as applies here) where the EFG is due to intramolecular charge

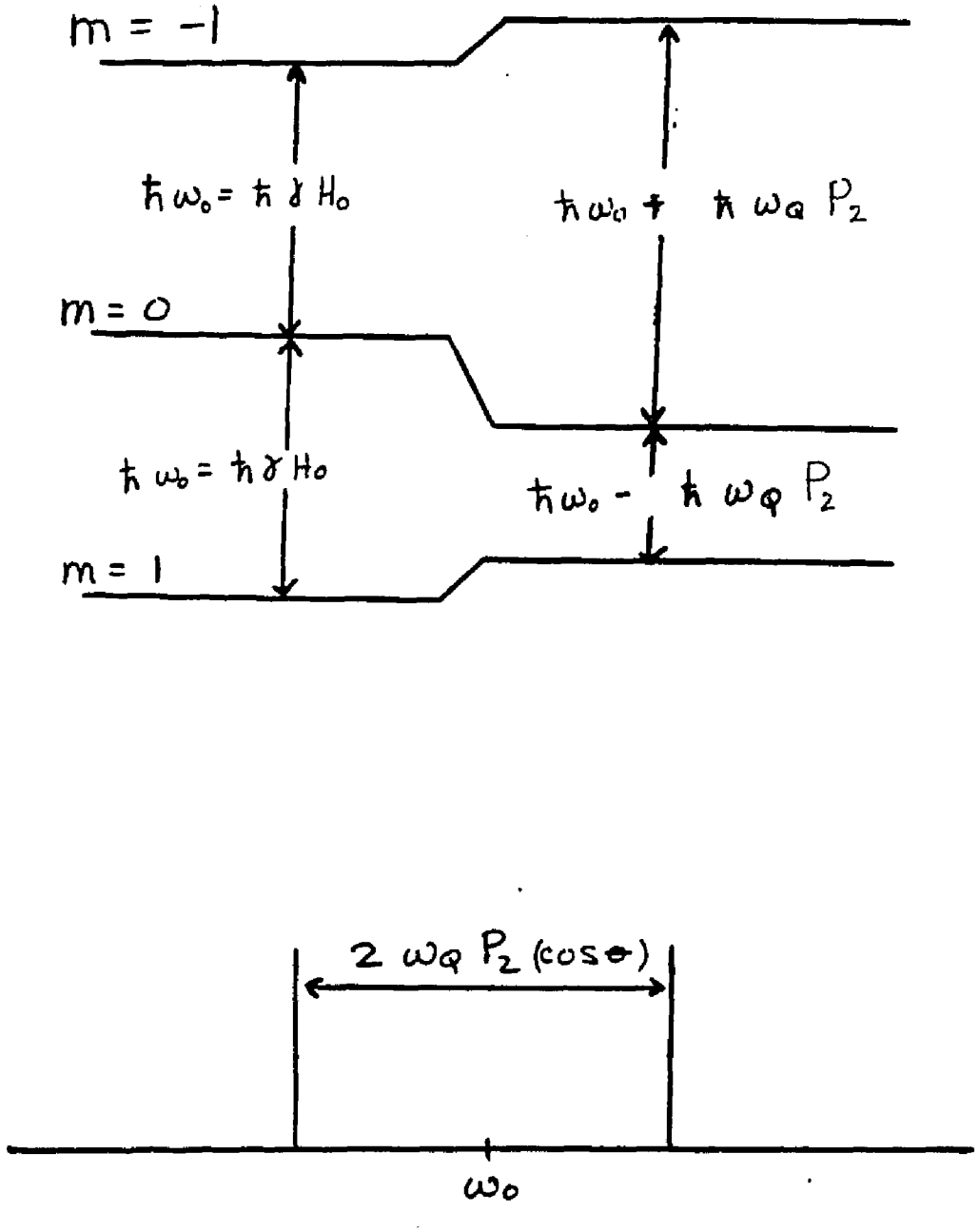

Figure 4.1 : Quadrupolar perturbation to the Zeeman interaction and the orientationally dependent splitting.

distribution and the unique principal axis is stationary in the reference frame of the molecule, the line shape can provide a quantitative measure of the orientational properties of the molecule at the microscopic level.

4.1 Line Shapes

As mentioned above, the EFGs are due to both the local charges (orbiting electrons) and the neighboring nuclei in the molecule.[34] It commonly occurs that the EFG's unique principal axis is collinear with a specific bond axis involving the resonating nucleus.[34] This is the case with the carbon-deuterium bond where the sp^3 hybridized bond results in an axially symmetric EFG with the unique principal axis of the EFG tensor lying along the bond axis. In this case $\eta = 0$ and the bond axis and the symmetry axis of the EFG tensor are one and the same. So in the discussion to follow, the quadrupole interaction will be discussed in terms of the angle between the C-D bond axis and the magnetic field.

The NMR frequency is a function of the angle between the bond axis and the magnetic field. In general, the bond axes are oriented over a range of angles, depending upon the physical problem being addressed. So in order to calculate the spectrum, we define an orientational probability density function $P(\Omega)$, $\Omega \equiv (\theta,\phi)$, that characterizes the orientational distribution of C-D bond directions. $P(\Omega)\, d\Omega$ is the probability that a C-D bond axis lies in the incremental solid angle $d\Omega$ centered around the solid angle Ω. This is easy to see pictorially on a unit sphere. We choose the north pole to lie along the magnetic field. We represent the C-D bond as a vector whose tip falls on the unit sphere at some angle $\Omega \equiv (\theta,\phi)$. Then $P(\Omega)\, d\Omega$ is then the number of points lying on the unit sphere in the solid area $d\Omega \equiv d(\cos\theta)d\phi$, about the solid angle Ω.

In the discussion above, we have picked the north pole to lie along the magnetic field. This is an arbitrary choice which simplifies the expression for the quadrupolar interaction. θ in Eq. 4.5 and θ in $P(\Omega)$ above are identical and the NMR frequency is degenerate for all ϕ. If we had not picked the unique axis to lie along H_o, but some other direction, say along the crystalline axis of a single crystal, it would be necessary to take the dot product between the vector H_o and each bond vector to get the orien-

tational dependence of the quadrupole interaction, i.e., the $\cos^2(\theta)$ term. Then, the interaction would depend upon two different angles, θ' and ϕ'. We address this issue to forewarn the reader that in section 6.0, the north pole axis will be defined by the stretch direction of PVF_2 and not the magnetic field. Hence the definitions of the angles θ and ϕ will neccessarily be different than in the above discussion. In the next section we will assume three different orientational distribution functions $P(\Omega)$ for the bond axes and calculate the NMR spectrum for each. We also choose H_o to point along the north pole to simplify the equations and to make the examples more straightforward.

4.1.1. Single Crystal

Consider a hypothetical single crystal containing C-D bonds which are all oriented at the same angle with respect to an arbitrary crystalline axis. The crystal itself is oriented at some angle with respect to the magnetic field H_o. Then all the bonds make an identical angle with H_o, .eg. θ_{sc}. The orientational parameter $P_2(\cos\theta)$ has the same value for all the spins

$$P_2(\cos\theta)=\frac{3\cos^2\theta_{sc}-1}{2}\ . \qquad 4.6$$

For a spin 1 system, we have two resonance frequencies corresponding to the

$$E_0 \rightarrow E_{-1} \text{ and } E_{+1} \rightarrow E_0$$

transitions. The resonance frequencies are given by Eq.4.5 :

$$\omega_{sc}^{\pm}=\omega_o \pm \omega_Q P_2(\cos\theta_{sc})$$

The NMR spectrum of the single crystal contains two lines , one shifted up in frequency and the other line down in frequency. The splitting is given by $2\times\omega_Q P_2(\cos\theta_{sc})$ and is centered about ω_o (fig. 4.1).

The condition that all bonds make an identical angle to H_o is equivalent to saying that $P(\Omega)$ is a delta function on our unit sphere, i.e., all the vector tips lie at one point on the sphere.

The most important thing to note is that the resonance frequency (or splitting) is a function of bond orientation. The orientational dependence of the resonance line

position is contained in the orientational parameter $P_2(\cos\theta)$ which ranges from +1 to -1/2 as θ is varied from 0° to 90°. As the single crystal is reoriented, the splitting varies according to a $\cos^2\theta$ function. If there exist other crystallites oriented at different angles with respect to the field, there will be more than one set of lines corresponding to different C-D bond orientations. In the limit of numerous randomly oriented crystallites, the NMR spectrum is called a *powder pattern* .[33-34,46,58]

4.1.2 Powder Pattern

A powder consists of numerous randomly oriented single crystals.[59] This gives rise to randomly oriented carbon-deuterium bonds. As before, we represent the bonds as vectors whose tips fall on the surface of the unit sphere. Randomly oriented bonds correspond to having randomly oriented vectors. It is equally likely to have the vector tips fall on one part of the sphere as on any other part of the unit sphere. The powder pattern then is characterized by a distribution that is constant over the sphere ($P(\Omega) = 1$ or $1/4\pi$). Choosing H_o along the north pole, each point corresponds to a definite relative orientation to the magnetic field and hence to a definite resonant frequency.[59] According to Eq. 4.5 the orientationally dependent frequency is a function of θ only;[59]

$$\omega^{\pm} = \omega_o \pm \omega_Q P_2(\cos\theta).$$

Using the equation above we draw curves of constant frequency on our unit sphere (figure 4.2).[15]

The NMR spectrum is the superposition of lines from all the nuclei from all the crystallites in the sample. For ease of calculation, we will consider only one of the transitions in our spin 1, three level system, $E_0 \rightarrow E_{-1}$. The intensity $I(\omega)$ of the spectrum when integrated over arbitrary limits ω_a to ω_b is proportional to the number of spins that lie in the interval $\omega_a \rightarrow \omega_b$.[59] This means that it is proportional to the area on the sphere between the curves of constant frequency ω_a and ω_b times the probability of finding a bond oriented between these curves :[59]

$$\int_{\omega_a}^{\omega_b} I(\omega)\,d\omega = \int_{\substack{\text{area between} \\ \omega=\omega_a \text{ and } \omega=\omega_b}} P(\Omega)\,d\Omega\,. \qquad 4.7$$

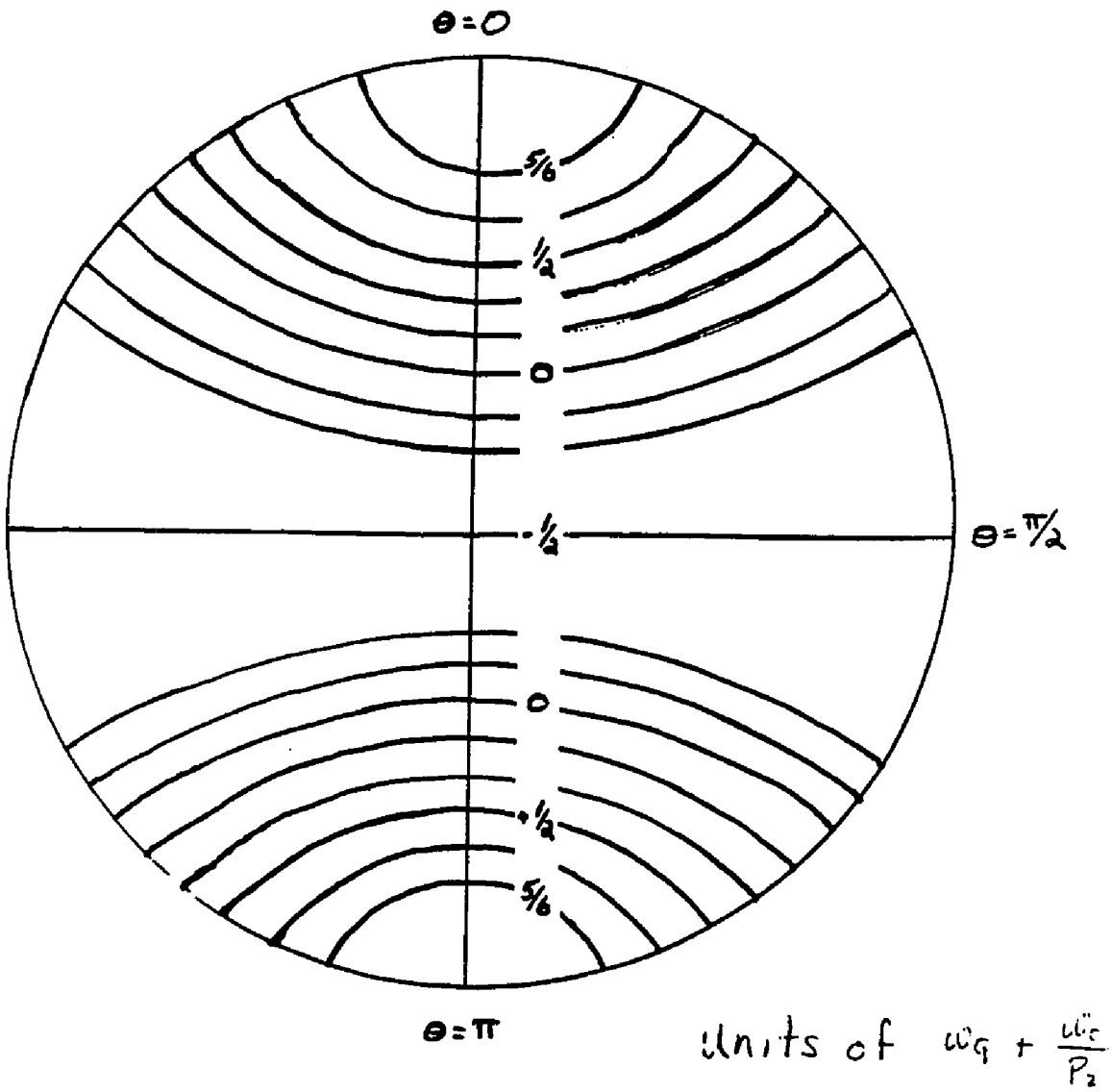

Figure 4.2 : Lines of constant ω on the unit sphere.

For a powder, $P(\Omega)$ is a constant over the entire sphere. After integrating over all ϕ we have :[59]

$$\int_{\omega_a}^{\omega_b} I(\omega)\,d\omega = N \int_{\substack{\text{area between} \\ \omega=\omega_a \text{ and } \omega=\omega_b}} \sin\theta\, d\theta \qquad 4.8$$

where N is a unimportant normalization factor. The integration over θ is performed using ω defined by Eq. 4.6 as the new integration variable. With

$$\omega = \omega_o + \omega_Q \frac{(3\cos^2\theta - 1)}{2}$$

as the new integration variable we have :

$$\int_{\omega_a}^{\omega_b} I(\omega)\,d(\omega) = \frac{N}{\omega_Q\sqrt{3}} \int_{\omega_a}^{\omega_b} \frac{d\omega}{\left[1+\frac{2}{\omega_Q}(\omega-\omega_o)\right]^{\frac{1}{2}}} \qquad 4.9$$

Since Eq.4.9 is valid for arbitrary values of ω_a and ω_b, the integrands can be equated:[59].

$$I(\omega) = \frac{N}{\sqrt{3}} \frac{1}{\left[\frac{2}{\omega_Q}(\omega-\omega_o)+1\right]^{\frac{1}{2}}} \qquad \omega_o - \frac{\omega_Q}{2} \le \omega \le \omega + 2\omega_Q \qquad 4.10$$

Figure 4.3 shows the NMR spectrum $I(\omega)$ for an isotropic powder. The intensity units are arbitrary. We see that the integrand diverges for $\omega \to \omega_o - \frac{\omega_Q}{2}$.

The above derivation has considered only one of the transitions for the spin 1, 3-level system. The complete spectrum is the sum of the line shapes obtained by considering both the $m = -1 \to 0$ and $0 \to +1$ transitions. We realize from the discussion in section 4.1 that we need only to sum the powder pattern in fig. 4.3 with its mirror image reflected about ω_o to obtain the entire spectrum. Figure 4.4 shows the entire line shape expected for our spin 1, 3-level system. The intensity units in both plots are

arbitrary.

4.1.3. Fiber pattern

The last general line shape we will discuss is the fiber pattern.[35,37,45,59] Let us consider the unit sphere with the bonds oriented with their vector tips distributed uniformly in ϕ but all lying on the equator. Instead of choosing the magnetic field oriented along the north pole, we now choose it to lie in the plane of the equator, $\theta_H = 90^\circ$. This is the orientational geometry that gives rise to the fiber pattern spectrum. It is called a fiber pattern because it is frequently seen in polymer materials that have been stretched creating alignment of molecular chains along the direction of the draw. If there was perfect alignment of chain axes along the stretch direction, all the bond vectors would lie in the equatorial plane of our unit sphere. We note this assumes that the bonds are oriented 90° to the chain axis. This corresponds to a delta function in $P(\theta)$ for $\theta = 90^\circ$. We assume the bonds are oriented uniformly in the plane. We mention that this not need be the case. In the next section in fact we will assign some orientational probability for the distribution of bonds in the plane about the stretch axis.

The spectrum for the fiber pattern geometry is then calculated by assuming a delta function for $P(\theta)$ peaked at 90°. In figures 4.5(a-j) we show a sequence of line shapes starting with the field oriented at 0^0. The bonds are oriented in a thin pancake about the equator. As the field is rotated down from $\theta_H = 0^\circ$ to $\theta_H = 90^\circ$, the single splitting eventually develops into the classic fiber pattern, figure 4.5j. These figures correspond to a uniform distribution in ϕ. In section 7.0 we will present more fiber patterns but they will have different functional forms for both the θ and ϕ distributions.

4.2 Experimental Techniques and Pulse Sequences

As was mentioned in chapter 3, PVF_2 and its copolymers exhibit ferroelectric properties which are thought to be due to the reorientation of electric dipoles in the unit cell. We have undertaken a line shape study of deuterated samples in order to examine the process of reorientation and to investigate to what extent dipole

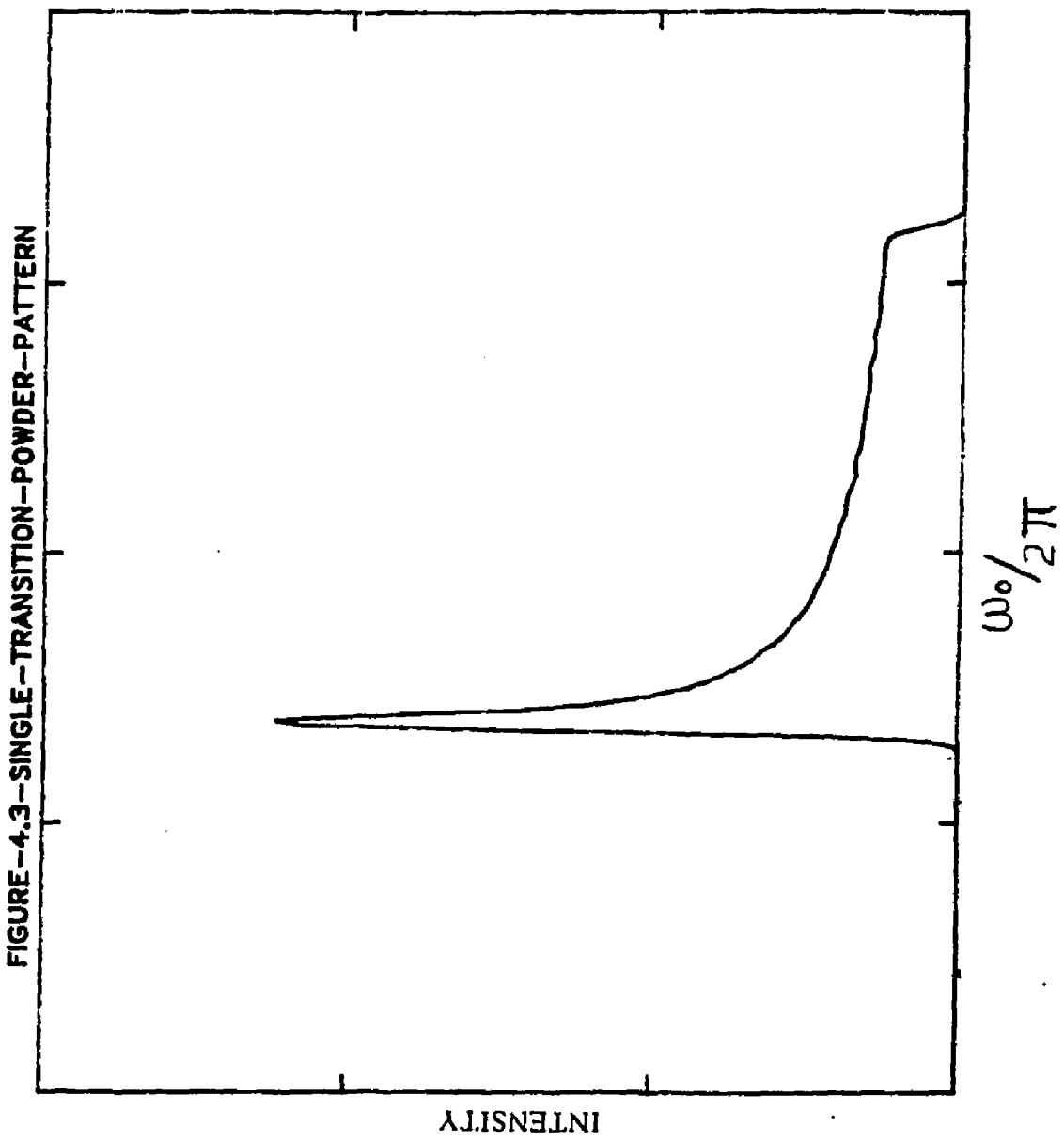

Figure 4.3 : The above spectrum is a simulated line shape which is calculated for the single NMR transition $m = 1 \rightarrow 0$ assuming randomly oriented bond vectors, i.e., a powder pattern. The maxiumum frequency width is approximately 164 Khz. The intensity is arbritrary.

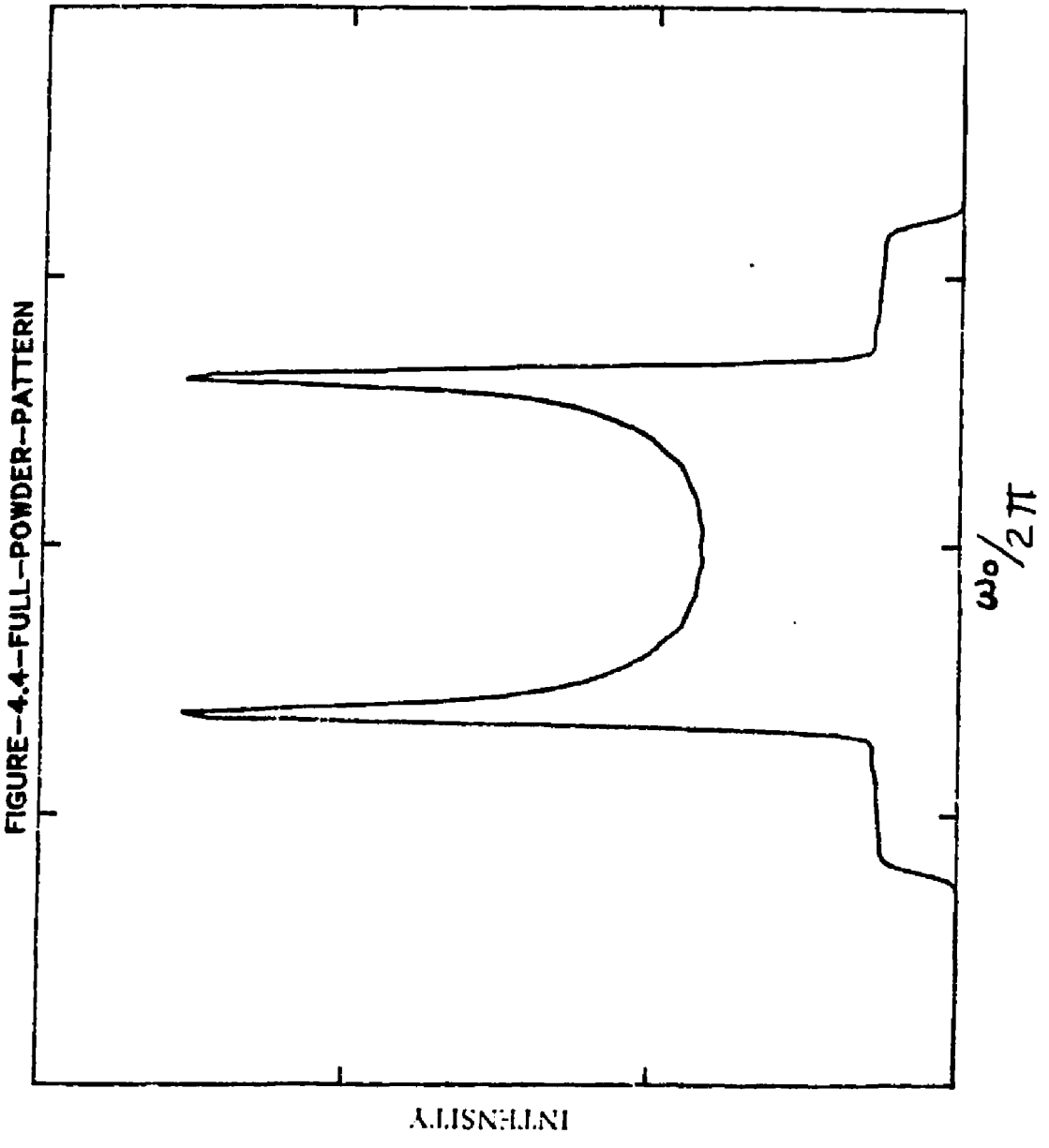

Figure 4.4 : The spectrum above is the symmetrized and summed version of the single transition spectra in fig.4.3. This spectra is the full powder pattern with a maximum splitting of ≈ 250 Khz. The intensity scale is arbritary.

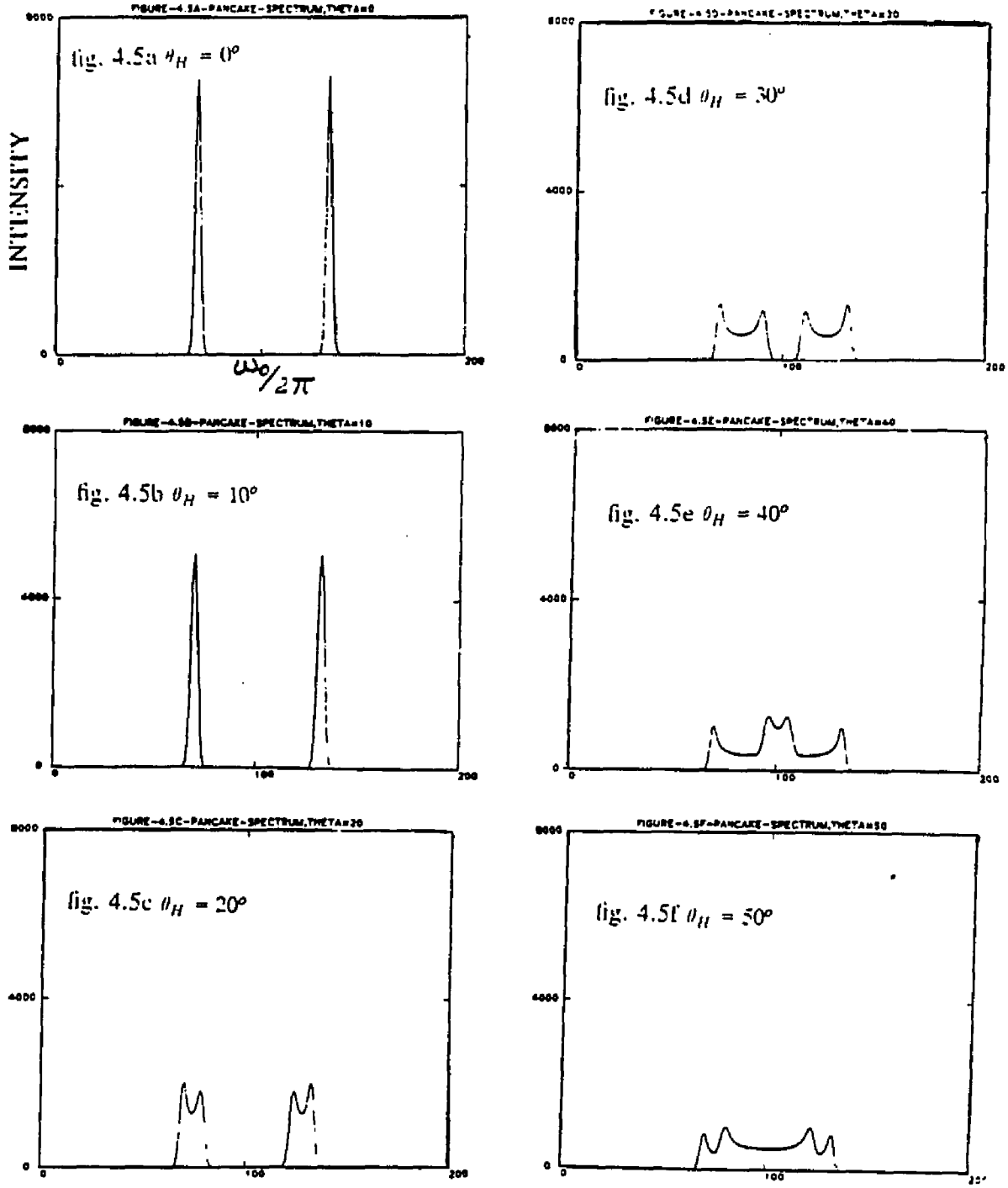

Figures 4.5(a-j) : Simualted line shapes calculated assuming a pancake distribution for the bond vectors about the equator.
The sequence of spectra start with $\theta_H = 0°$ in figure 4.5a and progresses to $\theta_H = 90°$ in figure 4.5j.

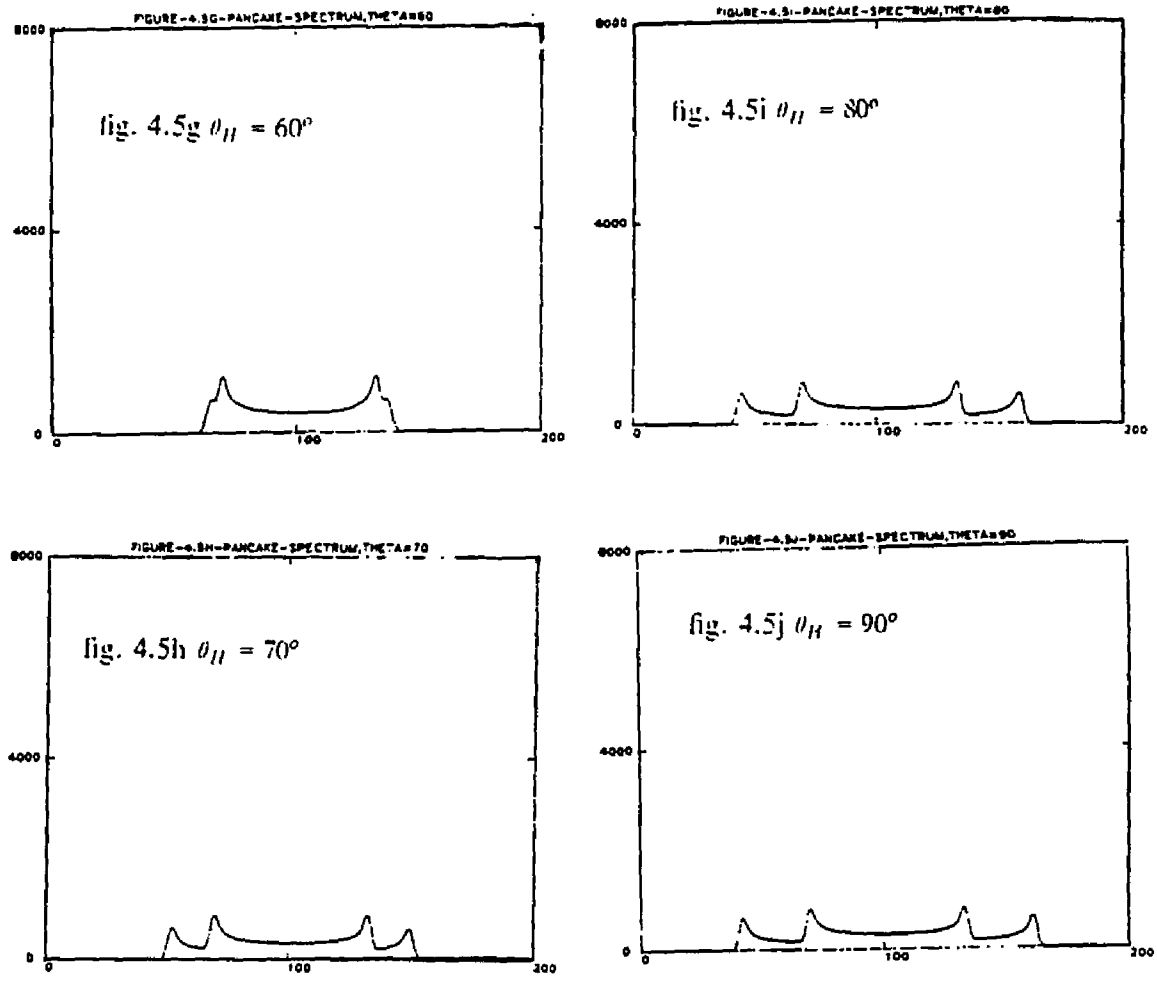

Figure 4.5 continued.

reorientation occurs. Both poled and unpoled samples of the homopolymer (PVF_2) and copolymer (PVF_2–F_4E) were examined at room temperature. The NMR pulse sequences will be described below followed by an analysis of experimental line shapes.

4.2.1 Pulse Sequences

The line shapes are derived from fast fourier transforms (FFT) of quadrupolar echoes.[37,41-42,44,60] The quadrupolar echo[37] pulse sequence involves two consecutive $\frac{\pi}{2}$ rf pulses phase shifted by 90^0 with respect to each other. The pulse sequence, $\frac{\pi}{2}_x - \tau - \frac{\pi}{2}_y - \tau -$ echo, contains two pulses separated by a waiting time τ which is of the order of 20 μseconds. The first pulse is phase inverted on odd cycles in order to subtract out any coherent noise in the received signal. The echo, which oscillates in sign with the phase of the first pulse, is multiplied by -1 on the odd cycle. When an even number of cycles are summed, the echoes will add and any coherent noise will be subtracted out.

The first pulse rotates the magnetization (at equilibrium along z-axis) into the x-y plane where it dephases due to the interaction of the nuclear electric quadrupole moment with local EFG's and spin-spin interactions. Dephasing in the transverse plane produces a free induction decay (FID) following the first pulse. The like-spin dipole-dipole interaction (deuterium-deuterium) and unlike-spin dipole-dipole interaction (deuterium-fluorine) cause dephasing but these are small compared to the quadrupole-EFG interactions.[33,42] The lines are inhomogeneously quadrupolar broadened.[36-37,42,45]

We can visualize the dephasing process in the following way. A spin situated in a molecule whose unique symmetry axis is at a specific angle to H_o has a different resonant frequency than another spin whose molecule is oriented at a different angle with respect to H_o. When these spins are rotated into the transverse plane, they will precess at their respective frequencies and dephase. If the molecules are static, the spins maintain their respective frequencies and the FID quickly decays in a time

comparable to the inverse of the rigid lattice line width (250 Khz). If the molecules are undergoing reorientations, the quadrupolar interactions and hence frequencies will change. In the extreme limit where the reorientations are very fast, all the spins will see the same average interaction and thus the same average frequency. In this case, the magnetization in the transverse plane will not dephase due to quadrupolar-EFG interactions.

The quadrupolar Hamiltonian can be divided into static secular and stochastic, time dependent contributions.[35] The dephasing due to the time dependent interactions cannot be "time reversed"; these interactions cause decay of the quadrupolar echo amplitude. The quadrupolar pulse sequence described above refocuses the static interactions, forming an echo.[35,42] The first pulse rotates the magnetization in the x-y plane where it dephases according to H_Q. After a waiting time τ, the second pulse is applied, phase shifted by 90°, effectively reversing the quadrupolar interaction and producing a quadrupolar echo. The echo can be thought of as two FIDs back to back. The magnetization increases along the appropriate direction in the transverse plane, goes through a maximum forming the peak of the echo and then dephases once again. This makes it easy to select the t=0 point of the FID at the top of the echo.

We mention that the experimental line shapes are artificially symmetrized. This entails replacing the imaginary portion in the time domain with zeroes.[44] That is, the quadruture channel of the data has been zeroed after the appropriate phasing has been performed. The line shapes were first inspected without the symmetrization process to insure that they were in fact symmetric about the center frequency ω_0. The purpose of symmetrizing was to increase the signal to noise ratio in the final spectra.

In addition to PVF_2 and PVF_2–F_4E line shapes, several runs were made on powder samples of deuterated biphenyl and polyethylene to investigate the bandwidth of the receiver section and the transmitter pulses. The FFT of quadrupolar echoes produced powder pattern line shapes which agree very well with a calculated powder pattern spectra. We especially note that the intensity in the wings of the experimental line shapes show no indication of instrumental reduction due to limited bandwidth of the receiver, probe, or rf pulses.

4.2.2 Short and Long T_1 Discrimination

When quadrupolar echoes were initially run on both the homo- and co-polymer samples, it was discovered that the amorphous and crystalline parts of the films had different longitudinal relaxation times, T_{1a} and T_{1c}. The amorphous component had a much shorter relaxation time, $T_{1a} \approx .02$ seconds, compared to the crystalline T_{1c}, which was of the order of 4 seconds. The NMR signals from the two different components were distinguished in the following way.

The separation of the amorphous and crystalline contributions was performed using short and long recycle times. Each quadrupole pulse sequence ($90_{\bar{x}x} - \tau - 90_y$) was preceded with a long saturation pulse (sat). The saturation pulse assures that the z-magnetization is initially zero every time the pulse sequence is initiated. The entire pulse sequence is then given by

$$\text{sat} - t - 90_{\bar{x}x} - \tau - 90_y$$

When the time t is set at 20 seconds, contributions from both the amorphous and crystalline components are collected in the echo since this is longer than either T_1. At shorter times (t = .1 sec.), however, the only contribution to the signal is from the amorphous component. The crystalline component is still saturated and does not contribute to the echo. So by varying the time t we can select a composite signal and an amorphous signal. By taking a series of scans with long t times and then the same number of scans with short t times, the two sets of scans can be subtracted from each other to isolate the crystalline contribution to the line shape. We note that the subtraction can be done in either the frequency or time domain. Both give identical results. The data presented here is subtracted in frequency domain.

Not only were the T_1's different for the two components but the line shapes of the amorphous and cystalline components were also different. The amorphous component of the polymer is made up of chains undergoing fast reorientations. Deuterium spins on these chains see a rapidly fluctuating quadrupole interaction due to the fast reorientations of chain segments. As discussed above, these spins see an averaged quadrupole interaction and hence the spins in the amorphous component produce a motionally narrowed NMR spectrum.[36-42] The chains in the crystalline component on

the other hand do not under go fast reorientations and hence the deuterium in the crystalline region see relatively static quadrupolar interactions. The NMR line from these spins are fully quadrupolar-broadened. It was possible then to distinguish the two different contributions to the composite NMR line by visual examination. The motionally narrowed amorphous component showed up as a narrowed hump in the NMR spectrum symmetrically positioned about ω_o.[36,38,40] The crystalline component gave rise to a fully broadened pattern. As expected, the subtracted "crystalline only" spectra did not contain the feature associated with the amorphous component.

The line shapes of both deuterated homopolymer and copolymer samples have been studied as a function of film orientation with respect to the static magnetic field H_o. We will discuss the line shapes of stretched samples (poled and poled) and then compare these results to simulated line shapes.

Figures 4.6(a,b) show the typical geometry of the experiments performed on both the poled and unpoled stretched PVF_2 and PVF_2–F_4E samples. In the first set of experiments, the sample stretch axis (3) was initially situated parallel to the magnetic field and then the film was rotated in 10^o increments about the 1 axis until the magnetic field was along the 2 axis. The magnetic field was always in the 2-3 plane during the rotation.

In the second set of experiments, the field was initially parallel to the 1 axis of the film and the film was rotated in 10^o increments about the stretch direction (3 axis) until the field was parallel to the 2 axis.

At each orientation, 500 scans were averaged together using the long recycle sequence outlined above. This was followed by 500 scans using the short recycle sequence.

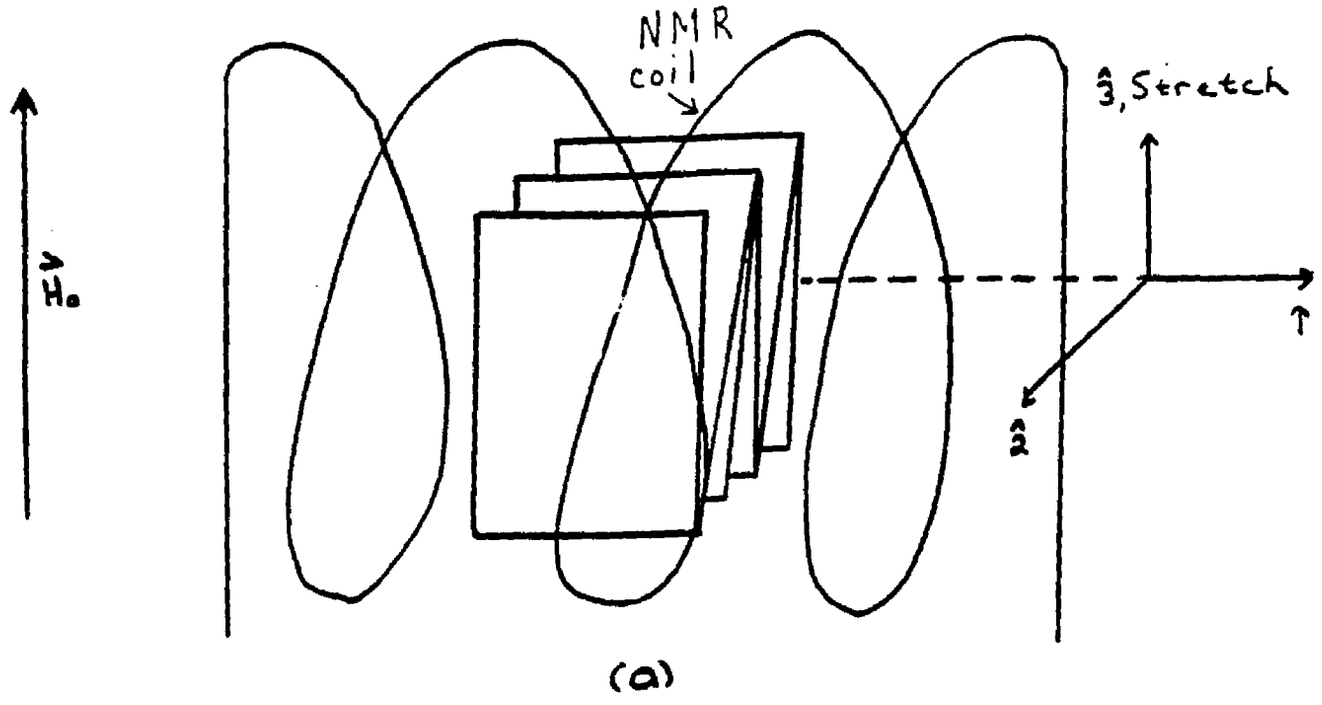

Figure 4.6(a-b) : Orientations of experimental films in the NMR coil.

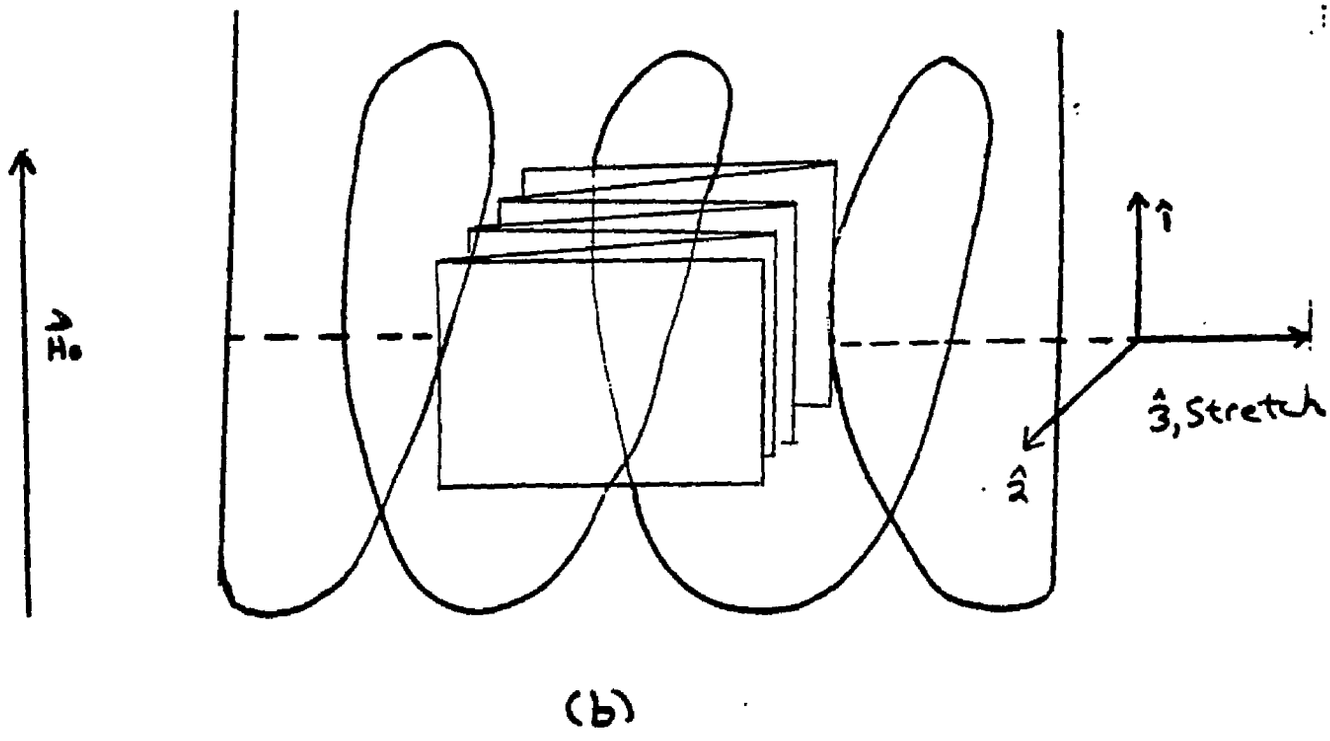

Chapter V

COMPUTER SIMULATIONS

5.0 Simulation Models

Computer simulations of the quadrupolar broadened deuterium NMR lines were made using two different models. Both simulations were based on the same method for calculating the NMR spectra. The line shapes can be calculated analytically but this can be very difficult.[37,42] A simpler approach is to do the direct calculation of the quadrupolar splitting for a given magnetic field direction, summing the partial spectra over a distribution of bond orientations. A given distribution of C-D bond orientations will then correspond to a certain density distribution of discrete points over the unit sphere. Once the orientation of the magnetic field is specified (by polar co-ordinates θ_H,ϕ_H), the quadrupolar splitting is calculated for each point on the sphere. The intensity of the spectrum for a certain splitting value is directly proportional to the number of points on the sphere that give rise to that splitting. By comparison of experimental spectra to simulated line shapes using different density distributions, we can characterize the actual distribution of bond orientations in the experimental samples. In both simulations, the stretch axis was defined to lie along the north pole of the unit sphere. Polar co-ordinates are measured with respect to the stretch direction for both the poled and unpoled samples.

5.0.1. First Simulation Model

In the first set of simulations, approximately 16,000 points were chosen on the unit sphere by specifying 90 θ points (0 to 180 every 2°) and 360 ϕ points (0 to 360 every 1°) (see fig. 5.1). We note that this distribution does not cover the unit sphere with an even density of points. The north and south poles are more densely covered (i.e. in points per unit of surface area) than the region on the equator. To correct for

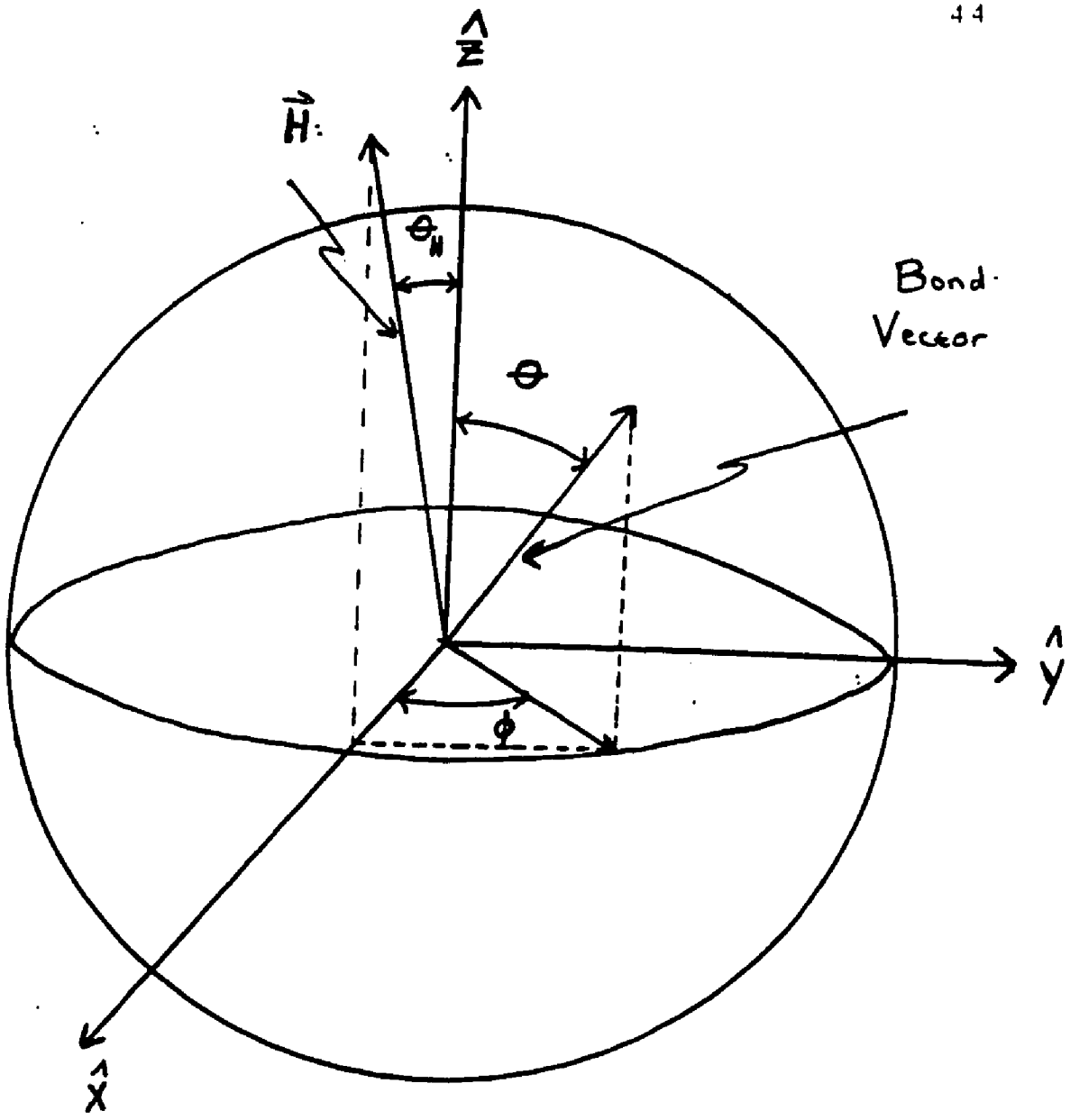

Figure 5.1 : First simulation model geometry.

this, an area weighting function (awf) was used to properly weight the intensity of each point on the sphere. The function awf is given by $\frac{\cos(\theta_1)-\cos(\theta_2)}{\text{no. of } \phi\text{'s}}$, the area of the band about θ divided by the number of ϕ's in that band. The intensity of each point was therefore corrected so that it represented unit intensity per unit area on the sphere. The next step involved assuming various orientational density distribution functions in θ and ϕ, given by $\mathbf{f}(\theta)$ and $\mathbf{g}(\phi)$ for the bond orientations. The total intensity for a point (θ,ϕ) is then given by the product, $\mathbf{I}(\theta,\phi) = \mathbf{awf}(\theta) \times \mathbf{f}(\theta) \times \mathbf{g}(\phi)$. We note that $\mathbf{f}(\theta) = 1$ and $\mathbf{g}(\phi) = 1$ corresponds to the case of an isotropic powder. The final line shape is developed for various orientations of the magnetic field by calculating the quadrupolar splitting for each point on the sphere. The quadrupolar interaction gives the corresponding frequency position in the NMR line. Once the position in the frequency spectrum is known, the appropriate $\mathbf{I}(\theta,\phi)$ intensity is assigned to that position in the line. This is performed for all points on the sphere and the intensities are summed.

The above program produces a stick spectrum for only one of the NMR transitions (for $m = +1 \rightarrow 0$ specifically). The entire NMR spectrum is a superposition of both the $m = +1 \rightarrow 0$ and $0 \rightarrow -1$ transitions. The entire spectrum was obtained by symmetrizing the line shape from a single transition about the center resonant frequency, ω_o. To realistically simulate the experimental data, the simulated spectra were gaussian broadened by convolution. Every point in each spectrum was replaced with a gaussian (FWHM = 6 kHz) whose height was equal to the intensity at that point. The chosen amount of broadening was estimated from the experimental data. The homogeneous broadening is due to the dipole-dipole interactions of the deuterium nuclei with each other and the ^{19}F nuclei.

5.0.2 Second Simulation Model

The second set of simulations used a different approach to generate the bond orientation distribution. Instead of assuming an orientational distribution for the bond directions themselves, the orientation of the chain axes about the north pole was specified. This model produces more closely the physics of the stretched samples (see

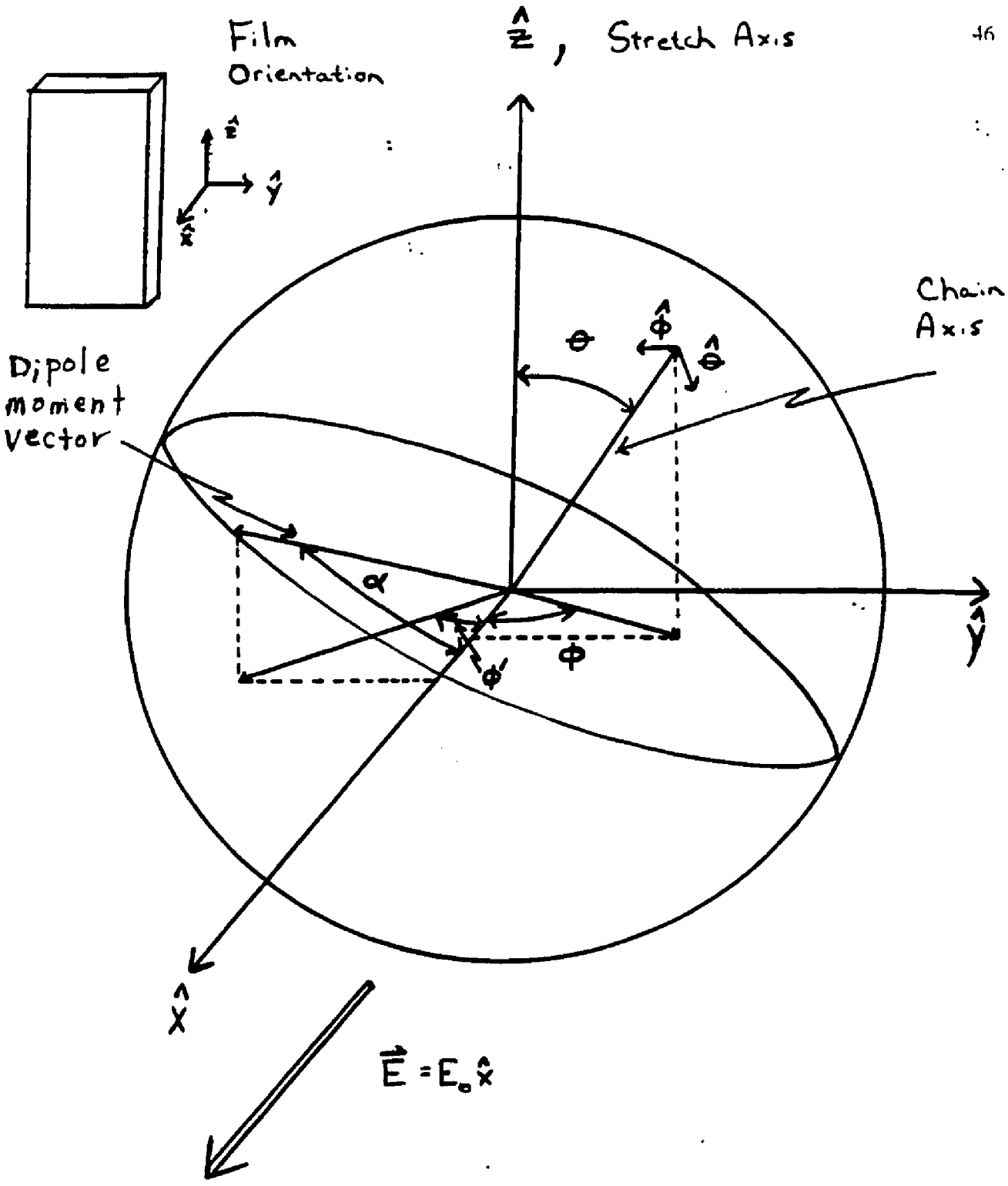

Figure 5.2 : Second simulation model geometry.

fig 5.2). As was mentioned before, when the polymer is stretched the chain axes are aligned in the stretch direction. The C-D bonds and the dipole moment vectors are perpendicular to the chain axis and can be thought to form a pancake about the chain axis. In this model it is necessary to specify three angles to uniquely define the geometry. The orientation of the chain axis is given by θ and ϕ and a final angle α specifies the orientation of the the dipole moment vector in the pancake with respect to angle $\phi = 0$. We recall that the dipole moment vector lies along the vectorial sum of the two C-D bonds and that the angle between the bonds is 109.5°. We incorporate this into the model by defining the vector oriented at α in the pancake as the direction of the dipole moment. The bonds are then at $\alpha \pm 54.75°$. As in the first simulation, θ and ϕ are incremented in 1° degree steps. α is incremented in 1° steps from 0° to 360°. As before, the intensity of the points on the unit sphere specifying the chain axis orientation is multiplied by the area weighting function so all orientations are properly weighted.

The orientational distribution function $f(\theta)$ now refers to the probability per unit solid angle of finding a chain axis oriented at θ about the north pole, i.e., about the stretch direction. Perfect alignment of the chain axis would correspond to having all the bonds lying on the equator. $f(\theta)$ in this case would be a delta function at the north pole. In the next section, we will consider a few different functional forms for f and compare this with the experimental line shapes. Given the chain axis orientation (θ,ϕ) and the angle α, we can calculate the angle of orientation for the corresponding dipole moment vector and C-D bonds in the pancake. Inspection of the quadrupolar interaction shows that only the direction cosines of the bonds with x,y,z axes are needed to determine the frequency splittings. Once we have the appropriate splitting, we assign the calculated spectral weight to that position in the line consistent with the probability function chosen.

We note that even though both of the models above reproduce the major features of the experimental line shapes, the second model imitates the physical system more closely. We can see this by considering for both models a gaussian distribution for $f(\theta)$. In the first model, a gaussian distribution for bond orientations would

would correspond to having the bonds peaked in intensity on the equator (this is for nearly ideal alignment of chain axes). The density of points would fall off uniformly according to the gaussian function as one moves away from the equator. In the second model however a gaussian distribution for the chain axes does not necessarily yield a gaussian distribution of bonds about the equator. Consider just one chain axis oriented at $\theta = 5^{\circ}$ with $\phi = 0^{\circ}$. The corresponding pancake tilted from the equator by 5° contains C-D bond axes from $\theta = 85^{\circ}$ to 90°, depending on the value of ϕ. Thus a specific chain orientation θ gives a distribution of bond orientations in θ; a gaussian distribution of chain axes orientations will give a more complicated distribution of bond orientations θ. Hence, the two models give different results. But the difference is slight when the sum over many ϕ's is taken. The following discussion will refer to the second model since it is the more physical, but it should be kept in mind that the first model gives almost indistinguishable results.

Simulating the effect of poling is not as straightforward as reproducing the stretching effect. In the simulation above, we assumed the dipole moment vectors to be lying in the pancake with their orientation angles given by α. The C-D bond vectors are located at $\alpha \pm 54.75^{\circ}$. We define the polarization axis to be along the x-axis (see figure 5.2); this simulates the application of a dc electric field perpendicular to the plane of the film and orthogonal to the stretch direction. The azimuthal co-ordinate of the dipole moment vector is defined to be ϕ'. The function $g(\phi')$ now refers to the probability of finding the x-y plane projection of the polarization vector oriented at some angle ϕ' with respect to the applied electric field. Note that g should be unity for a uniform distribution of dipole moment vectors about the chain axis.

To combine the effects of stretching and poling, the total intensity is just given by the product of f with g ; I(stretched,poled)= $\mathbf{awf}(\theta,\phi) \times \mathbf{f}(\theta) \times \mathbf{g}(\phi')$. Several different functional forms were tried for both f and g. These results will be presented below along with a comparison to our experimental results.

Chapter VI

EXPERIMENTAL RESULTS AND DISCUSSION

6.0 Experimental Results on Chain Axis Orientations

We begin by considering stretched samples of both homopolymer and copolymer films. For the convenience of the reader, figures 6.1 through 6.10 have been gathered together at the end of the text. We first draw attention to the general features of the experimental line shapes in figures 6.1(a-j), and 6.2(a-j). These are from the runs on the poled homopolymer and unpoled copolymer films respectively. The figure in both sequences has the magnetic field oriented along the stretch direction $\theta_H = 0^\circ$. The sequence progresses with the field eventually oriented perpendicular to the stretch direction. In both sets of data a single splitting occurs when $\theta_H = 0^\circ$. We deduce from this feature that virtually all the C-D bonds have the same value of $P_2(\cos(\theta))$ corresponding to $\theta \approx 90^\circ$. We recall that the splitting is given by Eq.4.5 :

$$\omega^{\pm} = \omega_o \pm \omega_Q P_2(\cos\theta). \qquad 4.5$$

As the field is rotated away from the stretch direction, the intensity in the peaks is redistributed and eventually at $\theta_H = 90^\circ$ the line shapes exhibit the features of a classical fiber pattern (section (4.1.3)).

These are the general features we would expect in a sample where the C-D bonds are perpendicular to the chain axes and the chain axes are aligned along the stretch direction. The single splitting occurs when all the bond angles are 90° with respect to the field. The value of P_2 is $\frac{-1}{2}$. From the splitting we measure the quadrupolar interaction strength ω_Q to be $\approx$ 124 kHz. This agrees very well with measurements of the quadrupolar interaction in the C-D bond in other polymers (e.g. PMMA, polyethylene).[35,38,43]

If we had perfect alignment of the chain axes after stretching we would expect the line shape to be very sharply peaked in figure 6.1-a and figure 6.2-a. These spectra show however more broadening than can be accounted for by dipole - dipole interactions. The non-zero intensity between the two peaks in both spectra comes from bonds that are not at 90° to the field. This can only occur if some of the chain axes in the sample are not aligned along the stretch direction. We assume all the C-D bonds are oriented 90° to the chain axis and hence any bonds not perpendicular to the field must be due to non-aligned chain axes.

In figure (6.1-j) we have labeled the frequency axis with the corresponding angle a bond would have to make with the field in order to resonate at that position in the spectrum. Zero splitting occurs at the magic angle, 54.7.°. The two inside peaks occur where P_2 is equal to $\pm\frac{1}{2}$, corresponding to angles 35.26° and 90°. The outside peaks occur for bonds oriented parallel to the field.

As the field is rotated away from the stretch direction, the intensity at the perpendicular edge in both spectra decreases and the area between the peaks begins to fill. This process occurs more rapidly for the homopolymer. At $\theta_H = 30°$, its center region has filled considerably compared to the copolymer spectrum. This indicates that the chain axes in the homopolymer are not aligned as well as they are in the copolymer films. As mentioned above, the central region of the spectrum is sensitive to bonds oriented between $\approx 35°$ and 90°. A broader distribution in orientations for the chain axes about the stretch direction produces a broader distribution of C-D bond angles. This result is consistent with the fact that the homopolymer film was very difficult to stretch and that the homopolymer stretch ratio was 3/1, compared to 4/1 for the copolymer film.

Near $\theta_H = 40°$ for the homopolymer and $\theta_H = 50°$ for the copolymer, shoulders start developing just outside the perpendicular edges in both spectra. This indicates that some bond axes are oriented at angles less than 35° to the field. As the field is rotated further the edges of the shoulders slowly move out and increase in intensity until they reach a splitting corresponding to parallel orientations. The intensity at both

the parallel and perpendicular edges have discontinuities (cusps) reflecting a fiber type configuration.

6.1 Simulation Results on Chain Axis Orientations

We were able to reproduce these general features in model simulations with the appropriate choice of $f(\theta)$ for the chain axis distributions. We assume for the moment that $g(\phi')$ is unity. Figures 6.3(a-j) and 6.4(a-j) are to be compared to the homopolymer and copolymer spectra in figures 6.1(a-j) and 6.2(a-j), respectively.

Figures 6.3(a-j) and 6.4(a-j) are simulated line shapes with a gaussian distribution for the spread of chain axes about the stretch direction, i.e., $f(\theta) = \exp-(\theta^2/\Delta\theta^2)$. In these particular sequences $\Delta\theta = 18^\circ$ and 22° respectively. Several other values of $\Delta\theta$ (HW1/cM) were tried but the above values gave the best agreement with experiment. The criterion for the choice of the functional form of $f(\theta)$ was its ability to reproduce the general features of the line shapes in the previous discussion. Several other functional forms for f were tried and although they gave rough agreement with experiment the gaussian distributions did a better job of reproducing the data. It was mentioned earlier that the rate at which the center part of the spectrum fills as θ_H goes from 0° to 90° is the property that characterizes the spread in bond orientations. The choices for $\Delta\theta$ above in both simulations reproduce this characteristic very well. The $\theta_H = 0$ line shapes in both simulations start out with the appropriate amount of intensity at angles greater than $\approx 35^\circ$, i.e., the area between the peaks. Note that the homopolymer simulation has more intensity in the center of the spectrum reflecting the wider distribution of chain axis orientations.

As the field is rotated toward field orientation $\theta_H = 90^\circ$, the peaks reduce in intensity at about the same rate as in the experimental data. The central region in the simulated line shapes fig. 6.3 (copolymer simulation) begins to increase substantially near $\theta_H = 20^0$ and levels out at $\theta_H = 40^0$. This agrees qualitatively with the experimental results. The homopolymer line shapes (experimental and simulated) are very similar in character but the filling process starts at lower angles, i.e.,10° to 30°, due to the lesser extent of chain axis alignment.

When the field reaches the perpendicular orientation $\theta_H = 90^0$, both simulations approximate the fiber pattern and are consistent with experimental results. Since there are some bonds which are oriented to the north and south of the equator, the line shapes at $\theta_H = 90^0$ are not true fiber patterns (all bonds in the equatorial plane). The parallel edges are not as high in intensity as in the case for a fiber pattern ; however, the perpendicular edges remain unchanged. We note again that the dipole moment vectors are distributed uniformly about the chain axis in the simulations discussed above, 6.3(a-j) and 6.4(a-j).

6.3 Experimental Results on b-Axis Orientation

We will now examine the effect that poling has on the line shapes of both the homopolymer and copolymer films. We remind the reader that the copolymer sample sustained a polarization of ≈ 3.0 μcoulombs per cm^2. This is about 60% of the polarization normally found in commercial films. The homopolymer on the otherhand showed a lower polarization of ≈ 1.0 μcoulombs per cm^2 due to problems outlined in section 2.1.3.. We have measured the polarization from our dielectric hysteresis loops and thermal light pulse techniques. We assume that the films remained poled throughout the experiments. The extent to which the samples were poled is central to the discussion to follow.

We begin by studying the spectra of the unpoled copolymer (figure 6.5(a-j)). The magnetic field is initially aligned along the +x direction ($\phi_H = 0$) and is rotated to $\phi_H = 90^\circ$. Upon inspecting the sequence from $\phi = 0^\circ$ to 90°, we conclude that the general features of the line shapes are not dependent on the orientation of the magnetic field. The cusps at the parallel and perpendicular edges do not vary in intensity as the field is rotated and the central region remains reasonably unchanged throughout the run. This is what we would expect for a uniform distribution of bond angles about the stretch axis. We note that even if the 6-site model proposed in section 3.0 is an accurate description of the physical system, we expect before poling that all orientations would be equally probable resulting in a uniform distribution in ϕ. Our deuterium NMR data indicate that the stretching process does not produce a preferred orientation for the dipole moment axis. X-ray studies on protonated stretched films also

show a uniform distribution in ϕ'.[1] Our results independently support this observation. We note that rolled material **does** have a preferred orientation even before poling, according to x-ray results.[1]

We now turn to the poled homopolymer and copolymer spectra, figures 6.6(a-j) and 6.7(a-j) respectively. Close examination of the homopolymer spectra show very little line shape variation as the field orientation is changed. We do not find this surprising in light of the poor poling conditions. We can only conclude that if the samples were poled , the poling process was not observable in the line shapes. We will discuss the consequences of this below in conjunction with the observations on the poled copolymer.

Close examination of figures 6.6(a-j) and figures 6.7(a-j) indicate that both sets of line shapes are independent of the orientation of the magnetic field. Though there are slight variations in the relative intensity between some of the spectra, the general features are not functions of the orientation of the magnetic field. We note that the intensity at the parallel edge of the spectrum is proportional to the number of bonds oriented parallel to the magnetic field. It is therefore very sensitive to any variation in the distribution function $g(\phi')$. We conclude that the reorientations taking place as a result of poling could not be seen with NMR line shape studies in our samples. We stress that our line shapes are only sensitive to the $l = 2$ parts of the distribution function $g(\phi')$. This is due to the nature of the quadrupolar interaction:

$$P_2(\cos(\theta)) = \frac{3\cos^2(\theta) - 1}{2}.$$

A reorientation of a bond by 180° would not be detectable since $\cos(\theta) = -\cos(\theta+180^\circ)$ and this goes into the above equation as the square. If the reorientations take place via 180° flips we would not be able to see this in our line shape data.

6.4 Simulation Results on b-axis Orientations

X-ray diffractometry experiments on rolled and poled films report a non-uniform distribution function for $g(\phi')$.[12] They define $g(\phi')$ as ;

$$g(\phi') = \sum_{p=0}^{\infty} C_{2p}\cos(2p\phi')$$

with

$$C_{2p} = \begin{cases} \pi/2 & \text{for } p = 0 \\ 1/\pi\langle\cos(2p\phi')\rangle & \text{for } p \geq 1. \end{cases}$$

It is important to note that their measurements as well as ours are only sensitive to the even terms in the above expansion. From their results they report that the p=1 term in the above expansion is by far the largest contribution in the series with a value of $\approx .8$ for the coefficient. This is for a film rolled and then poled at $\approx$ 800 Kv/cm at 100°C.[12] We note that this is comparable to the poling field used on our copolymer sample.

In order to make a quantitative comparison between our results and the x-ray data, we have run simulations with their $g(\phi')$ given by the above equation. To insure consistency with previous results, $f(\theta)$ is given by a gaussian; the HW1/eM is 18°. These are presented in Figures 6.8(a-j), 6.9(a-j) and 6.10(a-j). In the first two sets of simulations we present $g(\phi') = 1 + A\cos(2\phi')$ with different values for A. In the first sequence, (fig 6.8) A = .8 and in the second set of spectra (fig. 6.9) A=.5. Changes in the general features of the line shapes as a function of field orientation are detectable in all the runs. In figure 6.8(a-j) for instance, the perpendicular edges are much higher than the parallel edges for $\phi_H = 0$. As the field approaches $\phi_H = 90°$, the intensity in the perpendicular edges is transported into the parallel edges. This is the characterizing feature of this particular functional form of g. Clearly our line shapes do not reflect this behavior. Several other values of A were tried in the simulations in order to characterize the trend seen in the line shapes for different A's. We estimate an upper limit for A for the experimental spectra : $A \leq 0.2$.

The last set of figures (fig. 6.10(a-j)) are the line shapes obtained when $g(\phi')$ has

the following functional dependence;

$$g = \begin{cases} 1, & -30^{\circ} \leq \phi' \leq +30^{0} \\ 0, & \text{everywhere else.} \end{cases}$$

This distribution function corresponds to the maximum polarization possible in the 6-site reorientation model.[26,29] We assume that the initial distribution in ϕ' is uniform before poling. Then the maximum polarization occurs when all the dipole moments are oriented within $\pm 30^{\circ}$ of the applied field (i.e. as close as they can get). The simulation clearly does not reproduce the data.

In conclusion, we have found the orientational distribution function for the dipole moments in poled homopolymer and copolymer samples to be uniform in terms of even l variations. Simulated line shape studies were found to be sensitive to orientational distribution functions derived from experimental x-ray data. But the NMR experimental line shapes show no such behavior. If reorientations occurred by 180° flips in our samples, this would be consistent with our data. In general, NMR is insensitive to odd l components of the $g(\phi')$; we remark that dielectric polarization is an $l = 1$ quantity, involving the projection of the dipole vector onto the electric field.

Chapter VII

CONCLUSIONS

7.0 Conclusions

NMR line shape studies of deuterated poly(vinylidene fluoride) and its copolymer poly(vinylidene fluoride - tetrafluoroethylene) (80-20) are presented. The films were prepared at the National Bureau of Standards where powder samples obtained from Bell Labs were pressed into films, stretched and poled. Hysteresis loops obtained while poling indicate that the homopolymer (stretched 3/1) retained a polarization of $\approx$ 1.0 μ-coulombs/ cm^2. The copolymer (stretched 4/1) retained a more substantial polarization (3.0 μ-coulombs/cm^2) and produced hysteresis loops resembling those of commercial protonated samples. The polarization of both samples was also measured with a light pulse technique, confirming the hysteresis measurements.

The orientational distribution of carbon-deuterium bonds in both poled and unpoled samples were studied utilizing the quadrupolar interaction of the nucleus with the EFG of the C-D bond in the presence of an external magnetic field. The angular dependence of the quadrupolar interaction as a function of the magnetic orientation enabled us to measure the distribution of bond orientations. The orientational distribution functions for both the chain axis orientation, $f(\theta)$, and dipole moment (polar b-axis) orientation, $g(\phi')$, were measured for both the poled and unpoled samples.

Homopolymer experimental results give best agreement with simulated spectra using a gaussian distribution for $f(\theta)$ with HW1/eM value of 22°. $f(\theta)$ for the copolymer is also a gaussian but with a HW1/eM value of only 18°, reflecting a better alignment of the chain axes along the stretch direction.

The effects of poling on the dipole moment orientational distribution were also measured. The experimental line shapes indicated uniform distributions of dipole

moments about the chain axes both before and after poling. This is in contrast to X-ray results which have found an orientational distribution function given by, $g(\phi') = 1 + .8\cos(\phi')$ (for a well poled material) for the b-axis distribution. Simulation programs which used this particular $g(\phi')$ produced line shapes with pronounced ϕ_H dependence. We conclude therefore that if our samples were characterized by the same distribution function as found in the x-ray samples, we would have been able to see this in our line shape studies. However, no such variations were observed. Functional forms for g consistent with the 6-site model were also used in our simulation programs and the resulting line shapes did not resemble the experimental results.

We note that a reorientation process which proceeds by 180° flips is not detectable in our experiments due to the $I = 2$ symmetry of the quadrupolar interaction. The x-ray work is also insensitive to 180° reorientations.

Finally, we stress that we are comparing results on deuterated films to experimental results on commercially bulk produced protonated films. This must be taken into consideration since the bulk properties of the deuterated material are unknown. We do not believe that significant differences occur because of isotope effects, but because of unavoidable differences in the preparation techniques. The obvious procedure would be to perform the NMR and x-ray experiments on identical samples. However, the NMR interactions studied here are specific to deuterons. We are exploring the possibility of x-ray examination of the deuterated samples.

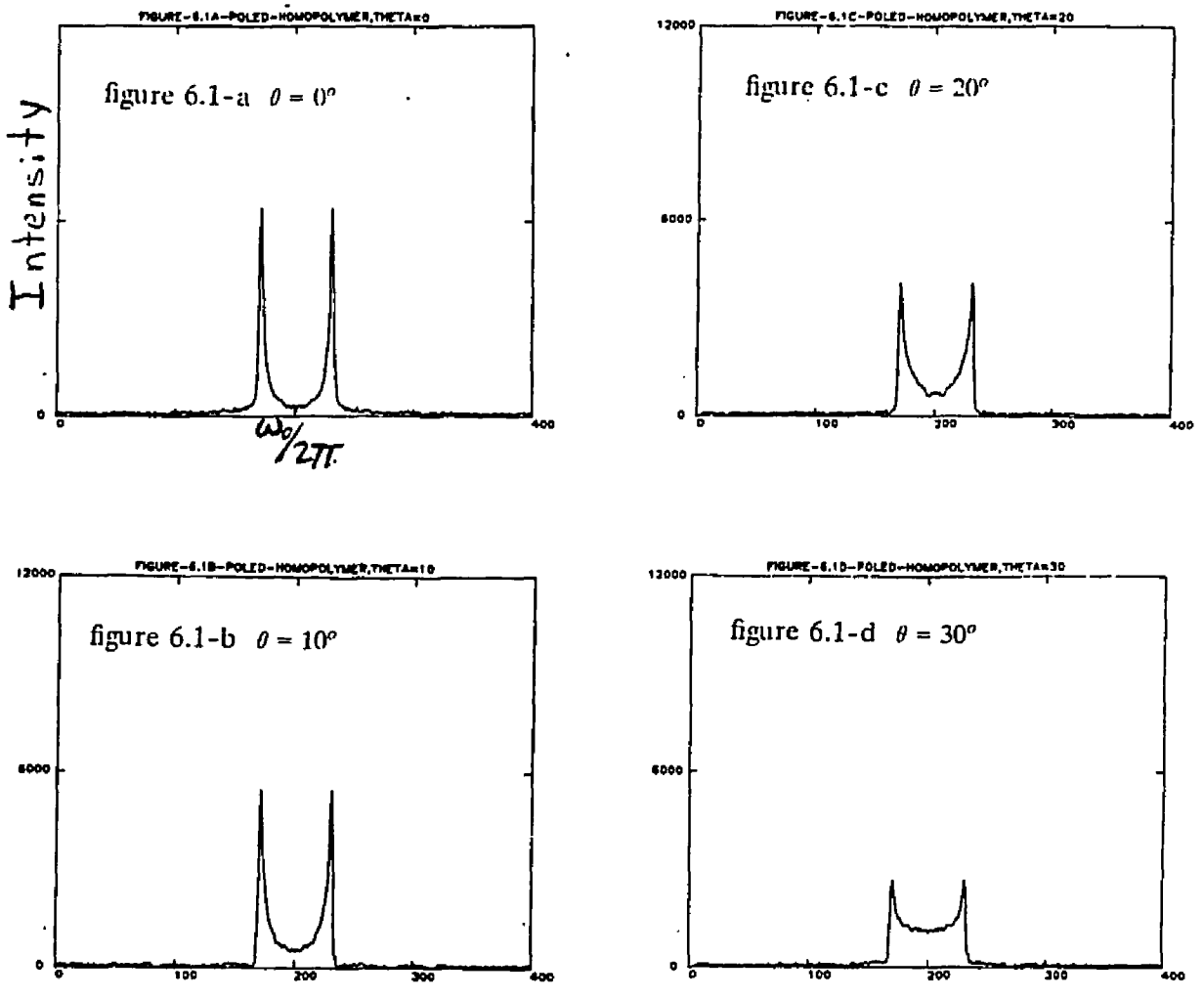

Figure-6.1(a-j)

Experimental line shapes of poled homopolymer PVF_2 as a function of field orientation. The sequence of spectra start with $\theta_H = 0^o$ in figure 6.1-a and progresses to $\theta_H = 90^o$ in figure 6.1-j. $\phi_H = 0^o$ in all runs. All intensities are normalized.

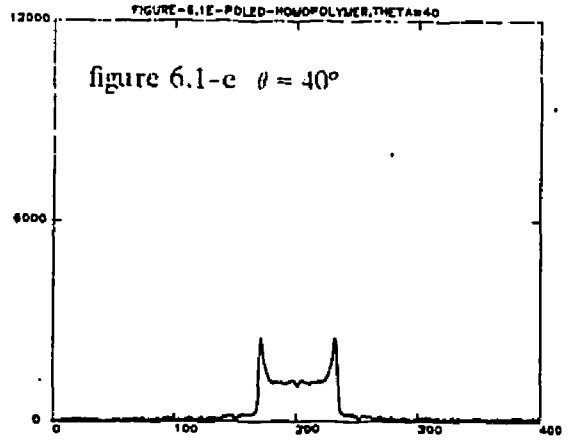

figure 6.1-e $\theta = 40°$

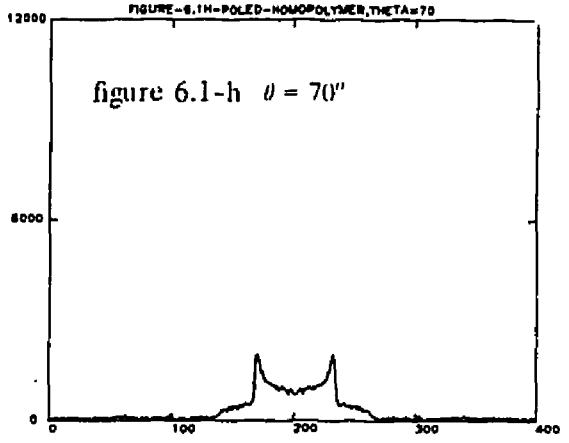

figure 6.1-h $\theta = 70°$

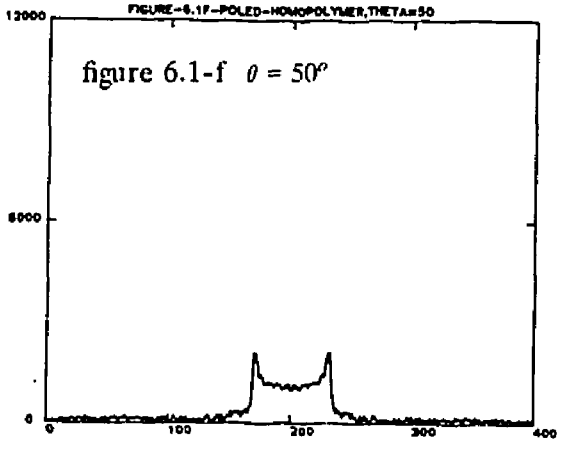

figure 6.1-f $\theta = 50°$

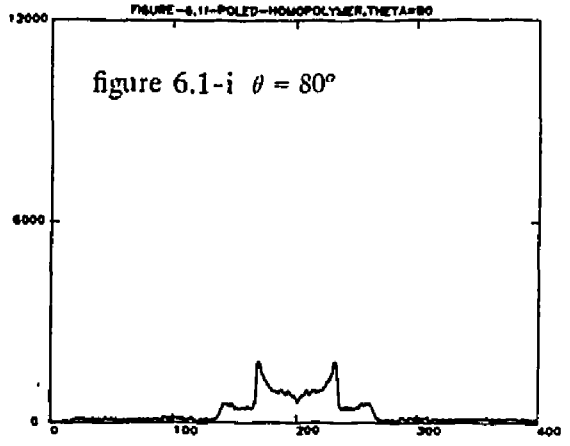

figure 6.1-i $\theta = 80°$

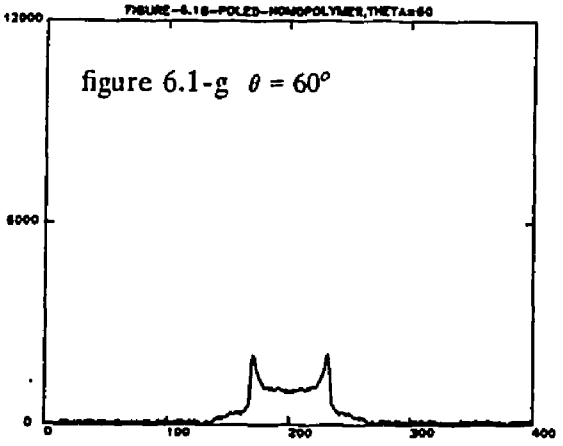

figure 6.1-g $\theta = 60°$

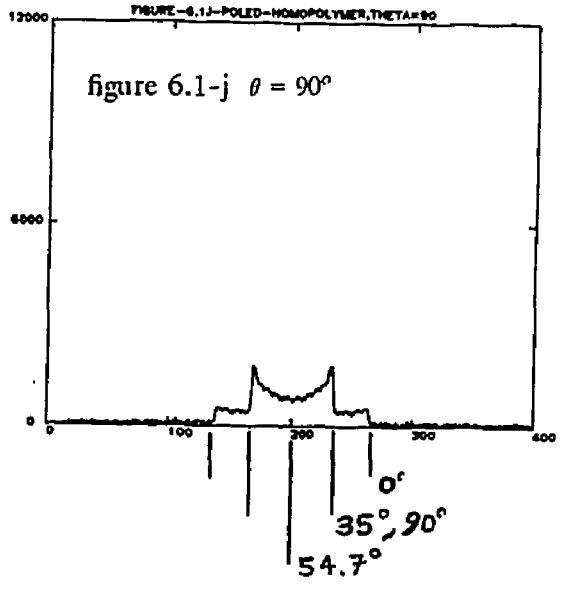

figure 6.1-j $\theta = 90°$

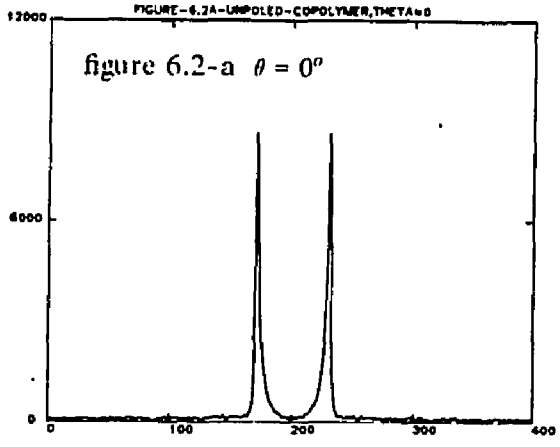

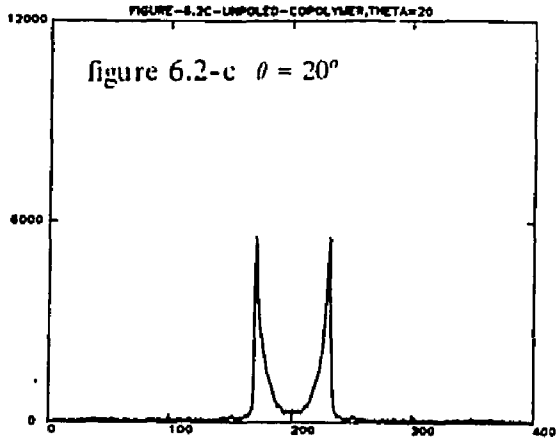

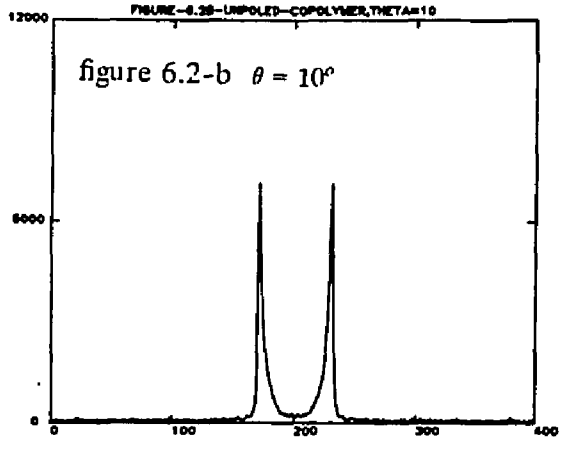

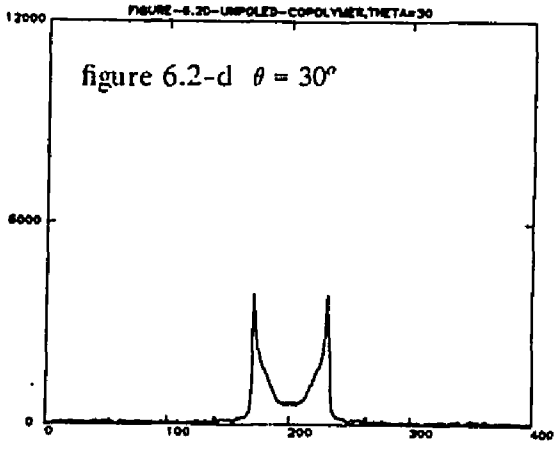

Figure-6.2(a-j)

Experimental line shapes of unpoled copolymer as a function of field orientation. The sequence of spectra start with $\theta_H = 0^o$ in figure 6.2-a and progresses to $\theta_H = 90^o$ in figure 6.2-j. $\phi_H = 0^o$ in all runs. All intensities are normalized.

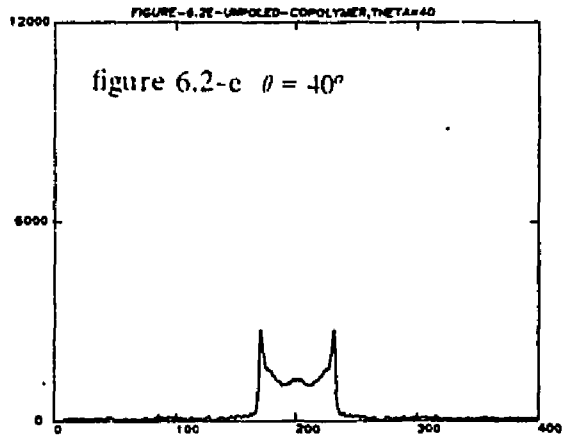

figure 6.2-e $\theta = 40^{o}$

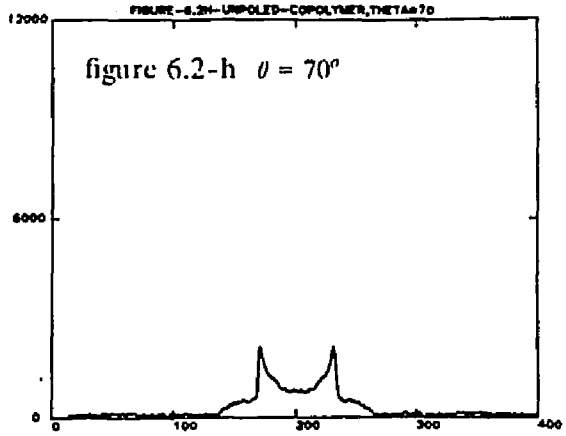

figure 6.2-h $\theta = 70^{o}$

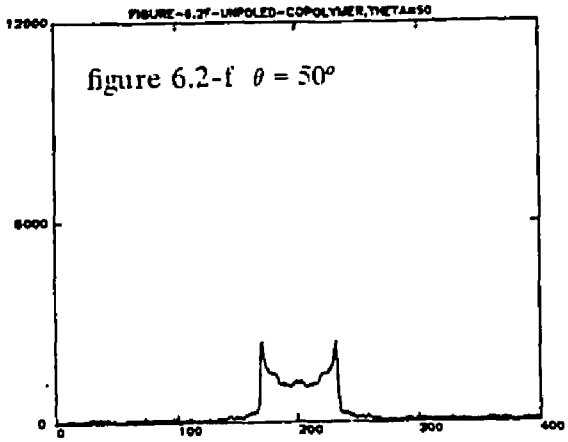

figure 6.2-f $\theta = 50^{o}$

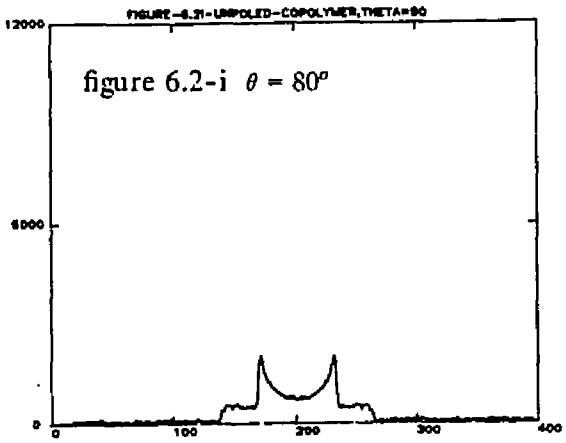

figure 6.2-i $\theta = 80^{o}$

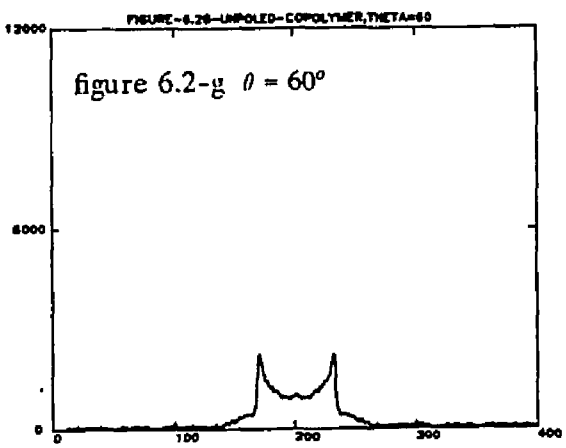

figure 6.2-g $\theta = 60^{o}$

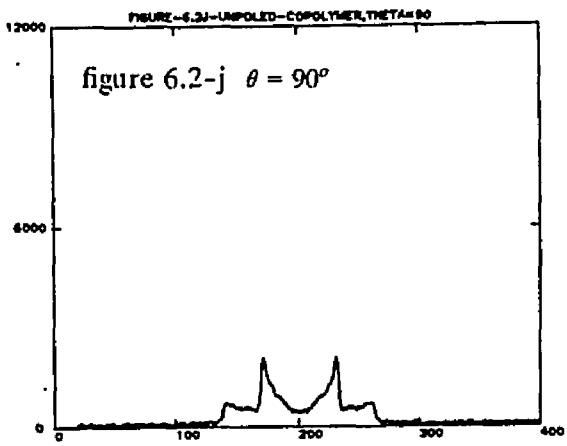

figure 6.2-j $\theta = 90^{o}$

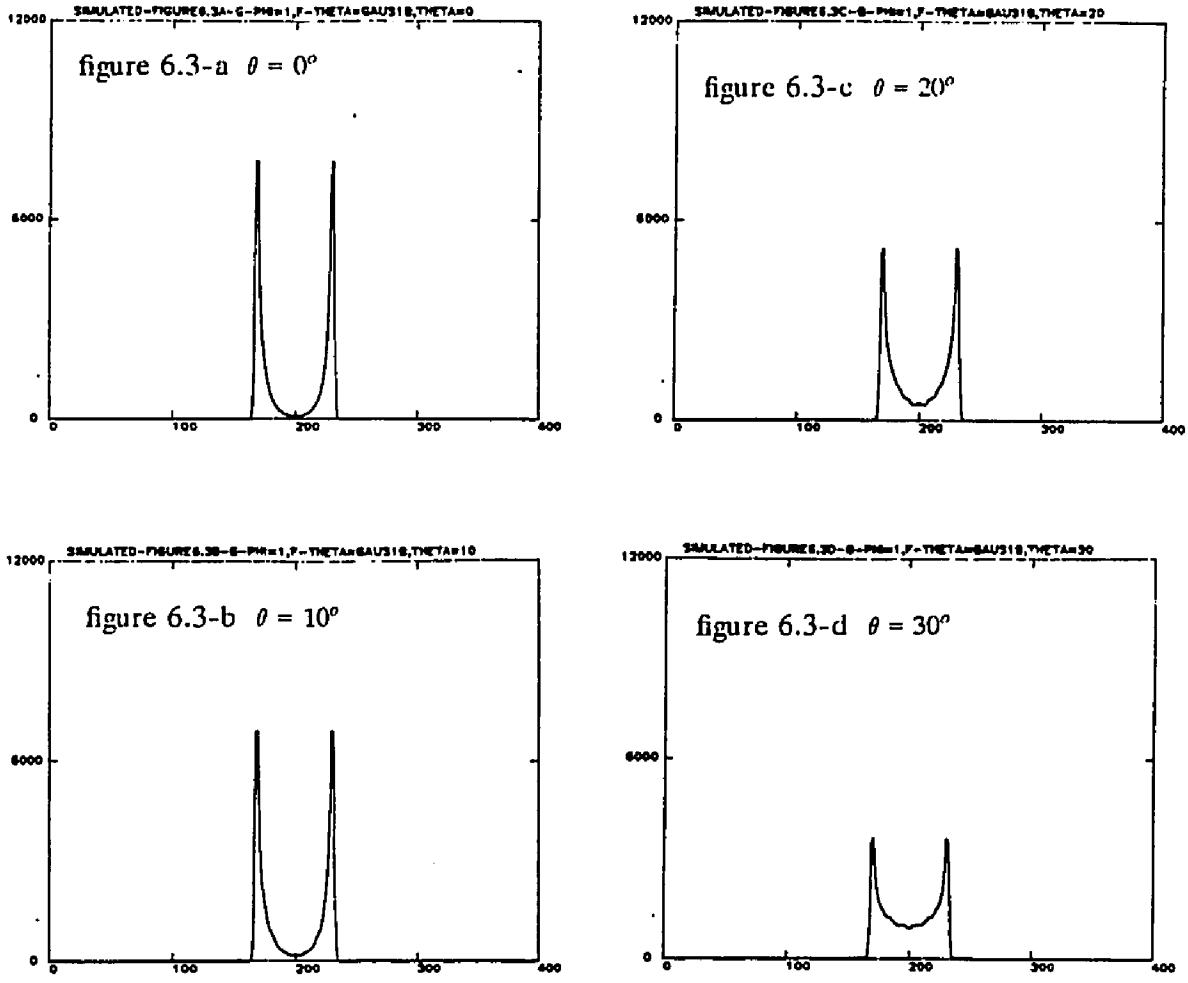

Figure-6.3(a-j)

Simulated line shapes with a gaussian distribution for $\mathbf{f}(\theta)$. HM1/eM = 18^o. The distribution in ϕ is uniform, $\mathbf{g}(\phi) = 1$. The sequence of spectra start with $\theta_H = 0^o$ in figure 6.3-a and progresses to $\theta_H = 90^o$ in figure 6.3-j. $\phi_H = 0^o$ in all runs. These simulated line shapes should be compared to figures 6.2(a-j). All intensities are normalized.

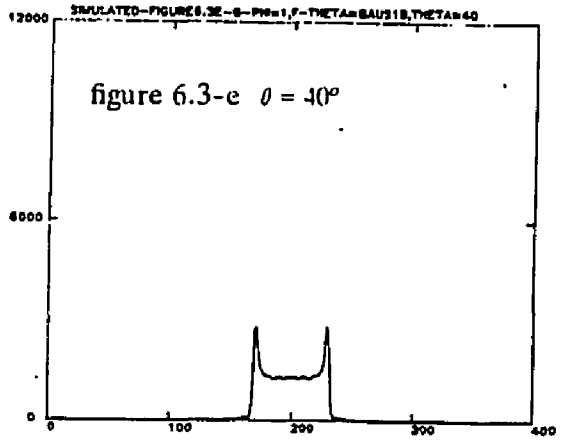

figure 6.3-e $\theta = 40^{o}$

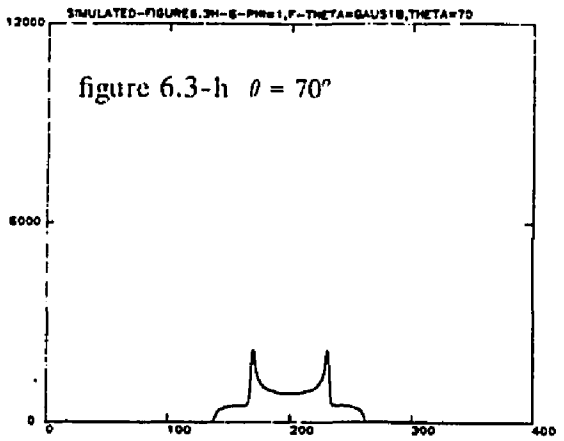

figure 6.3-h $\theta = 70^{o}$

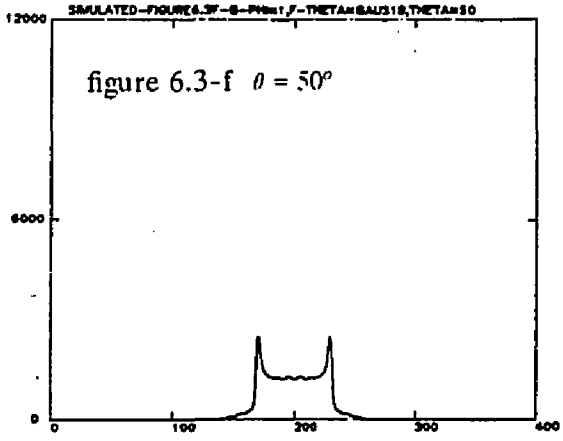

figure 6.3-f $\theta = 50^{o}$

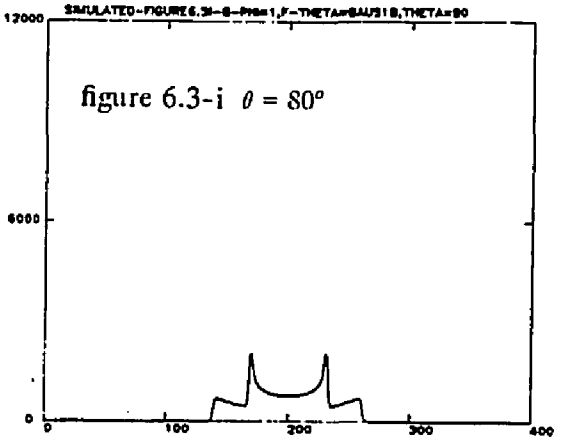

figure 6.3-i $\theta = 80^{o}$

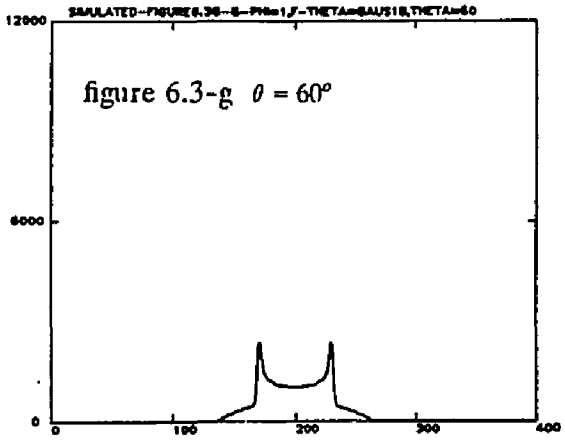

figure 6.3-g $\theta = 60^{o}$

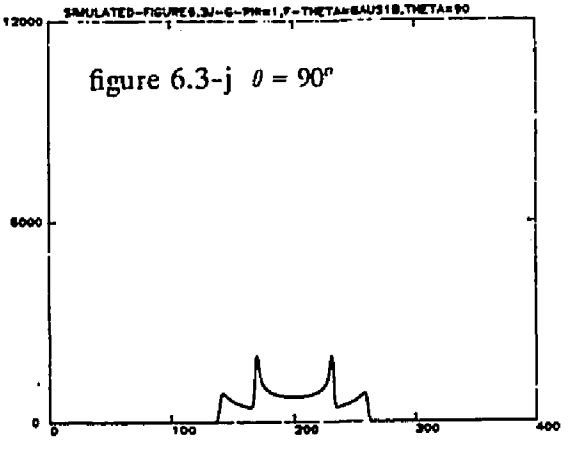

figure 6.3-j $\theta = 90^{o}$

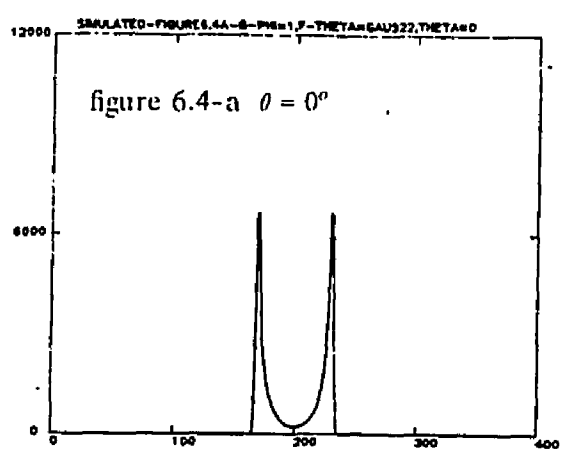

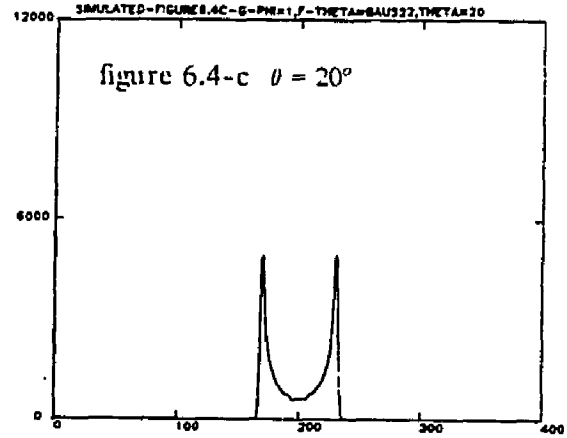

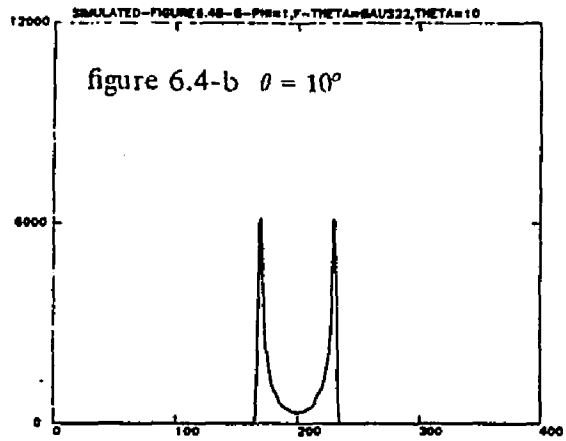

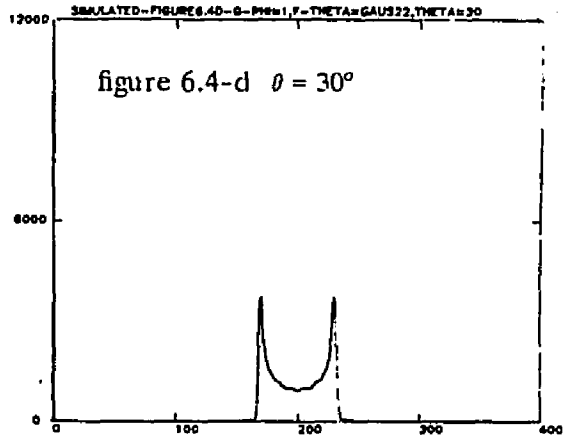

Figure-6.4(a-j)

Simulated line shapes with a gaussian distribution for $f(\theta)$. HM1/eM $= 22^o$. The distribution in ϕ is uniform, $g(\phi) = 1$ The sequence of spectra start with $\theta_H = 0^o$ in figure 6.4-a and progresses to $\theta_H = 90^o$ in figure 6.4-j. $\theta_H = 0^o$ in all runs. These simulated line shapes should be compared to those in figures 6.1(a-j). All intensities are normalized.

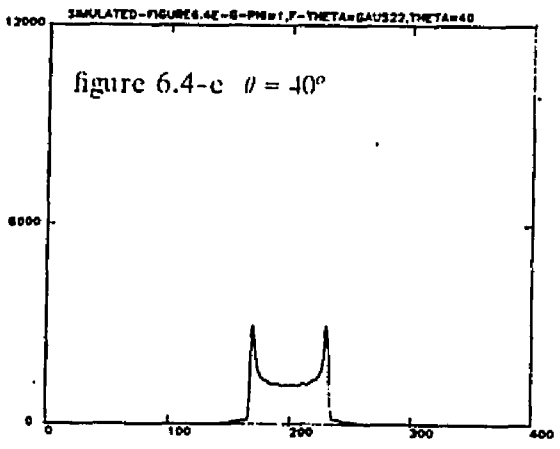

figure 6.4-e $\theta = 40°$

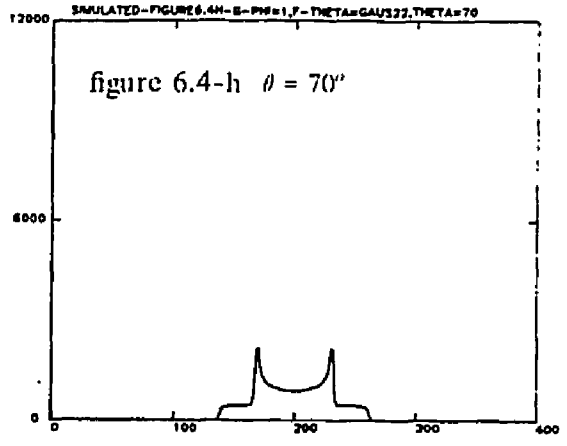

figure 6.4-h $\theta = 70°$

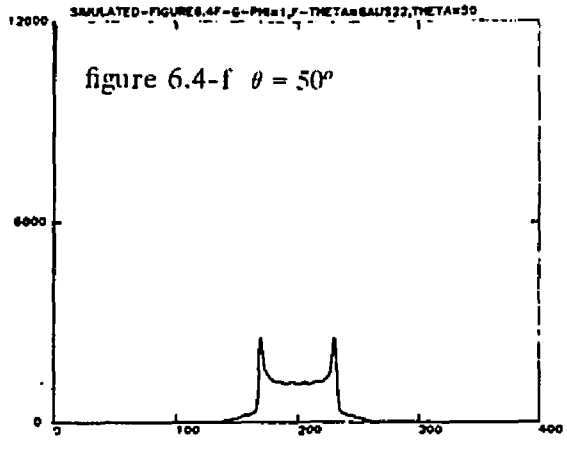

figure 6.4-f $\theta = 50°$

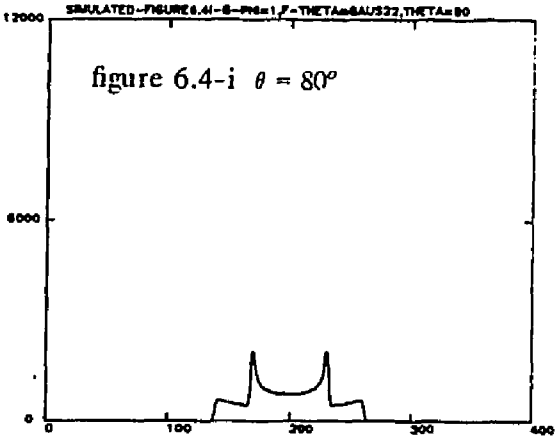

figure 6.4-i $\theta = 80°$

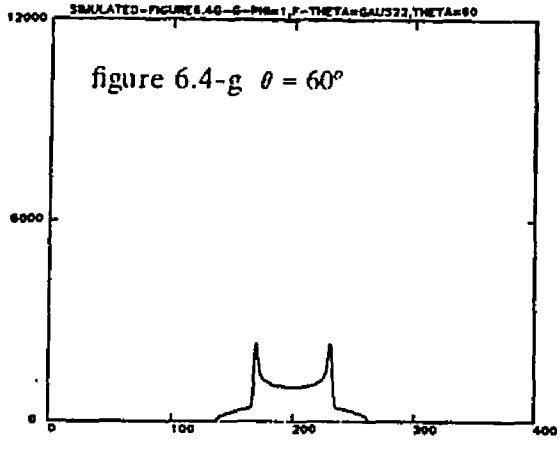

figure 6.4-g $\theta = 60°$

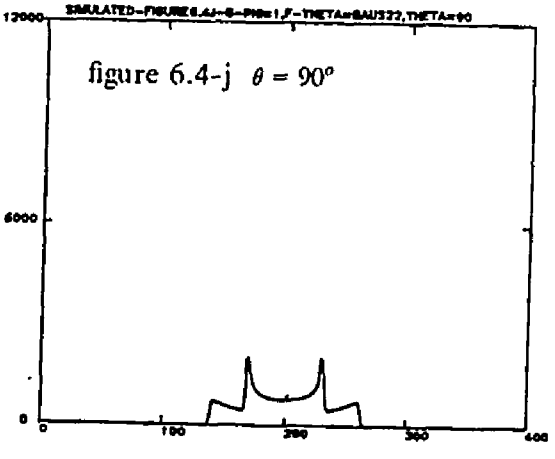

figure 6.4-j $\theta = 90°$

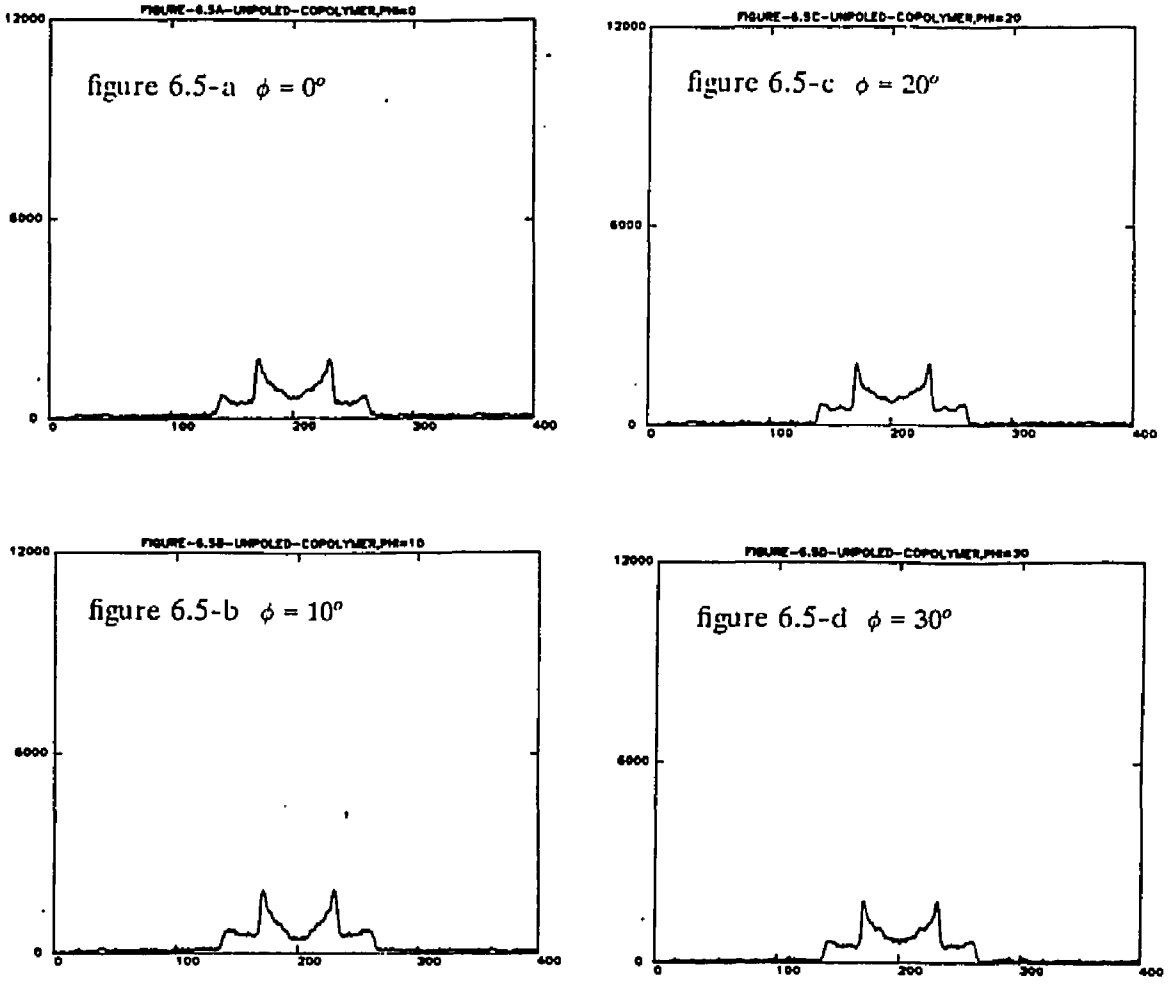

Figure-6.5(a-j)

Experimental line shapes of unpoled copolymer as a function of field orientation. The sequence of spectra start with $\phi_H = 0^o$ in figure 6.5-a and progresses to $\phi_H = 90^o$ in figure 6.5-j. $\theta_H = 90^o$ in all runs. There are essentially no differences between the spectra. All intensities are normalized.

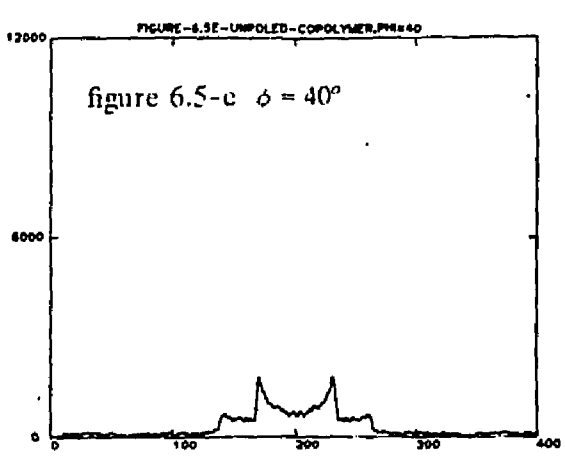

figure 6.5-e $\phi = 40^{\circ}$

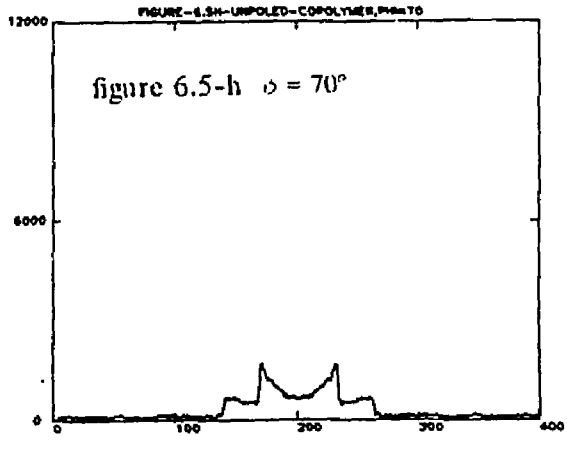

figure 6.5-h $\phi = 70^{\circ}$

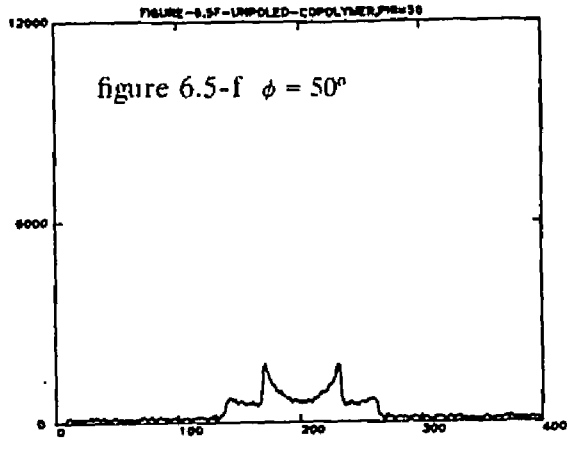

figure 6.5-f $\phi = 50^{\circ}$

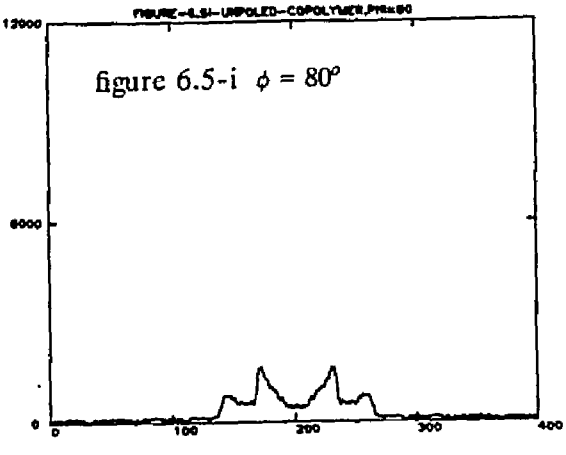

figure 6.5-i $\phi = 80^{\circ}$

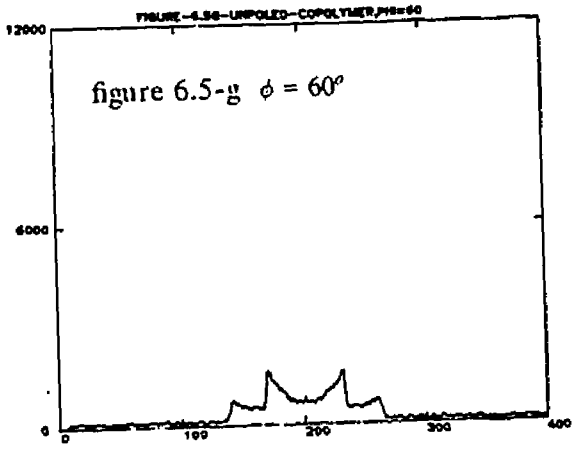

figure 6.5-g $\phi = 60^{\circ}$

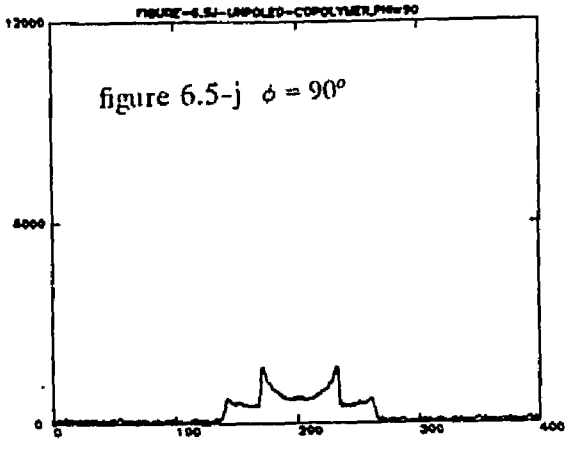

figure 6.5-j $\phi = 90^{\circ}$

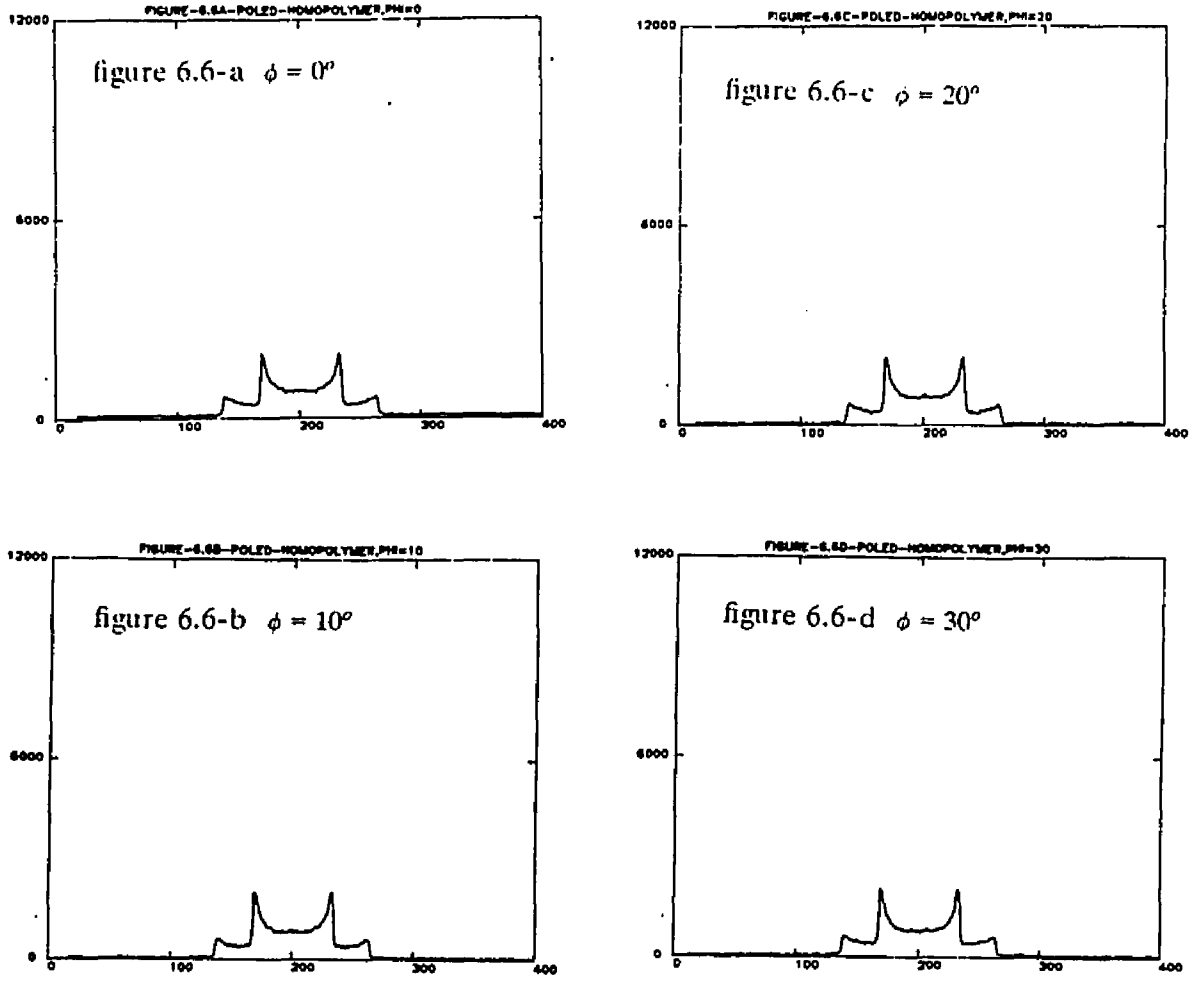

Figure-6.6(a-j)

Experimental line shapes of poled homopolymer (PVF_2) as a function of field orientation. The sequence of spectra start with $\phi_H = 0^o$ in figure 6.6-a and progresses to $\phi_H = 90^o$ in figure 6.6-j. $\theta_H = 90^o$ in all runs. There are essentially no differences between the spectra. All intensities are normalized.

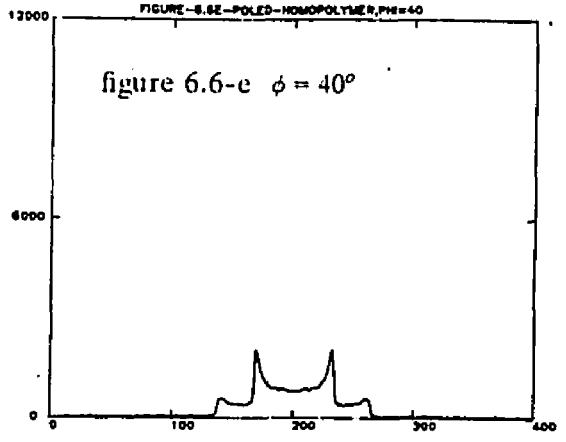

figure 6.6-e $\phi = 40°$

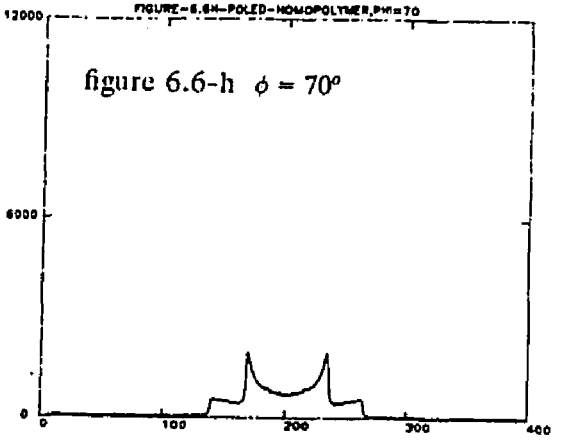

figure 6.6-h $\phi = 70°$

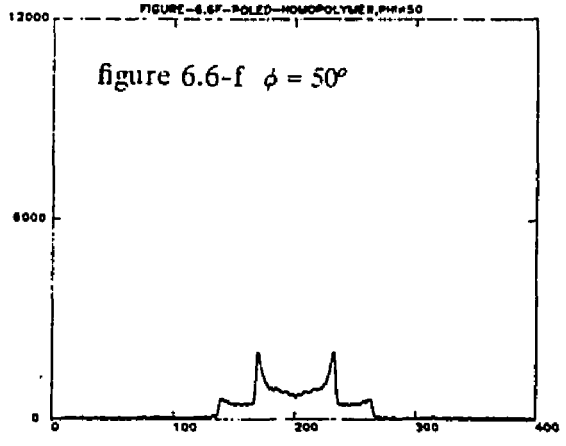

figure 6.6-f $\phi = 50°$

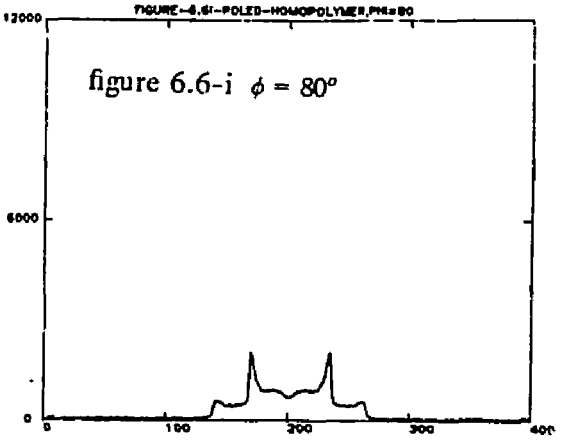

figure 6.6-i $\phi = 80°$

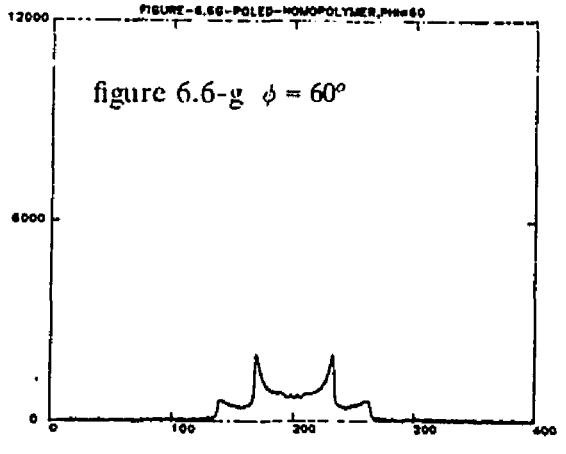

figure 6.6-g $\phi = 60°$

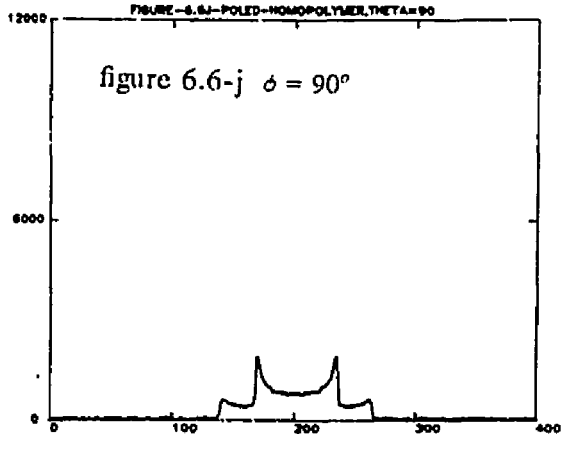

figure 6.6-j $\phi = 90°$

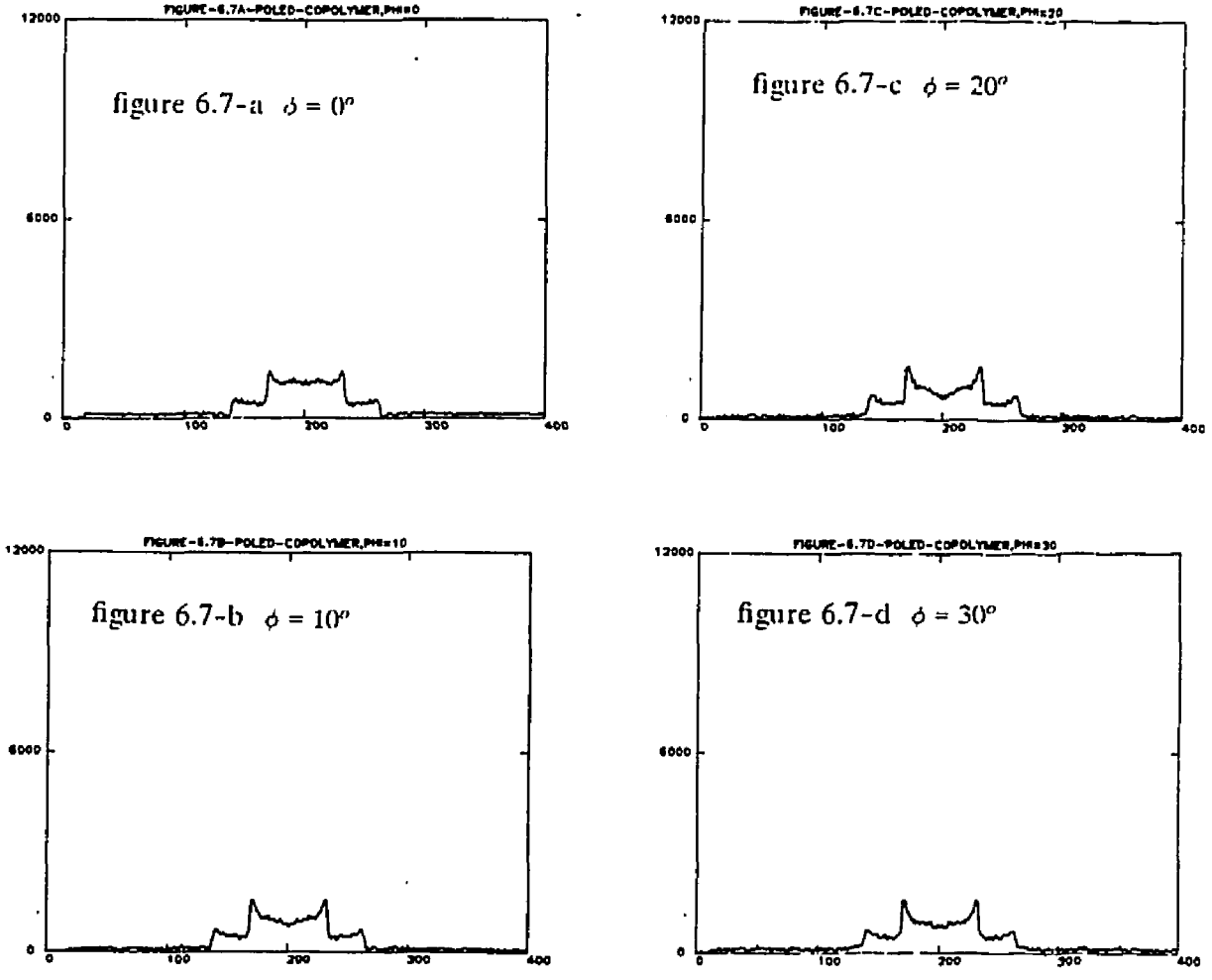

Figure-6.7(a-j)

Experimental line shapes of poled copolymer as a function of field orientation. The sequence of spectra start with $\phi_H = 0^o$ in figure 6.7-a and progresses to $\phi_H = 90_o$ in figure 6.7-j. $\theta_H = 90^o$ in all runs. There are essentially no differences between the spectra. All intensities are normalized.

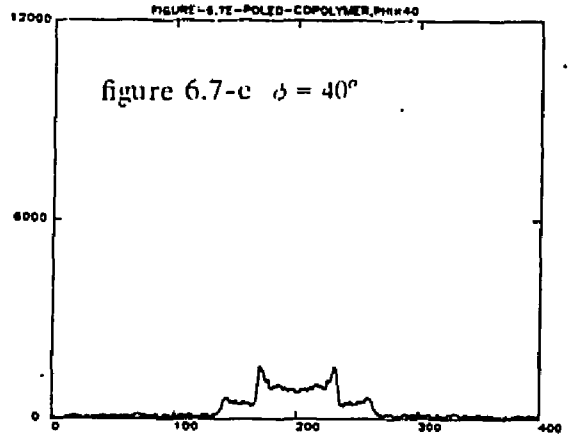

figure 6.7-e $\phi = 40°$

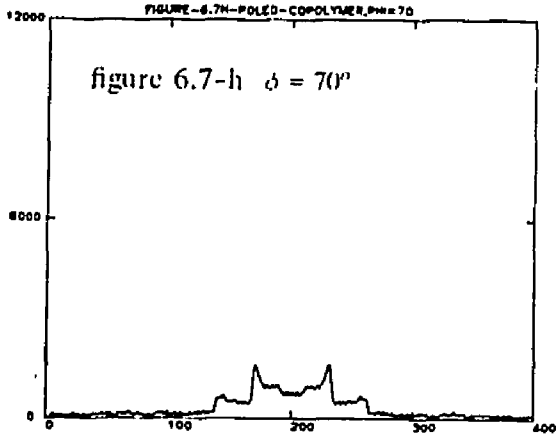

figure 6.7-h $\phi = 70°$

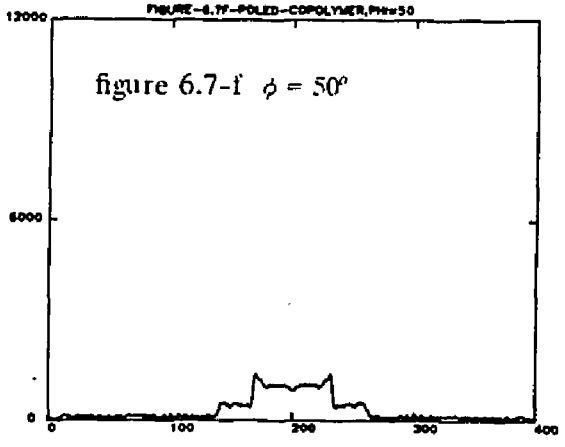

figure 6.7-f $\phi = 50°$

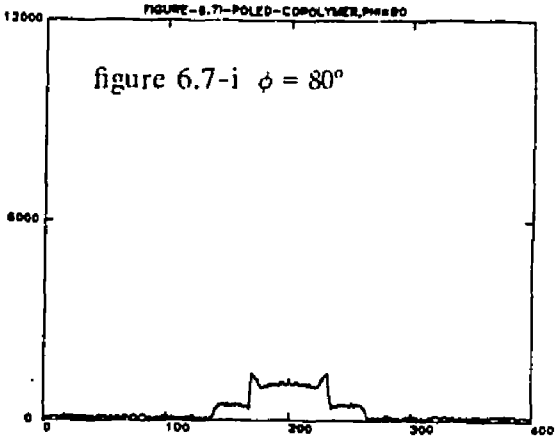

figure 6.7-i $\phi = 80°$

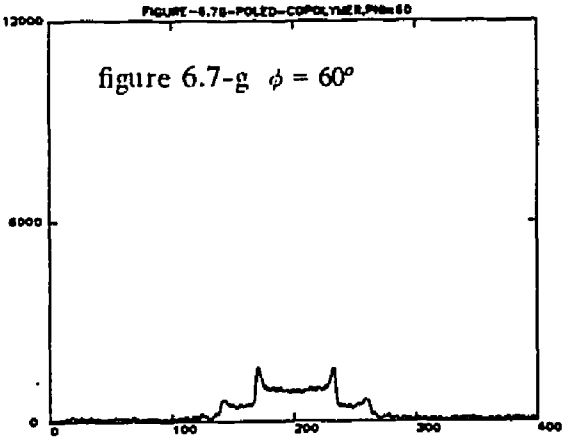

figure 6.7-g $\phi = 60°$

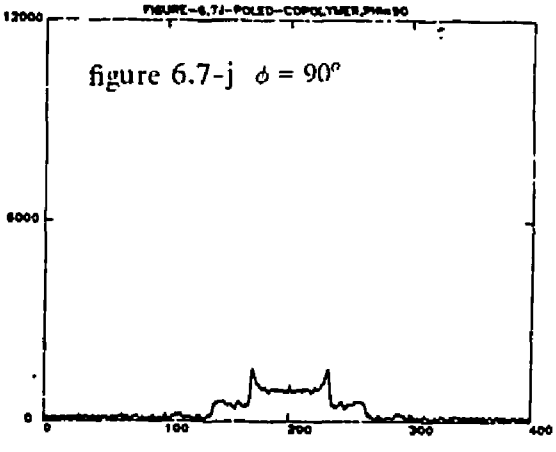

figure 6.7-j $\phi = 90°$

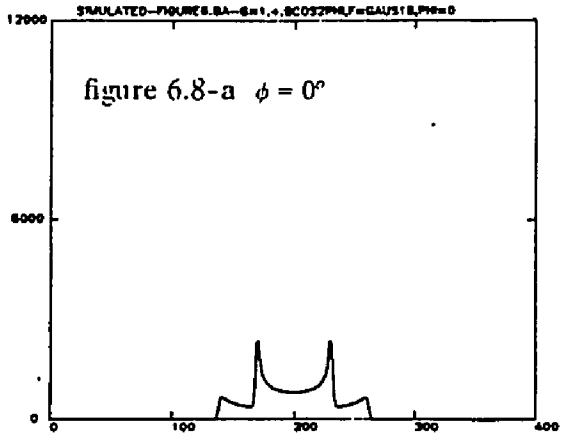

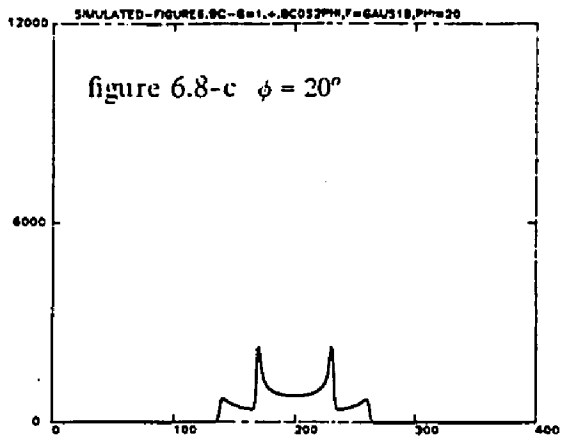

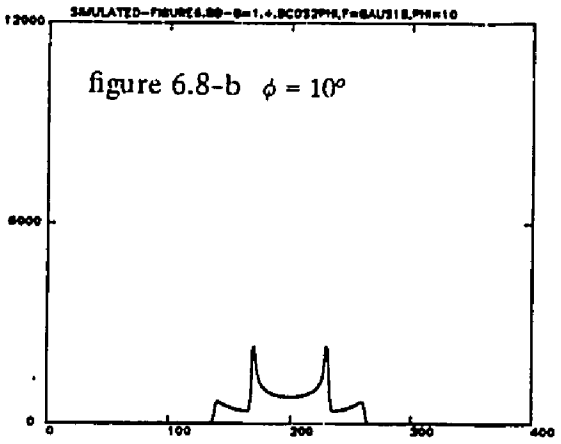

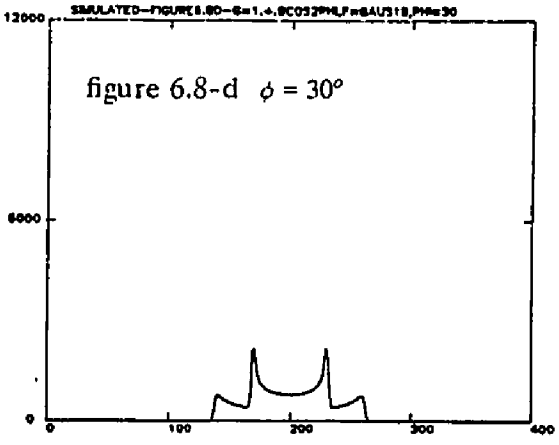

Figure-6.8(a-j)

Simulated line shape with a gaussian distribution for f(θ). HM1/eM = 18°. The distribution in ϕ is given by g(ϕ) = 1 +.8*cos*(2ϕ). The sequence of spectra start with $\phi_H = 0^o$ in figure 6.8-a and progresses to $\phi_H = 90^o$ in figure 6.8-j. $\theta_H = 0^o$ in all runs. Note that the relative heights of the cusps vary (see a and j for most prominent effect). Intensities are normalized.

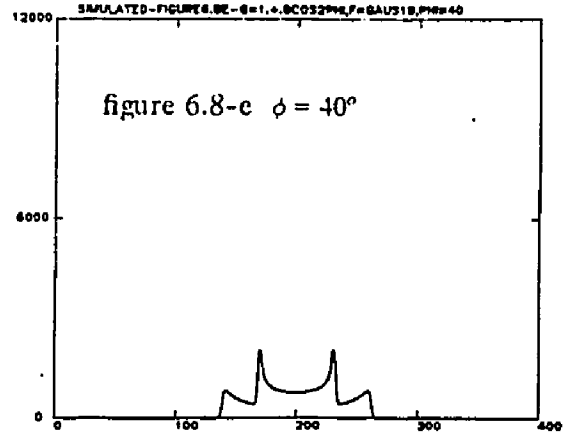

figure 6.8-e $\phi = 40^{o}$

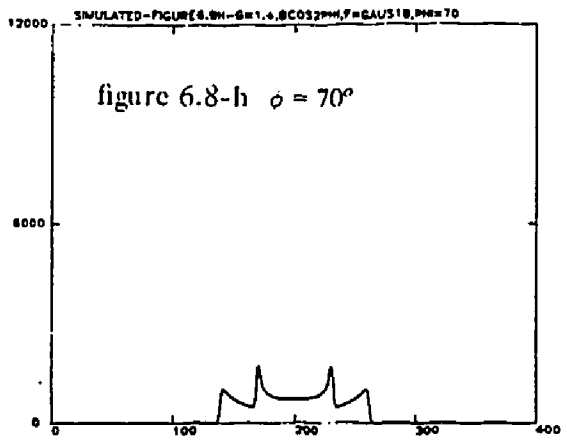

figure 6.8-h $\phi = 70^{o}$

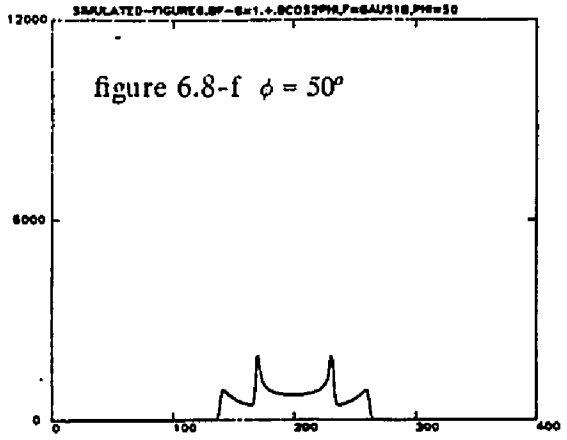

figure 6.8-f $\phi = 50^{o}$

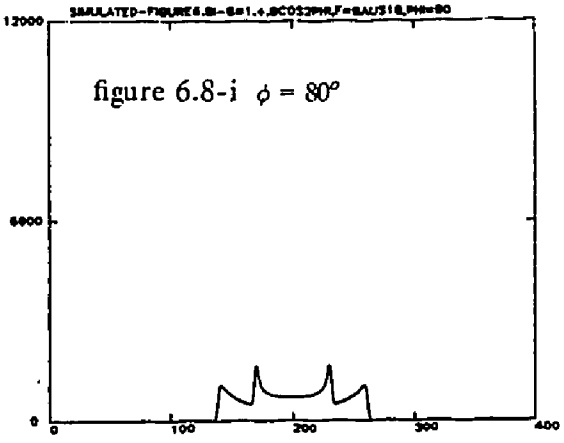

figure 6.8-i $\phi = 80^{o}$

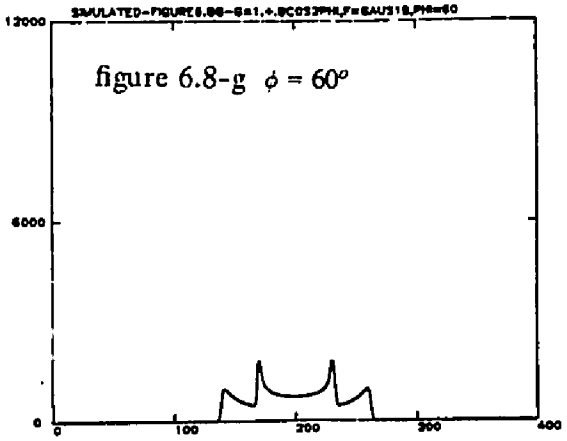

figure 6.8-g $\phi = 60^{o}$

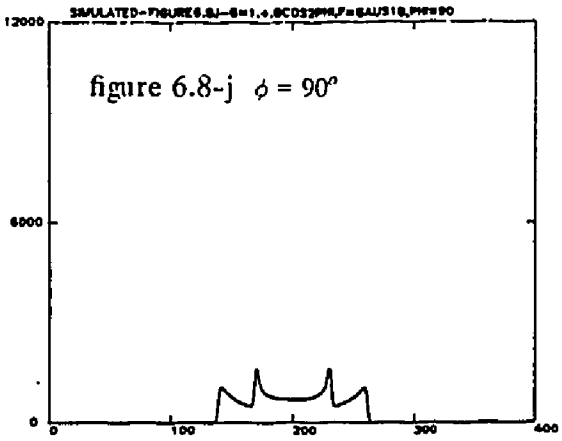

figure 6.8-j $\phi = 90^{o}$

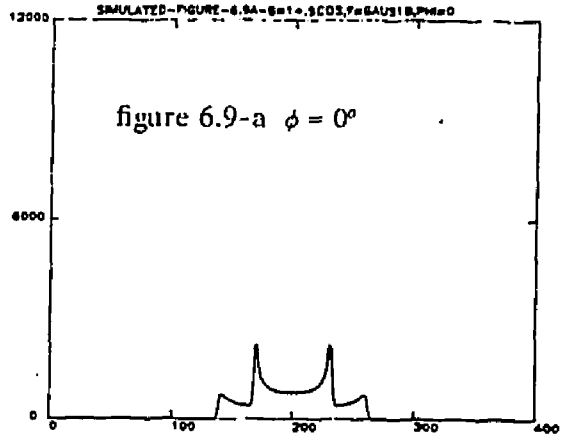

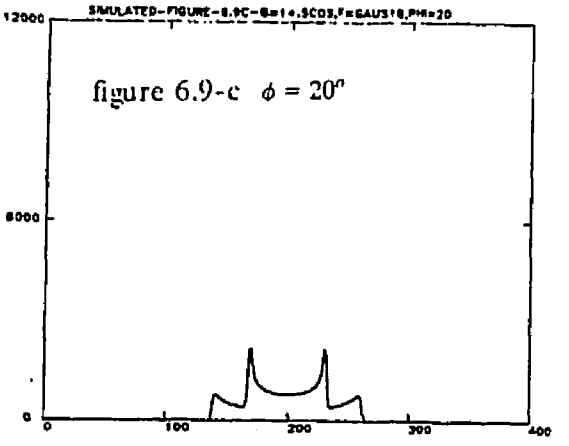

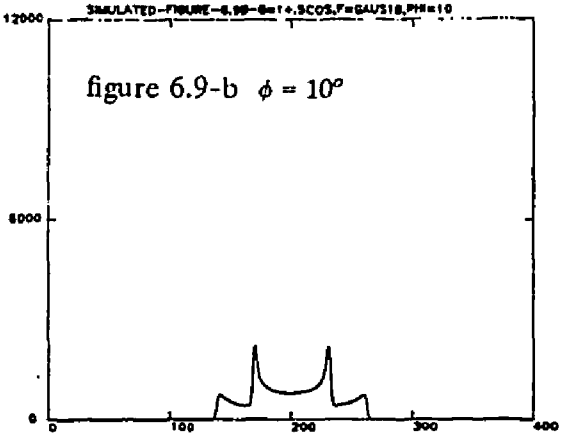

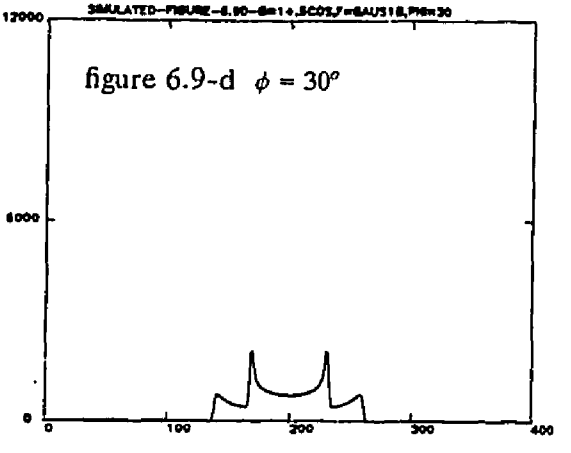

Figure-6.9(a-j)

Simulated line shape with a gaussian distribution for f(θ). HM1/eM = 18°. The distribution in ϕ is given by $g(\phi) = 1 + .5\cos(2\phi)$. The sequence of spectra start with $\phi_H = 0^o$ in figure 6.9-a and progresses to $\phi_H = 90^o$ in figure 6.9-j. $\theta_H = 0$ in all runs. Note that the relative height of the cusps vary (see a and j for most prominent effect), but the variation is smaller than that in figure 6.8. Intensities are normalized.

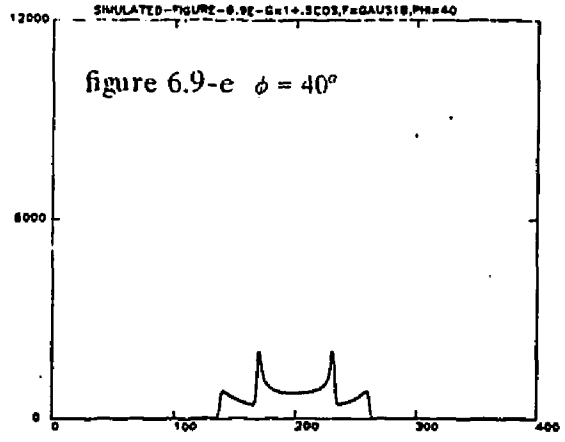

figure 6.9-e $\phi = 40^{o}$

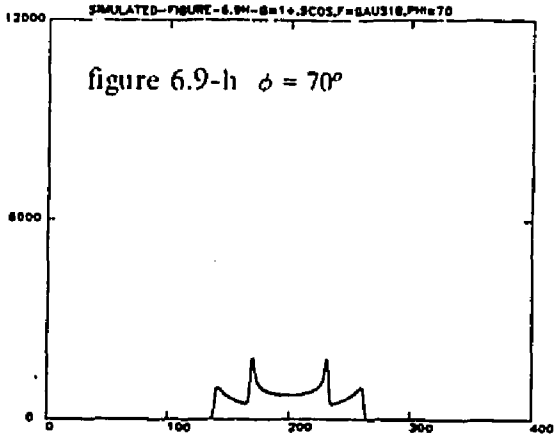

figure 6.9-h $\phi = 70^{o}$

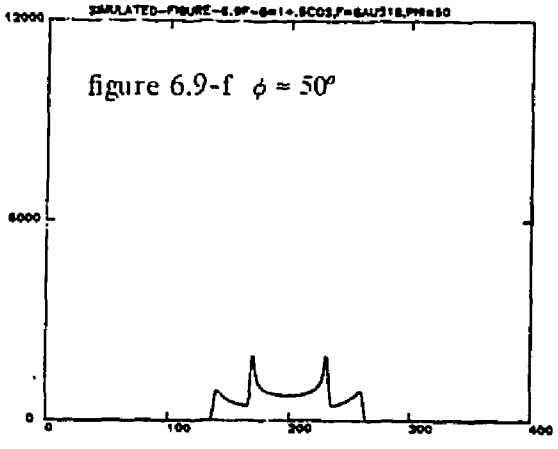

figure 6.9-f $\phi = 50^{o}$

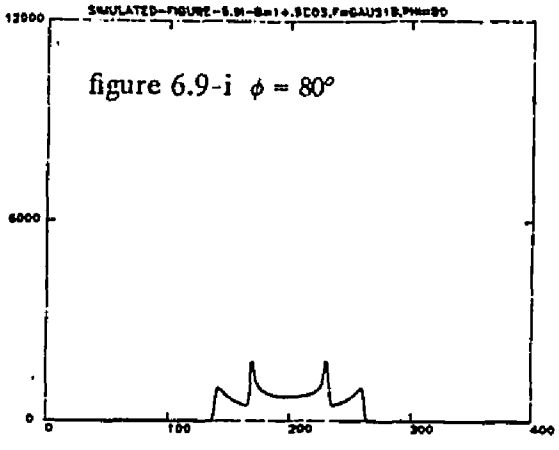

figure 6.9-i $\phi = 80^{o}$

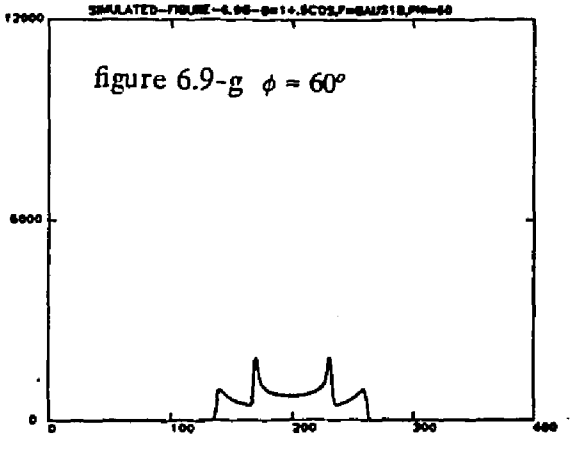

figure 6.9-g $\phi = 60^{o}$

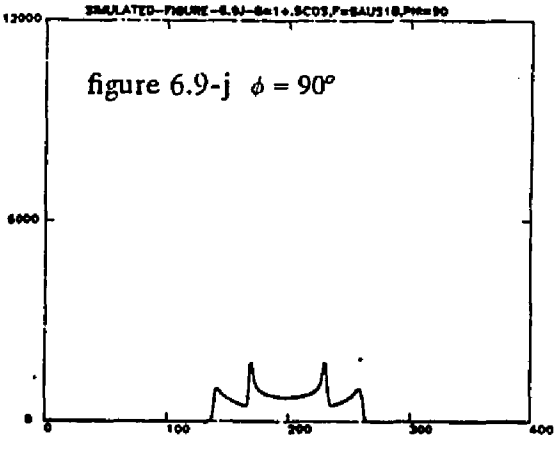

figure 6.9-j $\phi = 90^{o}$

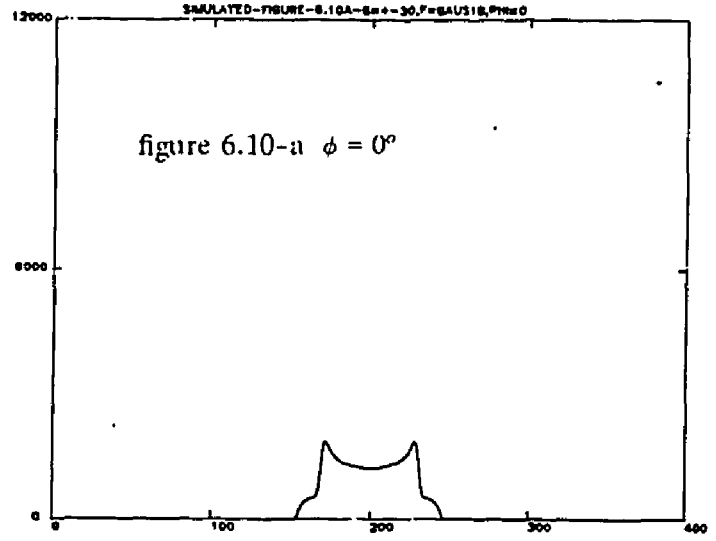

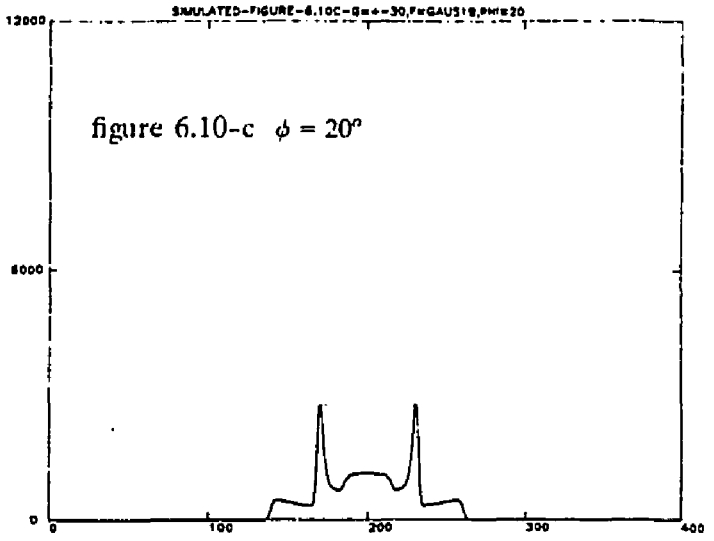

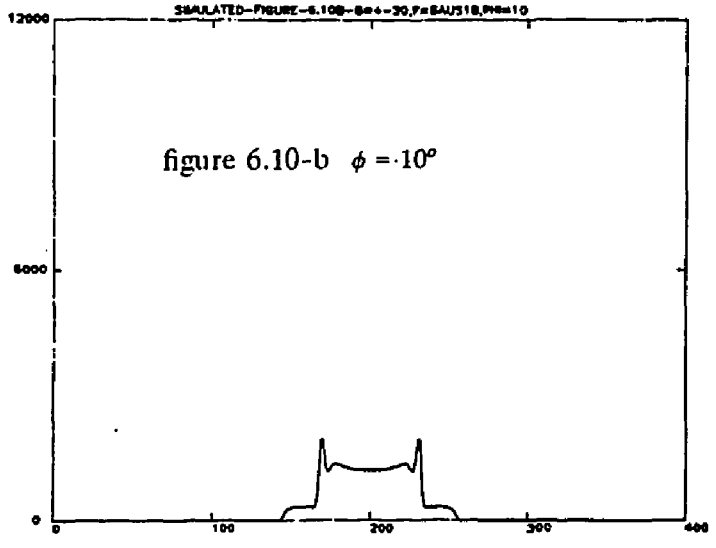

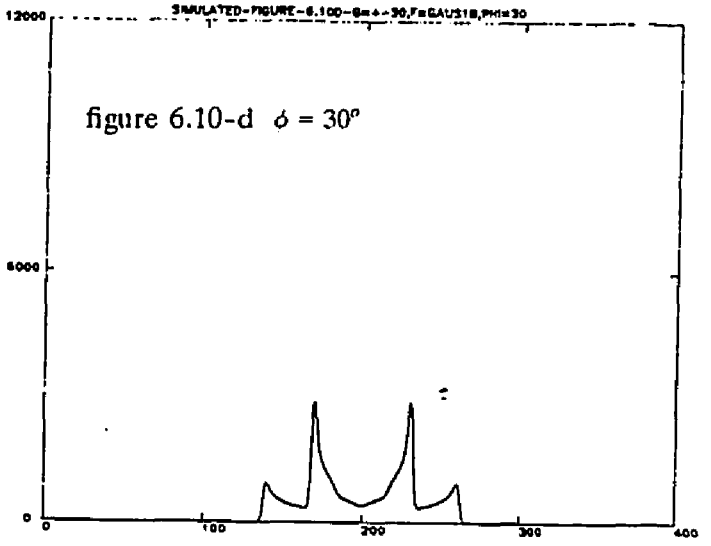

Figure-6.10(a-j)

Simulated line shape with a gaussian distribution for $\mathbf{f}(\theta)$. HM1/eM $= 18^o$. The distribution in ϕ is given by $\mathbf{g}(\phi) = 1$ for $-30^o < \phi < 30^o$ $\mathbf{g}$ is zero everywhere else. This corresponds to complete polarization in the 6-site model. The sequence of spectra start with $\phi_H = 0^o$ in figure 6.10-a and progresses to $\phi_H = 90^o$ in figure 6.10-j. $\theta_H = 0^o$ in all runs. The intensity in these runs were not normalized to the other spectra.

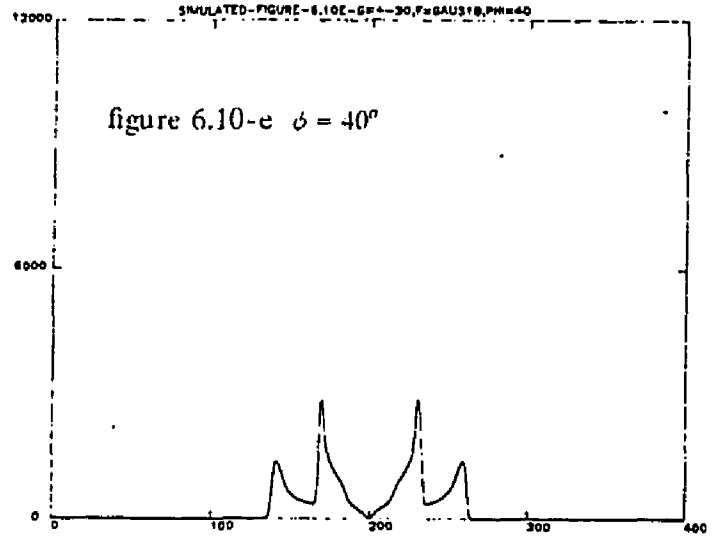

figure 6.10-e $\phi = 40^{o}$

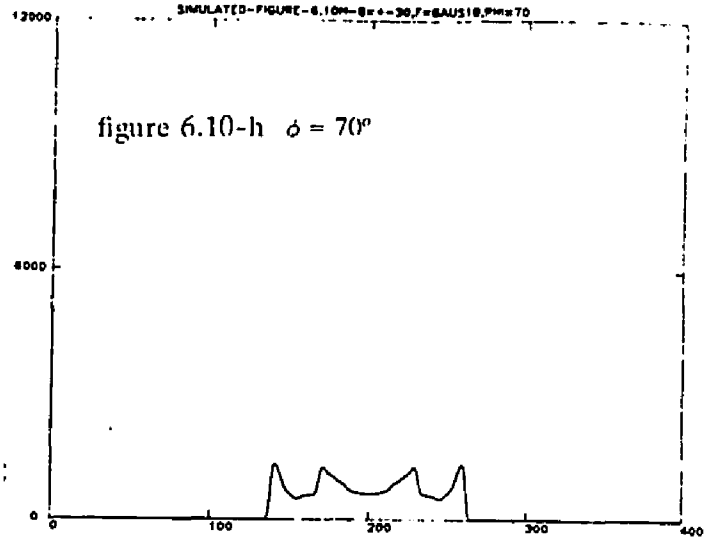

figure 6.10-h $\phi = 70^{o}$

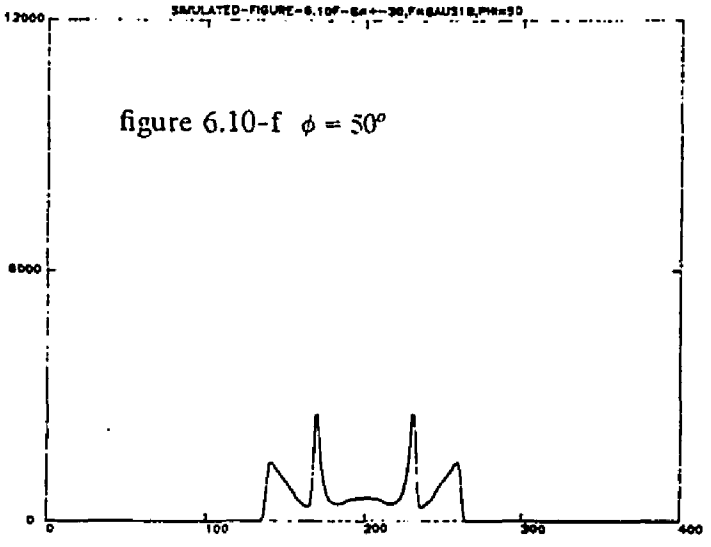

figure 6.10-f $\phi = 50^{o}$

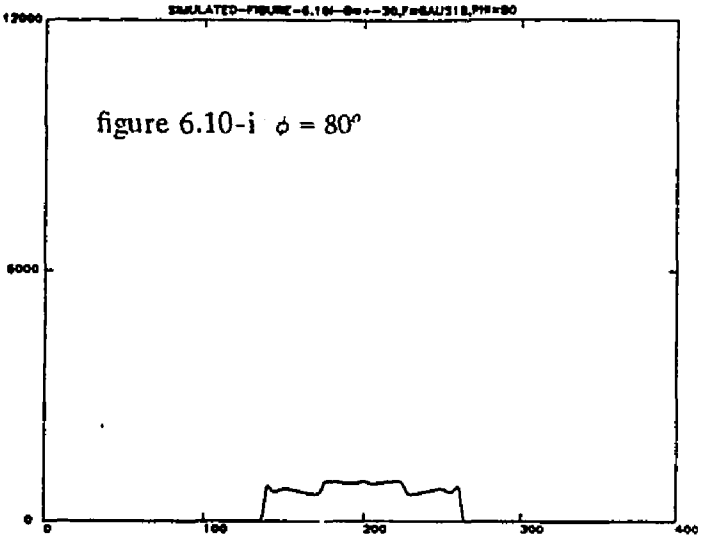

figure 6.10-i $\phi = 80^{o}$

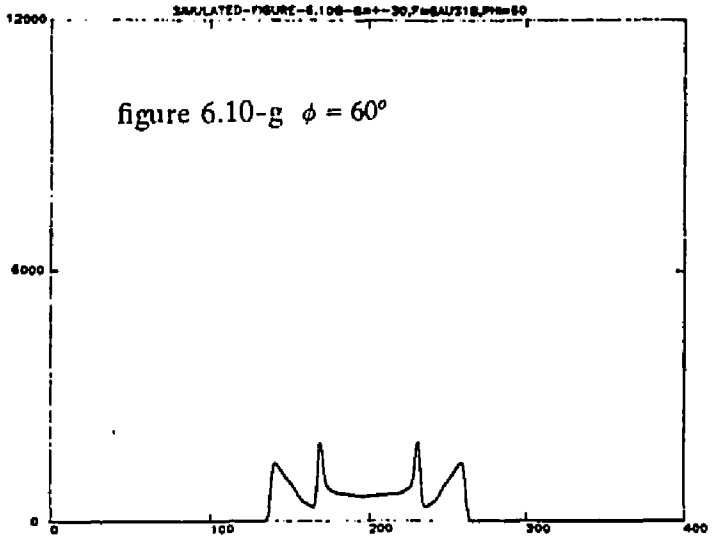

figure 6.10-g $\phi = 60^{o}$

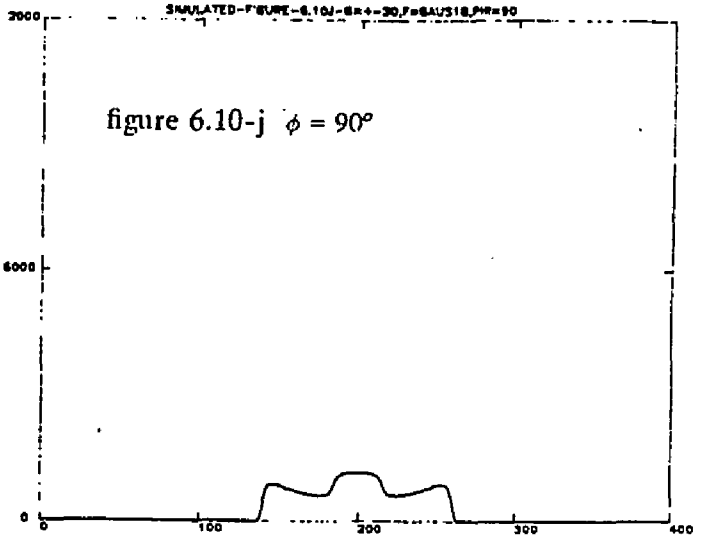

figure 6.10-j $\phi = 90^{o}$

References

1. A.J. Lovinger, "Poly(vinylidene fluoride)," in *Developments in Crystalline Polymers. 1.*, ed. D.C. Basset, pp. 195-273, Applied Science Publishers, London, 1981.

2. R. Gerhard-Multhaupt, G.M. Sessler, J. E. West, K. Holdik, M. Haardt, and W. Eisenmenger, "Investigation of piezoelectricity distributions in poly(vinylidene fluoride) by means of quartz or laser-generated pressure pulses," *J. Appl. Phys.*, vol. 55, pp. 2769-2775, 1984.

3. Danilo DeRossi, Aime S. DeReggi, Martin G. Broadhurst, Steven C. Roth, and G. Thomas Davis, "Method of Evaluating the Thermal Stability of the Pyroelectric Properties of Polyvinylidene Fluoride: Effects of Poling Temperature and Field," *J. Appl. Phys.*, vol. 53, pp. 6520-6525, 1982.

4. G. Pfister, M. Abkowitz, and R.G. Crystal, "Pyroelectricity in Polyvinylidene Fluoride," *J. Appl. Phys.*, vol. 44, pp. 2064-2071, 1973.

5. Behruz Rezvani and John G. Linvill, "Measurement of Piezoelectric Parameters Versus Bias Field Strength in Polyvinylidene Fluoride(PVF2)," *Appl. Phys. Lett.*, vol. 34, pp. 828-830, 1979.

6. Aime S. DeReggi, "Transduction Phenomena in Ferroelectric Polymers and Their Role in Biomedical Applications.," *Ferroelectrics*, vol. 60, pp. 83-105, 1984.

7. J.G. Bergman,Jr., J.H. McFee, and G.R. Crane, "Pyroelectricity and Optical Second Harmonic Generation in Polyvinylidene Fluoride Films," *Appl. Phys. Lett.*, vol. 18, pp. 203-205, 1971.

8. Tetsuo Takahashi, Munehiro Date, and Eiichi Fukada, "Dielectric Hysteresis and Rotation of Dipoles in Polyvinylidene Fluoride," *Appl. Phys. Lett.*, vol. 37, pp. 791-793, 1980.

9. J. Clements, G.R. Davis, and I.M. Ward, "A Broad Line N.M.R. Study of Oriented Poly(vinylidene fluoride)," *Polymer*, vol. 26, pp. 208-218, 1985.

10. Yasuhiro Takahashi and Kazuhiro Miyaji, "Long-Range Order Parameters of Form II of Poly(vinylidene fluoride) and Molecular Motion in the α_c Relaxation," *Macromolecules*, vol. 16, pp. 1789-1792, 1983.

11. Yasuhiro Takahashi and Hiroyuki Tadokoro, "Structure And Disorder Of Poly(Vinylidene Floride)," *Ferroelectrics*, vol. 57, pp. 187-201, 1984.

12. N. Takahashi and A. Odajima, "Ferroelectric Reorientation of Crystallites in Polyvinylidene Fluoride," *Ferroelectrics*, vol. 32, pp. 49-59, 1981.

13. Andrew J. Lovinger, G.T. Davis, T. Furukawa, and M.G. Broadhurst, "Crystalline Forms in a Copolymer of Vinylidene Fluoride and Trifluoroethylene(52/48 mol%)," *Macromolecules*, vol. 15, pp. 323-328, 1982.

14. Bernard Servet, Simone Ries, Dominique Broussoux, and Francois Micheron, "Bulk and Surface Dipolar Orientation Induced by Two Poling Techniques in Rolled PVF_2 Films," *J. Appl. Phys.*, vol. 55, pp. 2763-2768, 1984.

15. A.J. Bur, J.D. Barnes, and K.J. Wahlstrand, *A Study of Thermal Depolarization of Polyvinylidene Fluoride Using X-ray Pole Figure Observations.*, Center for Materials Science, Polymers Division, National Bureau of Standards, Gaithersburg, MD, 1985.

16. Nobuyuki Takahashi and Akira Odajima, "On the Structure of Poly(vinylidene Fluoride) Under a High Electric Field ," *Ferroelectrics*, vol. 57, pp. 221-228, 1984.

17. M. Koboyashi, K. Tashiro, and H. Tadokoro, *Macromolecules*, vol. 8, p. 158, 1975.

18. F.A. Bovey, F.C. Schilling, T.K. Twei, and H.L. Frisch, *Macromolecules*, vol. 10, p. 559, 177.

19. M.A. Bachmann, W.L. Gordon, J.L. Koenig, and J.B. Lando, *J. Appl. Phy.*, vol. 50 P 6106, 1979.

20. D. Naegele and D.Y. Yoon, "Orientation of Crystalline Dipoles in Poly(vinylidene fluoride) Films Under Electric Field," *Appl. Phys. Lett.*, vol. 33, pp. 132-134, 1978.

21. C.W. Wilson III, *J. Polymer Sci. A*, vol. 1, p. 1305, 1963.

22. C.W. Wilson III and E.R. Santee, Jr., *8*, p. 97, 1965.

23. D.C. Douglass, V.J. McBrierty, and T.T. Wang, "The Use of NMR Linewidths to Study b-axis Distributions in Poled and Unpoled PVDF," *J. Chem. Phys.*, vol. 77 , pp. 5826-5834, 1982.

24. G.T. Davis, M.G. Broadhurst, A.J. Lovinger, and T. Fukukawa, "Hysteresis in Copolymers of Vinylidene Fluoride and Trifluoroethylene," *Ferrolectrics*, vol. 57, pp. 73-84, 1984.

25. G.T. Davis, T. Furukawa, A.J. Lovinger, and M.G. Broadhurst, "Stuctural and Dielectric Investigation on the Nature of the Transition in a Copolymer of Vinylidene Fluoride and Trifluoroethylene(52/48 mol%)," *Macromolecules*, vol. 15, pp. 329-333, 1982.

26. M.G. Broadhurst and G.T.Davis, "Ferroelectric Polarization in Polymers," *Ferroelectrics*, vol. 32, pp. 177-180, 1981.

27. T. Furukawa, M. Date, and E. Fukada, "Hysteresis Phenomena in Polyvinylidene Fluoride Under High Electric Field," *J. Appl. Phys.*, vol. 51, pp. 1135-1141, 1980.

28. T. Furukawa and G.E. Johnson, "Measurements of ferroelectric switching characteristics in polyvinylidene fluoride," *Appl. Phys. Lett.*, vol. 38, pp. 1027-1029, 1981.

29. R.G. Kepler and R.A. Anderson, "Ferroelectricity in Polyvinylidene Fluoride," *J. Appl. Phys.*, vol. 49, pp. 1232-1235, 1978.

30. Masahiko Tamura, Kiyohide Ogasawara, Nobuyuki Ono, and Sumio Hagiwara, "Piezoelectricity in Uniaxially Stretched Poly(vinylidene fluoride)," *J. Appl.Phys.*, vol. 45, pp. 3768-3771, 1974.

31. A. J. Lovinger, T. Furukawa, G. T. Davis, and M.G. Broadhurst, "Curie Transitions in Copolymers of Vinylidene Fluoride," *Ferroelectrics*, vol. 50, pp. 227-236, 1983.

32. Ken'Ichi Nakamura, Yoshikichi Teramoto, and Naohiro Murayama, "Rotation of Polar Axis of β-Form Poly(vinylidene fluoride) Under High Electric Field," *Ferrolectrics*, vol. 57, pp. 139-149, 1984.

33. A. Abragam, in *Principles of Nuclear Magnetism*, ed. D.H. Wilkinson, Oxford University Press, New York, 1983.

34. C.P. Slichter, in *Principles of Magnetic Resonance*, ed. Hans-Joachim Queisser, Springer-Verlag, Berlin Heidelberg New York, 1980.

35. H.W. Spiess, "Deuterium NMR - A new Tool for Studying Chain Mobility and Orientation in Polymers.," in *Advances in Polymer Science*, vol. 66, p. 23, Springer-Verlag, Berlin Heidelberg, 1985.

36. H.W. Spiess, "Deuterium spin alignment: A probe for studying ultraslow motions in solids and solid polymers," *J. Chem. Phys.*, vol. 72, pp. 6755-6762, June, 1980.

37. R. Hentschel, J. Schlitter, H. Sillescu, and H.W. Spiess, "Orientational distributions in partially ordered solids as determined from NMR and ESR line shapes.," *J. Chem. Phys.*, vol. 68, pp. 56-66, Jan. 1978.

38. Alexander J. Vega, "Characterization of Macromolecular Motion in Bulk PMMA by Deuterium NMR," *Central Research and Development Department E.I. du Pont de Nemours and Company*.

39. Kenneth R. Jeffrey and Roderick E. Wasylishen, "Molecular reorientation in sodium Hydrosulfide: a deuterium nmr study," *Can. J. Phys.*, vol. 59, p. 1585, 1981.

40. James H. Davis, "Deuterium Magnetic Resonance Study of the Gel and Liquid Crystalline Phases of Dipalmitoyl Phosphatidylcholine," *Biophysical Journal*, vol. 27, p. 339, 1979.

41. M. Lausch and H.W. Spiess, "Ultraslow Tetrahedral Jumps in Hexamethylenetetramine Studied by Deuteron Spin Alignment," *Chemical Physics Letters*, vol. 71, p. 182, 1980.

42. J.H. Davis, K.R. Jeffrey, M. Bloom, M.I. Valic, and T.P. Higgs, "Quadrupolar Echo Deuteron Magnetic Resonance Spectroscopy in Ordered Hydrocarbon Chains," *Chemical Physics Letters*, vol. 42, p. 392, 1976.

43. P.M. Henrichs , J.M. Hewitt, and M. Linder, "Experimental Aspects of Deuterium NMR of Solids," *Journal of Magnetic Resonance*, vol. 60, p. 280, 1984.

44. R. Hentschel, "Deuterium Fourier Transform NMR in Solids and Solid Polymers," *Journal of Magnetic Resonance*, vol. 35, pp. 157-162, 1979.

45. R. Hentschel, H. Sillescu, and H.W. Spiess, "Orientational distribution of polymer chains studied by Deuterium n.m.r. line shapes," *Polymer*, vol. 22, pp. 1516-1521, 1981.

46. M.H. Cohen and F. Reif, "Quadrupole Effects in Nuclear Magnetic Resonance Studies of Solids," in *Solid State Physics*, ed. David Turnbull, vol. 5, p. 332, Academic Press, New York, N.Y., 1957.

47. D.I. Hoult, "The NMR Receiver: A Description and Analysis of Design," *Progress in NMR Spectroscopy*, vol. 12, 1978.

48. in *Radio Amateur's Handbook*, American Radio League, Inc., Newington, Conn., 1973.

49. Eiichi Fukushima and Stephen B. Roeder, in *Experimental Pulse NMR, A Nuts and Bolts Approach*, Addison-Wesley Publishing Company,Inc., Reading, Massachusettes, 1981.

50. *Private communications with Aime DeReggi and T. Davis at the National Bureau of Standards..*

51. *NBS - All this work was done at the National Bureau of Standards with the help and direction of Aime DeReggi and T. Davis..*

52. Aime DeReggi, C.M. Guttman, F.I. Mopsik, G.T. Davis, and M.G. Broadhurst, "Determination of Charge or Polarization across Polymer Electrets by the Thermal Pulse Method and Fourier Analysis," *Physical Review Letters*, vol. 40, p. 413, 1978.

53. A.J. Lovinger, T. Furukawa, G.T. Davis, and M.G. Broadhurst, "Crystallographic changes characterizing the Curie transistion in the ferroelectric copolymers of vinylidene fluoride and trifluoroethylene:1. As-crystallized samples," *Polymer Papers*, vol. 24, pp. 1225-1239, 1983.

54. G.J. Welch, *Polymer*, vol. 15, p. 429, 1974.

55. V.J. McBrierty, D.C. Douglass, and T.A. Weber, "Nuclear Magnetic Relaxation and Molecular Motion in Poly(vinylidine fluoride)," *Journal of Polymer Science*, vol. 14 , pp. 1271-1286, 1976.

56. Martin Broadhurst, "Rigorous Bounds for the Calculated Dielectric Constants of Ferroelectric Polymers," *Ferroelectrics*, vol. 49, pp. 159-167, 1983.

57. J.F. Legrand, P.J. Schuele, V.H. Schmidt, and M. Minier, "N.M.R. Study of the Ferroelectric Phase Transition in a 70/30 mol% Copolymer of Vinylidene Fluoride (VF_2) and Trifluoroethylene (TrFE)," *Polymer*, vol. 26, pp. 1683-1688, 1985.

58. G.E. Pake, "Nuclear Resonance Absorption in Hydrated Crystals: Fine Structure of the Proton Line," *The Journal of Chemical Physics*, vol. 16, p. 327, 1947.

59. Ulrich Haeberlen, "High Resolution NMR in Solids," in *Advances in Magnetic Resonance: Suppl. 1.*, pp. 24-30, Academic Press, New York, N.Y., 1976.

60. M. Bloom, J.H. Davis, and M.I. Valic, "Spectral Distortion effects due to finite widths in deuterium nuclear magnetic resonance spectroscopy," *Can. J. Phys.*, vol. 58, p. 1510, 1980.

VITA

MONTEE A. DOVERSPIKE

The author was born in Stillwater, Okalahoma on March 5, 1955. He received a B.S. degree (May, 1979) from the College of William and Mary; he received his M.S. degree (December, 1981) from the College of William and Mary. He received his Ph.D. (November, 1986) from the College of William and Mary. He accepted a postdoctoral position at the Naval Research Lab in Washington, D.C..